Crystal structures of leucites – past, present, and future?

BELL, Anthony <http://orcid.org/0000-0001-5038-5621>

Crystal structures of leucites – past, present, and future?

Anthony Martin Thomas Bell*

Materials and Engineering Research Institute, Sheffield Hallam University, Sheffield, S1 1WB, United Kingdom

Anthony.Bell@shu.ac.uk

Tony Bell is Senior X-ray Technician in the Materials and Engineering Research Institute, Sheffield Hallam University where he manages an X-ray (X-ray Powder Diffraction and X-ray Fluorescence) Laboratory. He has a Ph.D. in solid-state chemistry from the University of Cambridge. He was formerly employed as a synchrotron X-ray powder diffraction beamline scientist at the Daresbury Synchrotron Radiation Source in Cheshire, UK, and at the DORIS-III synchrotron at the DESY laboratory in Hamburg, Germany. He has worked on many different materials in his solid-state chemistry research over the years but has kept coming back to leucites.

ORCID

Anthony Martin Thomas Bell 0000-0001-5038-5621

Acknowledgements. This paper is not funded by a specific grant. I wish to thank all my colleagues who have collaborated with me in my leucite research over the years. I particularly wish to thank Michael Henderson, Emeritus Professor of Petrology in the Department of Earth and Environmental Sciences, University of Manchester. He started me on my research into leucites over 30 years ago and has collaborated with me for many years. I also wish to acknowledge the use of the EPSRC funded National Chemical Database Service hosted by the Royal Society of Chemistry.

Abstract

The synthetic anhydrous analogue of the mineral leucite has the chemical formula $KAlSi_2O_6$, it has a silicate framework crystal structure with the same topology as the zeolite analcime. In this crystal structure Al partially replaces Si in the framework, a K extraframework cation is incorporated to balance the charges. Synthetic analogues of leucite are known with the general formulae ACX_2O_6 and $A_2BX_5O_{12}$, where *A* is a monovalent cation, *B* is a divalent cation, *C* is a trivalent cation and *X* is Si or Ge. The crystal structures of these analogues have the same topology but otherwise show differences in crystal structure symmetry and framework cation ordering. This paper reviews the work done on leucite analogue crystal structures over the years and looks forward to work that could be done on these fascinating materials in the future.

Keywords: leucite minerals, silicate framework structures, zeolites, X-ray powder diffraction, synchrotron radiation, Rietveld method.

Contents

1. Substitution into silicate framework structures .....**Error! Bookmark not defined.**
2. Leucite and pollucite 7
3. Leucite analogue structures 14
4.1 Initial ion exchange - Barrer 14
4.2 More leucite analogues - West 15
4.3 Cation-ordered leucite structures 16
4.4 Cation disordered leucite structures since 1990 22
4. Leucite phase transitions. 25
5.1 Initial leucite phase transitions 25
5.2 Non-cation disordered leucite phase transitions since 1990. 27
5.3 Cation ordered leucite phase transitions 30
5.4 Pressure induced leucite phase transitions. 35
5. Ge leucites. 38
6. Comparison of leucite structure types. 40
7. Future work. 59
8. Conclusions. 61
1. References. 89

Silicate minerals are rock-forming minerals consisting of silicate groups. They are the largest and most important class of minerals and make up approximately 90 percent of the earth's crust ***(1)***. The chemically simplest silicate mineral is silicon dioxide, SiO_2. It is mostly found in nature as quartz which is a major component of sand. The crystal structures of silicon dioxide polymorphs (***(2)***, ***(3) (4) (5)***) have silicon in an infinite three-dimensional array with each silicon bonded to four oxygens and each oxygen bonded to two silicon atoms.

Partial replacement of Si atoms by Al atoms (or other trivalent atoms such as B, Ga, or Fe) in silicate framework structures means a net negative charge on the framework, incorporation of metal (and other) cations into the framework balances the charge. Inclusion of monovalent (e.g., Na, K, Cs) or divalent (e.g., Ca) extraframework cations increases the sizes of channels between the tetrahedral framework units. Henderson ***(6, 7)*** reviewed the composition, thermal expansion, and phase transitions in these framework silicates. These channels in the crystal structures of framework structures can also accept water. Some of these hydrated metal aluminosilicate framework materials are **zeolites** ***(8)***.

These zeolites occur naturally and can also be synthesised. The large internal surface areas of these channels in zeolite framework structures give them extremely useful technological properties such as ion-exchange and catalysis.

One zeolite material is analcime ($NaAlSi_2O_6.H_2O$), this has the zeolite ANA framework ***(9)***. In this zeolite 1/3 of Si atoms are replaced by Al, Si and Al are

disordered over the tetrahedrally coordinated sites (**T-sites**) in the silicate framework. Na^+ cations are incorporated into the structure to balance charge; water is also incorporated into one of the channels present in the framework structure. Analcime has an *Ia*-3*d* cubic crystal structure ***(10-12)***. An analogous structure to analcime (with the same silicate framework topology) is wairakite ($Ca(Al_2Si_4O_{12}).2H_2O$; ***(13, 14)***). However, in the wairakite structure Si and Al are ordered onto separate T-sites, wairakite has a *I*2/*a* monoclinic structure.

Figures 1ab show the crystal structures of analcime and wairakite with Si and Al on the T-sites, water molecules are sited on the W site in the larger central channel of this framework, Na^+ cations in analcime are sited on the S site in a smaller channel, these S sites are only 2/3 occupied by Na^+. In wairakite there are only half the number of Ca^{2+} cations compared to Na^+ cations due to the charge difference. Ca^{2+} cations in wairakite are on three different partially occupied on S sites occupancy, one S site is not occupied. All crystal structures in this paper are plotted using VESTA ***(15)***.

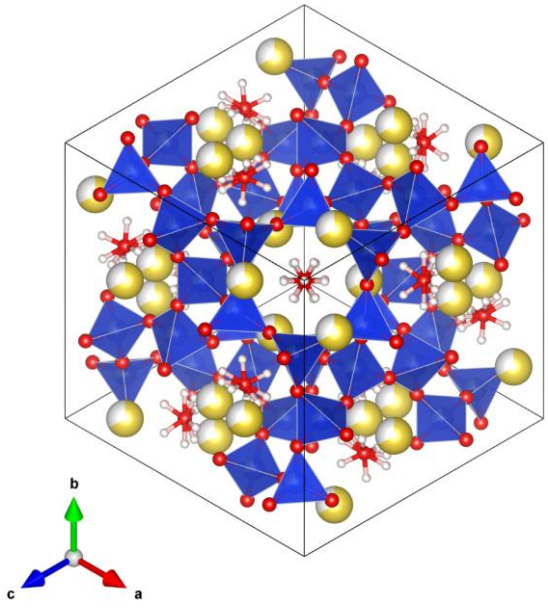

Figure 1a. *Ia-3d* cubic crystal structure of $NaAlSi_2O_6.H_2O$ analcime. Yellow spheres

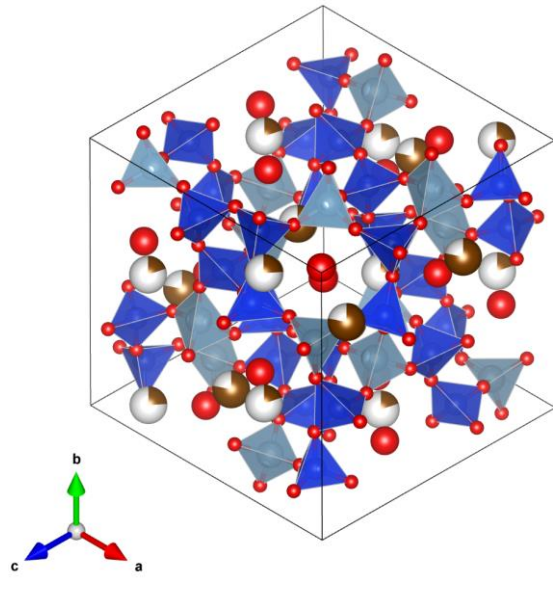

Figure 1b. *I*2/*a* monoclinic crystal structure of $CaAl_2Si_4O_{12}.2H_2O$ wairakite.

show Na^{+} cations (2/3 occupied S sites), red spheres show O^{2-} anions and white spheres (W sites) show H atoms in the water molecule. Blue tetrahedra show $(Si/Al)O_4$ units.	Brown spheres show Ca^{2+} cations (partially occupied S sites). Blue tetrahedra show SiO_4 units, pale blue tetrahedra show AlO_4 units. Small red spheres show O^{2-} anions, large red spheres (W-sites) show oxygen from water molecules.

1. Leucite and pollucite

If the analcime structure is modified by removal of water and the Na^+ cation is replaced by the larger K^+ cation, then the **leucite** crystal structure ($KAlSi_2O_6$) is formed. In this structure there is an infinite framework structure consisting of $(Si/Al)O_4$ tetrahedra with Si and Al disordered (as in analcime but not as in wairakite) over the same site, the K^+ cations sit in the W site extraframework channels in the structure and are 12 coordinated to O. These K^+ cations do not sit on the smaller S sites. The analcime topology is retained but the crystal structure is lowered in symmetry from *Ia*-3*d* cubic to $I4_1/a$ tetragonal ***(16-20)***. Leucite is a naturally occurring mineral ***(21)***, but it can also be synthesised. The substituted silicate framework structure of leucite consists of 6-rings,4-rings and 8-rings of $(Si/Al)O_4$ tetrahedral units. Figures 2abc show these 6-rings,4-rings and 8-rings in the leucite structure.

Uses of leucite include sources of potassium and aluminium and dental ceramics ***(22)***

A similar mineral to leucite is pollucite, the naturally occurring mineral ***(23)*** has the stoichiometry $(Cs,Na)AlSi_2O_6.nH_2O$ but synthetic pollucite has the stoichiometry $CsAlSi_2O_6$. For the rest of the paper pollucite refers to synthetic pollucite as opposed to mineral pollucite Comparison of the crystal structures of leucite (Figure 2ac) and pollucite (Figure 3) show that these structures have the same topology, with K and Cs cations on the W sites.

As the pollucite structure contains caesium then this mineral is a potential material for storage of caesium from radioactive waste materials ***(24-26)***

Name	a (Å)	c (Å)	V (Å^3)	SG	Ref
analcime	13.73		2588	*Ia-3d*	*(10)*]
analcime	**13.73**		**2588**	***Ia-3d***	*(11)*
leucite	**12.95**	**13.65**	**2289**	***I*4$_1$/*a***	*(16, 17)*
leucite	**13.09(1)**	**13.75(1)**	**2356(4)**	***I*4$_1$/*a***	*(19)*
leucite	**13.0548(2)**	**13.7518(2)**	**2343.69(7)**	***I*4$_1$/*a***	*(20)*
pollucite	13.71		2577	*Ia-3d*	*(27)*]
pollucite	**13.74**		**2594**	***Ia-3d***	*(28)*
pollucite	**13.682(3)**		**2561.2(6)**	***Ia-3d***	*(29)*
pollucite	**13.69**		**2565.72641**	***Ia-3d***	*(30)*
pollucite	**13.6645(3)**		**2551.42(6)**	***Ia-3d***	*(31)*
pollucite	**13.6914(6)**		**2566.5(1)**	***Ia-3d***	*(26)***]**
pollucite	**13.6808(6)**		**2560.6(1)**	***Ia-3d***	*(26)*
pollucite	13.653		2545.0	*Ia-3d*	*(32)*
pollucite	13.678		2559.0	*Ia-3d*	*(33)*

pollucite	13.682		2561.2	*Ia*-3*d*	***(33)***
pollucite	13.677		2558.4	*Ia*-3*d*	***(33)***
pollucite	**13.6735(2)**		**2556.46(4)**	***Ia*-3*d***	***(34)***

Table 1a. Lattice parameters for analcime, leucite and pollucite. SG = space group. If the original reference doesn't quote a unit cell volume, then these have been calculated. **Bold type shows that crystal structure is given in this reference.**

However, $KAlSi_2O_6$ leucite has a $I4_1/a$ tetragonal structure but the $CsAlSi_2O_6$ pollucite has an *Ia*-3*d* cubic structure ***(12)(27-31)***. Comparison of Figures 2a and 3 show that the 6-ring in leucite is distorted compared to the corresponding 6-ring in pollucite. The pollucite 6-ring has sixfold symmetry, but the leucite 6-ring is less symmetrical having twofold symmetry. The crystal ionic radii ***(35)*** for 12 coordinate Cs^+ and K^+ are respectively 2.02Å and 1.78Å. Replacing the Cs^+ cation with the smaller K^+ cation in this structure will cause a framework collapse ***(36)*** of the crystal structure and a consequent lowering of symmetry from cubic to tetragonal.

However, the $LiAlSi_2O_6$ ***(37)*** and $NaAlSi_2O_6$ ***(38)*** structures have crystal structures with a different topology to that for leucite due to the smaller sizes of the extraframework cations, the crystal ionic radii for 8-coordinate Na^+ and Li^+ are respectively 1.32Å and 1.06Å ***(35)***. $LiAlSi_2O_6$ and $NaAlSi_2O_6$ are isostructural, with Al and Si are completely ordered (unlike in leucite) onto AlO_6 and SiO_4 polyhedra with Li/Na cations sitting in the extraframework channels, see Figures 4ab.

Table 1a shows lattice parameters for analcime, leucite and pollucite. Table 1b shows lattice parameters for two different wairakite crystal structure determinations.

a (Å)	**b (Å)**	**c (Å)**	**β (°)**	**V (Å^3)**	**SG**	**Ref**
13.692(3)	13.643(3)	13.560(3)	90.5(1)	2533(2)	*I*2/*a*	***(13)***
13.694(6)	13.644(7)	13.576(6)	90.46(2)	2536(4)	*I*2/*a*	***(14)***

Table 1b. Lattice parameters for wairakite crystal structure determinations. SG = space group. If the original reference doesn't quote a unit cell volume, then these have been calculated.

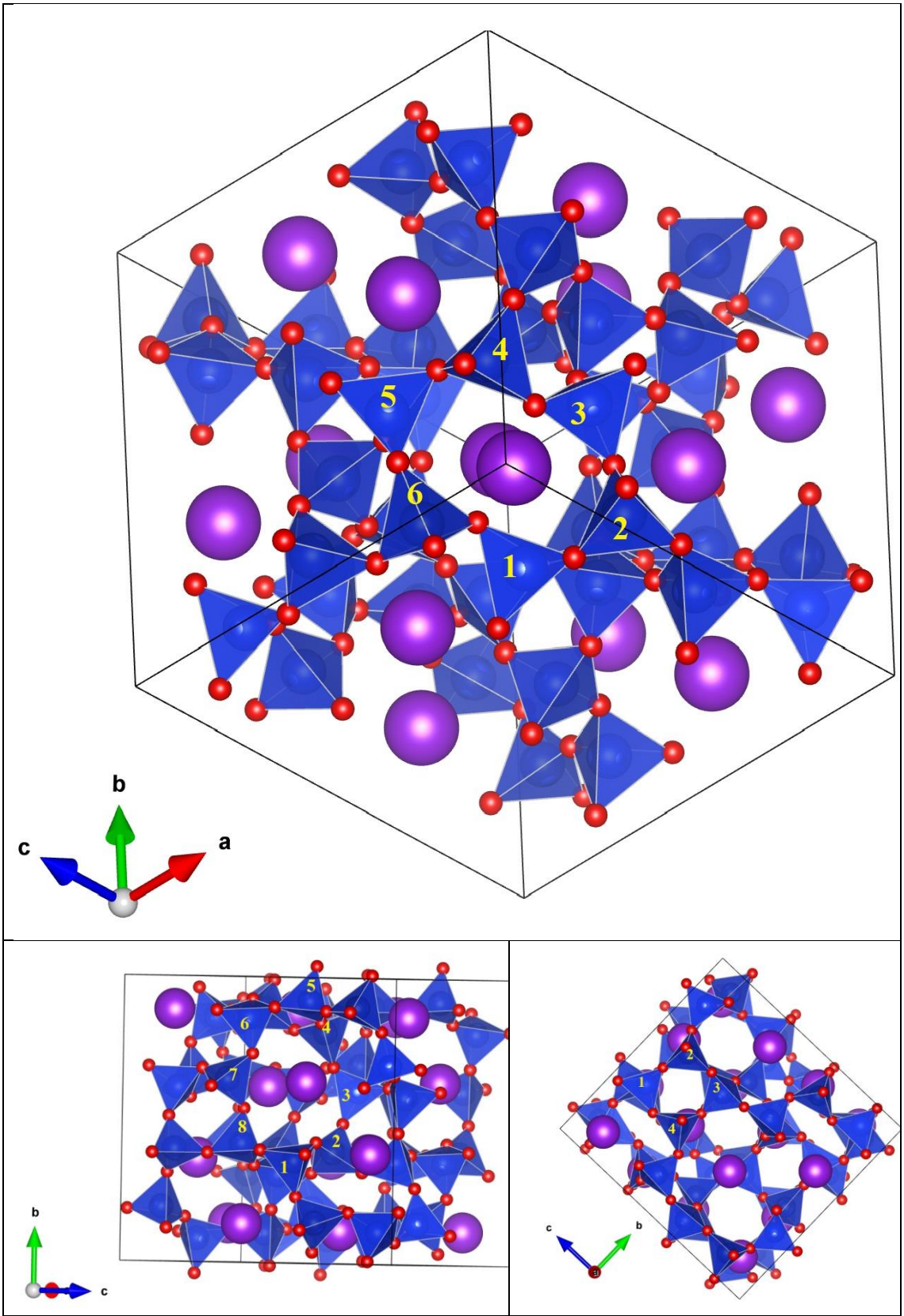

Figures 2a (top), 2b (bottom left) and 2c (bottom right). $I4_1/a$ tetragonal crystal structure ***(19)***of $KAlSi_2O_6$ leucite indicating the 6-rings, 4-rings and 8-rings of

tetrahedral $(Si/Al)O_4$ units, shown in blue. Purple spheres (W-sites) show K^+ cations, red spheres show O^{2-} anions.

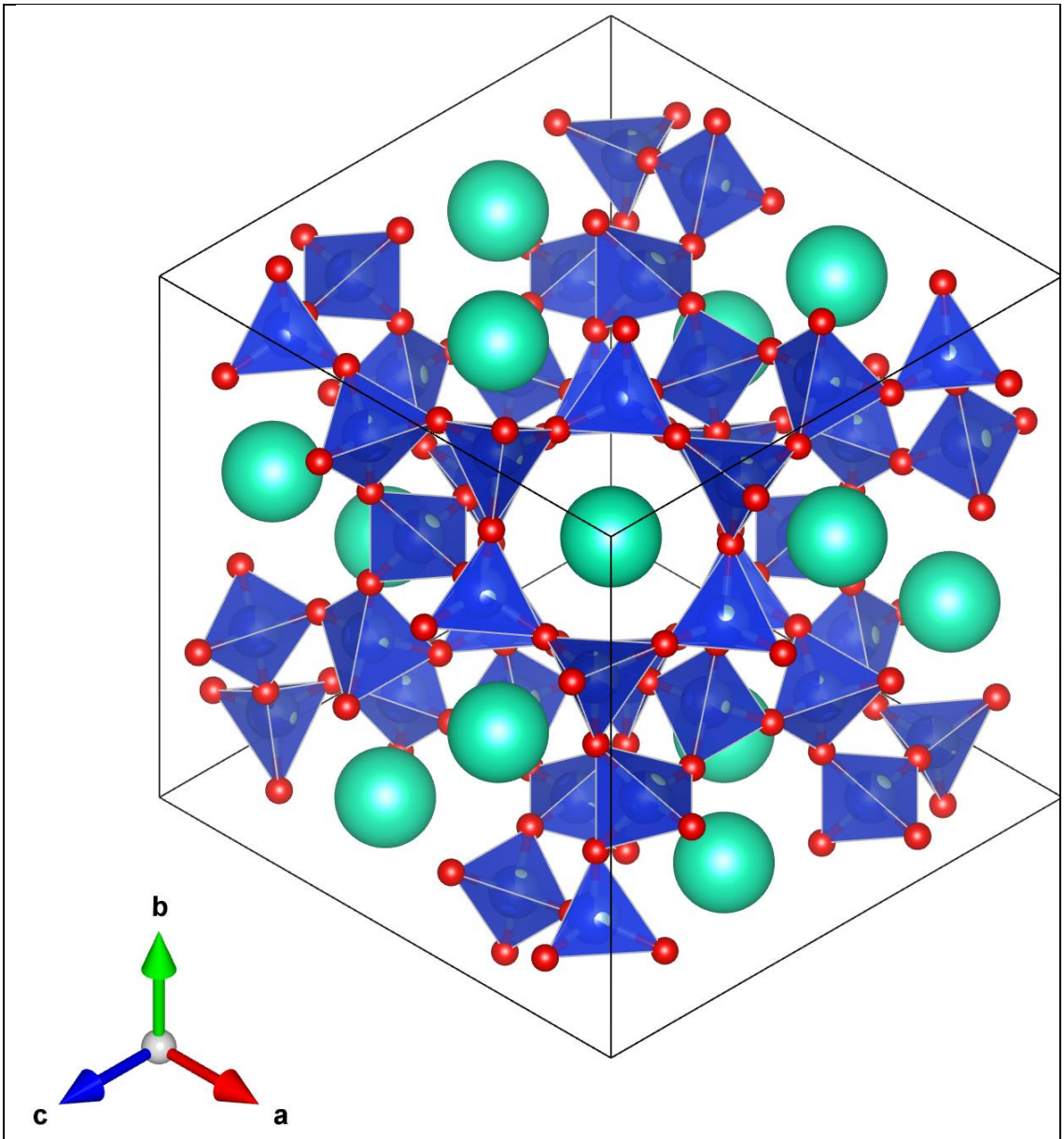

Figure 3. *Ia*-3*d* cubic crystal structure of $CsAlSi_2O_6$ pollucite. Turquoise spheres show Cs^+ cations, red spheres show O^{2-} anions, tetrahedral $(Si/Al)O_4$ units are in blue. Note the difference in symmetry in the central channel 6-ring in pollucite compared to that in leucite (see Figure 2a).

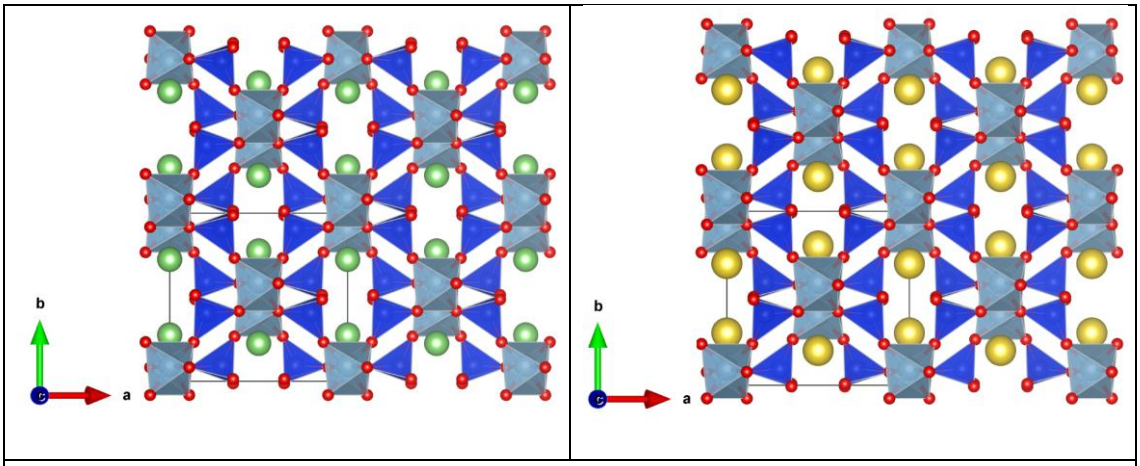

Figures 4a (left) and 4b (right). *C*2/*c* monoclinic crystal structure of $LiAlSi_2O_6$ spodumene and of $NaAlSi_2O_6$ jadiete. Green spheres show Li^+ cations, yellow spheres show Na^+ cations, red spheres show O^{2-} anions. Grey octahedra show AlO_6 units and blue tetrahedra show SiO_4 units.

2. Leucite analogue structures

4.1 Initial ion exchange - Barrer

These leucite structures have channels containing cations, such K and Cs as the W site cations in leucite and pollucite. It is possible to do ion-exchange on these framework structures to replace the extraframework cations. The research group of Professor Barrer at the University of Aberdeen did some work in the 1950s to synthesise new leucite and pollucite analogue by ion-exchange and by synthesis from gel precursor materials. Hereafter all of these analogues of leucite and pollucite are referred to as leucite analogues.

Initial ion-exchange experiments ***(39)*** on analcime showed that Na^+ could be ion-exchanged with K^+, NH_4^+, Rb^+, Cs^+, Ag^+ and Tl^+. These ion-exchanged samples gave X-ray powder diffraction patterns similar to those for leucite, pollucite and analcime. The Tl^+ ion-exchanged sample has an X-ray powder diffraction pattern identical to that for a Tl-analcime crystallised hydrothermally from a $Tl_2O.Al_2O_3.4SiO_2$ gel ***(40)***. Further ion-exchange experiments ***(41)*** showed that leucite could be ion-exchanged with Tl^+ and that Tl-analcime could be ion-exchanged with Rb^+.

Hydrothermal synthesis from gel starting materials ***(42, 43)*** produced synthetic anhydrous $A AlSi_2O_6$ samples where $A = K^+$, NH_4^+, Rb^+, Cs^+ and Tl^+. Hydrated $A AlSi_2O_6.nH_2O$ samples were produced where $A = Li^+$, Na^+ and Ag^+. Table S1 shows lattice parameters for these anhydrous $A AlSi_2O_6$ samples ***(43)***.

At the end of the paper ***(43)*** the authors refer to some other substituted analogues of $KAlSi_2O_6$, where the Al^{3+} framework cation has been replaced by other divalent and trivalent cations. These include $KGaSi_2O_6$ ***(44)*** and $K_2MgSi_5O_{12}$ ***(45, 46)***.

The authors ended the paper by suggesting that the analcime-leucite structure type could potentially contain many different chemical compositions.

4.2 More leucite analogues - West

Thirty years after the work of Professor Barrer, more work was done at the University of Aberdeen by the research group of Professor West. This work greatly expanded the number of known leucite structures, especially for the $A_2BSi_5O_{12}$ leucites where 2 Al atoms are replaced with one Si and one divalent (*B*) cation. Additionally, more $ACSi_2O_6$ leucites were synthesised where Al is replaced by other trivalent (*C*) cations.

Tables S2a ($ACSi_2O_6$) and S2b ($A_2BSi_5O_{12}$) show the lattice parameters for leucite samples synthesised by the West group and other leucite structures (except leucite and pollucite) up to 1989. All the lattice parameters for which definite space group assignments are given are either *Ia*-3*d* cubic (pollucite), *I*-43*d* cubic ($KBSi_2O_6$ - boroleucite) or $I4_1/a$ (leucite). The papers of Professor West suggest that other space groups are possible, including those with lower than tetragonal symmetry, but no definite space group assignments are given. These structures include a leucite where the extraframework cation is not an alkali metal, ammonioleucite $(NH_4)AlSi_2O_6$ ***(47)***.

In boroleucites, when the $ACSi_2O_6$ *C* cation is now boron (the smallest trivalent cation, 4-coordinate crystal ionic radius 0.25 Å ***(35)***) and the *A* cation is either K or Rb, this cubic space group is no longer the highest symmetry space group *Ia*-3*d* cubic (space group 230 out of 230), which is centrosymmetric. The cubic space group for $KBSi_2O_6$ and $RbBSi_2O_6$ is now *I*-43*d* cubic (space group 220), which is non-centrosymmetric.

4.3 Cation-ordered leucite structures

Up to the end of the 1980s almost all known leucite structures had disordered cations on the T-sites. These were high symmetry body centred tetragonal and cubic structures with the divalent and trivalent cations disordered onto the same T-sites as the quadrivalent Si cations. $K_{0.2}Rb_{0.8}GaSi_2O_6$ ***(48)*** was hydrothermally synthesised. The single-crystal structure for this sample was $I4_1/a$ tetragonal and had partial T-site cation ordering. However, this doesn't match the $I4_1/a$ tetragonal structures for $KGaSi_2O_6$ ***(49)*** and $RbGaSi_2O_6$ ***(50)*** which have complete T-site cation disorder for Ga and Si.

Samples of $K_2MgSi_5O_{12}$ leucite analogues were synthesised dry (heated up in air) and hydrothermally (heated up under pressure in the presence of water). 29-Si NMR spectra on these two samples gave very different results ***(51)***. The hydrothermal NMR spectrum shows 10 different resonances of approximately the same intensity, see Figure 5. This suggested that there were 10 different chemical environments for Si in the hydrothermal sample.

High-resolution synchrotron X-ray powder diffraction showed that dry $K_2MgSi_5O_{12}$ leucite has the *Ia*-3*d* cubic structure, isostructural with pollucite ***(52, 53)***. However, high-resolution synchrotron X-ray powder diffraction, together with electron diffraction, NMR spectroscopy and Rietveld refinement ***(54)***, showed that hydrothermal $K_2MgSi_5O_{12}$ had a previously unknown *cation-ordered* leucite crystal structure. This was $P2_1/c$ monoclinic with 10 different fully occupied Si T-sites and 2 different fully occupied Mg T-sites, the structure contains distinct SiO_4 and MgO_4 tetrahedral units. Table S3 shows ambient temperature lattice parameters for $P2_1/c$ monoclinic *cation-ordered* leucite crystal structure for $K_2BSi_5O_{12}$ (*B* = Mg, Fe, Co, Zn ***(52, 53, 55)***), these

are all isostructural with monoclinic $K_2MgSi_5O_{12}$. Figures 6ab shows crystal structure plots for cubic and monoclinic $K_2MgSi_5O_{12}$ leucites.

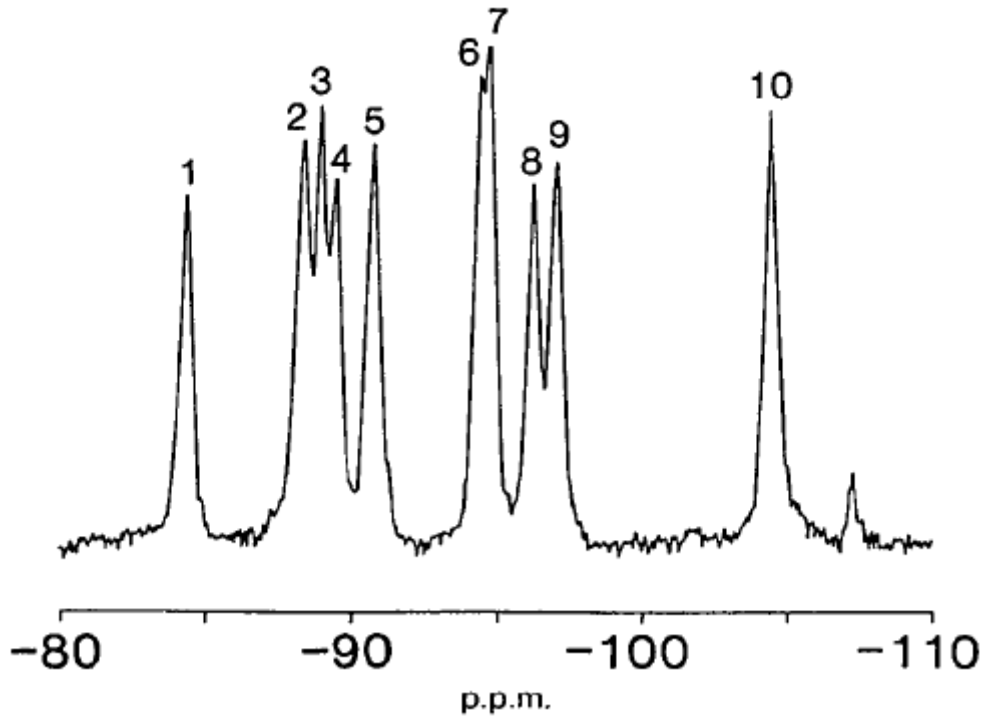

Figure 5. 29-Si NMR spectrum for hydrothermally synthesised $K_2MgSi_5O_{12}$ leucite (***(51-53)***]. The 10 large peaks indicate 10 different Si environments, the weak peak at about -107ppm is due to SiO_2 impurity.

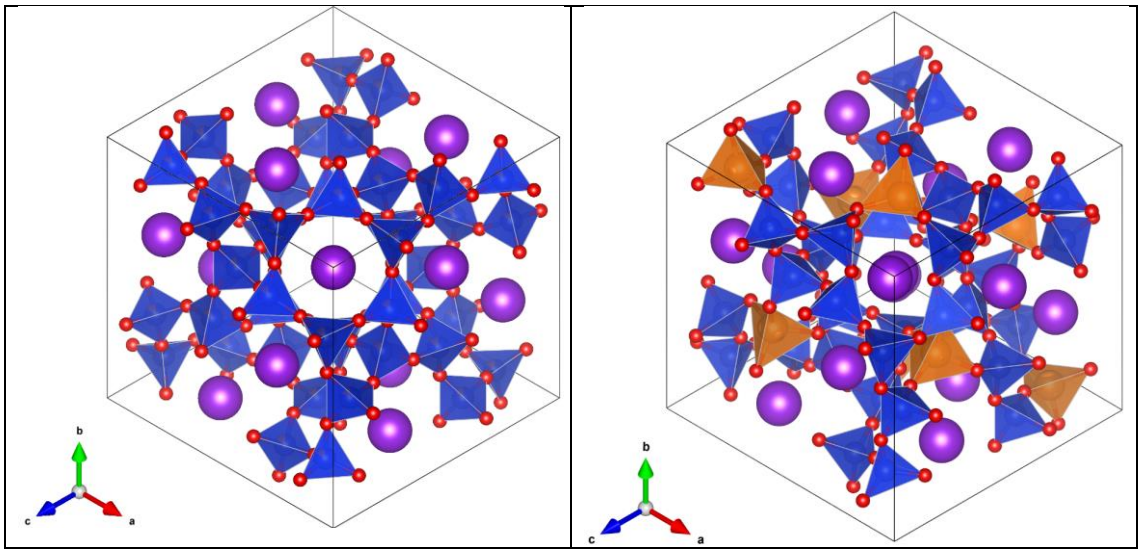

Figures 6a (left) and 6b (right). Plots of crystal structures for $K_2MgSi_5O_{12}$. Left structure is for *Ia*-3*d* cubic cation disordered $K_2MgSi_5O_{12}$. Right is for $P2_1/c$ monoclinic cation ordered $K_2MgSi_5O_{12}$. $(Si/Mg)O_4$ and SiO_4 units are shown in blue, MgO_4 units are shown in orange. Purple spheres show K^+ cations, red spheres show O^{2-}anions. Note how the monoclinic structure has the same topology as the cubic structure but is more distorted.

More NMR work was done some other leucite analogues [***(56-58)***] to look for the number of different chemical environments in these analogues. One of these analogues had the stoichiometry $Cs_2CdSi_5O_{12}$, (see Figure 7). The 29-Si NMR spectrum on this sample showed 5 different resonances of approximately the same intensity, suggesting that there were 5 different chemical environments for Si in the structure.

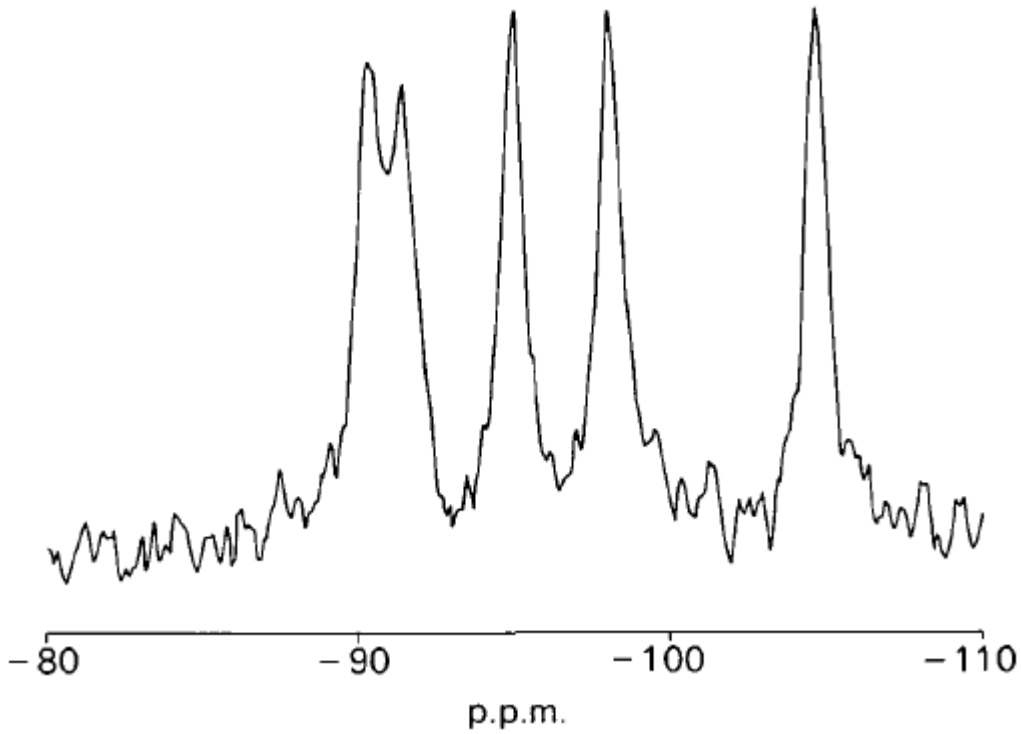

Figure 7. 29-Si NMR spectrum for dry $Cs_2CdSi_5O_{12}$ leucite analogues [***(56)***, ***(59)***].

However, high-resolution synchrotron X-ray powder diffraction, NMR spectroscopy and Rietveld refinement showed that $Cs_2CdSi_5O_{12}$ leucite also had a previously unknown *cation-ordered* leucite crystal structure [***(59)***], see Figure 8. This was *Pbca* orthorhombic with 5 different fully occupied Si T-sites and 1 fully occupied Cd T-site. Table S4 shows ambient temperature lattice parameters for *Pbca* orthorhombic *cation-ordered* leucite crystal structure for $A_2BSi_5O_{12}$ (A = Rb, Cs, B = Mg, Mn, Co, Cu, Ni, Zn, Cd. These structures also include three with two different alkali-metal extraframework cations (***(60)*** $RbCsXSi_5O_{12}$, X = Mg, Ni and Cd), these all have complete T-site order. These structures are all isostructural with $Cs_2CdSi_5O_{12}$. A high-resolution synchrotron radiation X-ray powder diffraction and NMR study on $Cs_2ZnSi_5O_{12}$ ***(61)*** showed some partial T-site disorder. However, another synchrotron radiation X-ray powder diffraction study on $Cs_2ZnSi_5O_{12}$ ***(62)***, with a lower-resolution X-ray detector, showed full T-site cation ordering.

Lattice parameters for three low temperature (8-10 K) *Pbca* leucite $Cs_2BSi_5O_{12}$ structures (B = Cu, Zn and Cd; ***(63)***) are given in Table S5. Apart from thermal contraction the structures are isostructural with the corresponding ambient temperature structures.

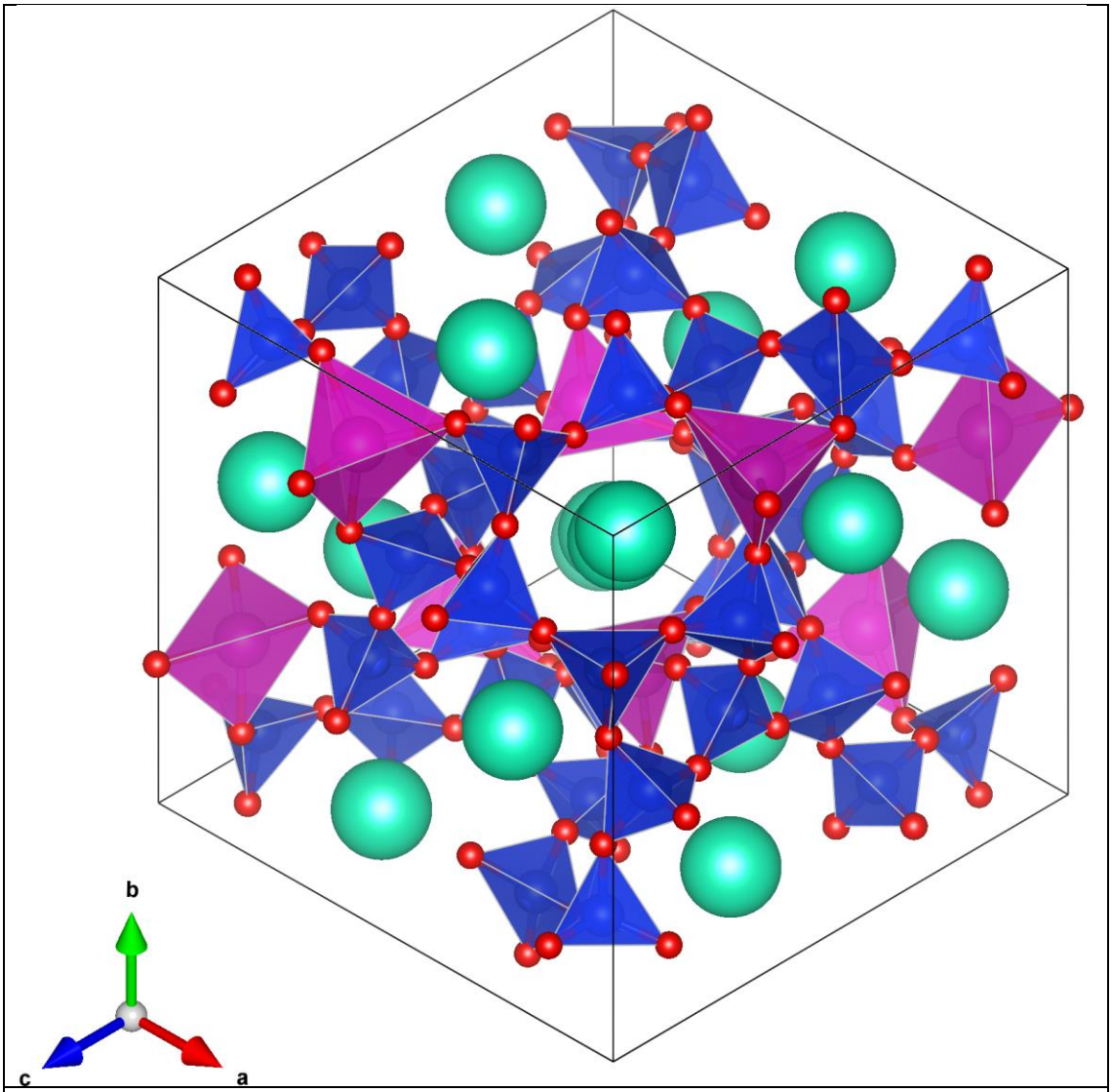

Figure 8. Plot of *Pbca* cation ordered crystal structure for $Cs_2CdSi_5O_{12}$. SiO_4 units are shown in blue, CdO_4 units are shown in pink. Turquoise spheres show Cs^+ cations, red spheres show O^{2-} anions. Note that this structure is more distorted than cubic $K_2MgSi_5O_{12}$ but less distorted than monoclinic $K_2MgSi_5O_{12}$.

A crystal structure for $Cs_2CuSi_5O_{12}$ was predicted [***(64)***], this had a different topology to that for other leucite analogues. A combined synchrotron X-ray and neutron powder diffraction study on this material [***(65)***] showed that the structure of this material could be better described as isostructural with cation ordered *Pbca* $Cs_2CdSi_5O_{12}$ [***(59)***].

The $A_2BSi_5O_{12}$ cation-ordered leucite structures with A = K are all $P2_1/c$ monoclinic at room temperature. However, the corresponding structures with A= Rb and Cs are all *Pbca* orthorhombic. The smaller K cation means that there is framework collapse to monoclinic structures for the A = K structures. However, with the larger A= Rb and Cs cations the crystal structures are less collapsed from monoclinic to orthorhombic. The same framework collapse effects as observed earlier ***(36)*** are seen in these cation-ordered leucite structures.

There is a different $ACSi_2O_6$ cation ordered structure for $CsCSi_2O_6$ (C = Al, B), these are $I4_1/acd$ tetragonal. $CsAlSi_2O_6$ was first reported as tetragonal ***(28)*** as a pseudocubic modification of *Ia*-3*d*. The first true $I4_1/acd$ tetragonal structure leucite was for $Cs_{0.7\text{-}0.8}Na_{0.1}Al_{0.8}Si_{2.2}O_6\bullet(0.3\text{-}0.2)H_2O$ ***(66)***. A similar structure for a mineral sample with the composition $(Cs_{1.02}K_{0.01})B_{0.96}Si_{2.02}O_6$ was reported ***(67)***. There is also a low-temperature $I4_1/acd$ tetragonal structure for $CsAlSi_2O_6$ at 248K ***(31)***

Figure 9 shows the $I4_1/acd$ tetragonal structure of $CsAlSi_2O_6$ ***(67)***.

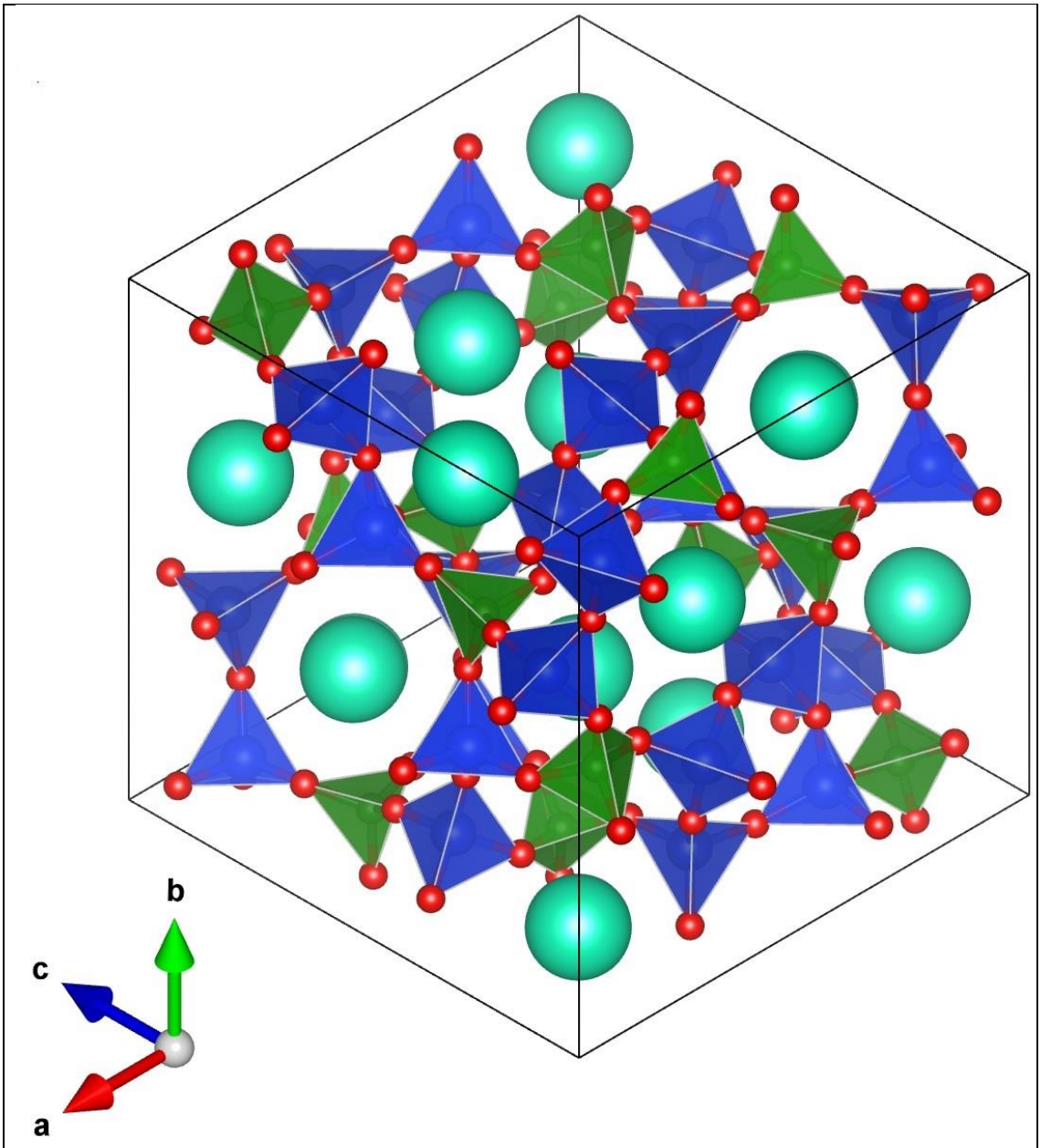

Figure 9. $I4_1/acd$ tetragonal crystal structure $(Cs_{1.02}K_{0.01})B_{0.96}Si_{2.02}O_6$, Turquoise spheres represent Cs^+ cations, red spheres represent O^{2-} anions. Blue tetrahedra represent ordered SiO_4 units and green tetrahedra represent ordered AlO_4 units.

4.4 Cation disordered leucite structures since 1990

After the work of Professor West in the 1980s several more $ACSi_2O_6$ and $A_2BSi_5O_{12}$ (*A* = K, Rb, Cs, NH_4, Tl; *B* = Mg, Cu, Zn, Mn, Ni, Co; *C* = B, Fe, Al, Ga) leucite analogues were synthesised. Almost all leucite structures have an average unit cell length of about 13.5 Å.

However, one interesting leucite is a hydrothermally synthesised $KBSi_2O_6$ ***(68, 69)***, this has a $P2_1/a$ structure which has a monoclinic modification of the leucite topology, in this case the unit cell length **is not** about 13.5 Å. $P2_1/a$ is a different setting of the $P2_1/c$ space group, which is the same space group as the cation-ordered $K_2MgSi_5O_{12}$ structure. Figure 10 shows this monoclinic leucite structure, which is cation-disordered, it has Si and B *disordered* over T-sites. This is different to the cation-ordered $K_2MgSi_5O_{12}$ structure ***(52, 53)***, which has Si and Mg *ordered* over different T-sites. The lattice parameters for these analogues are summarised in Table S6.

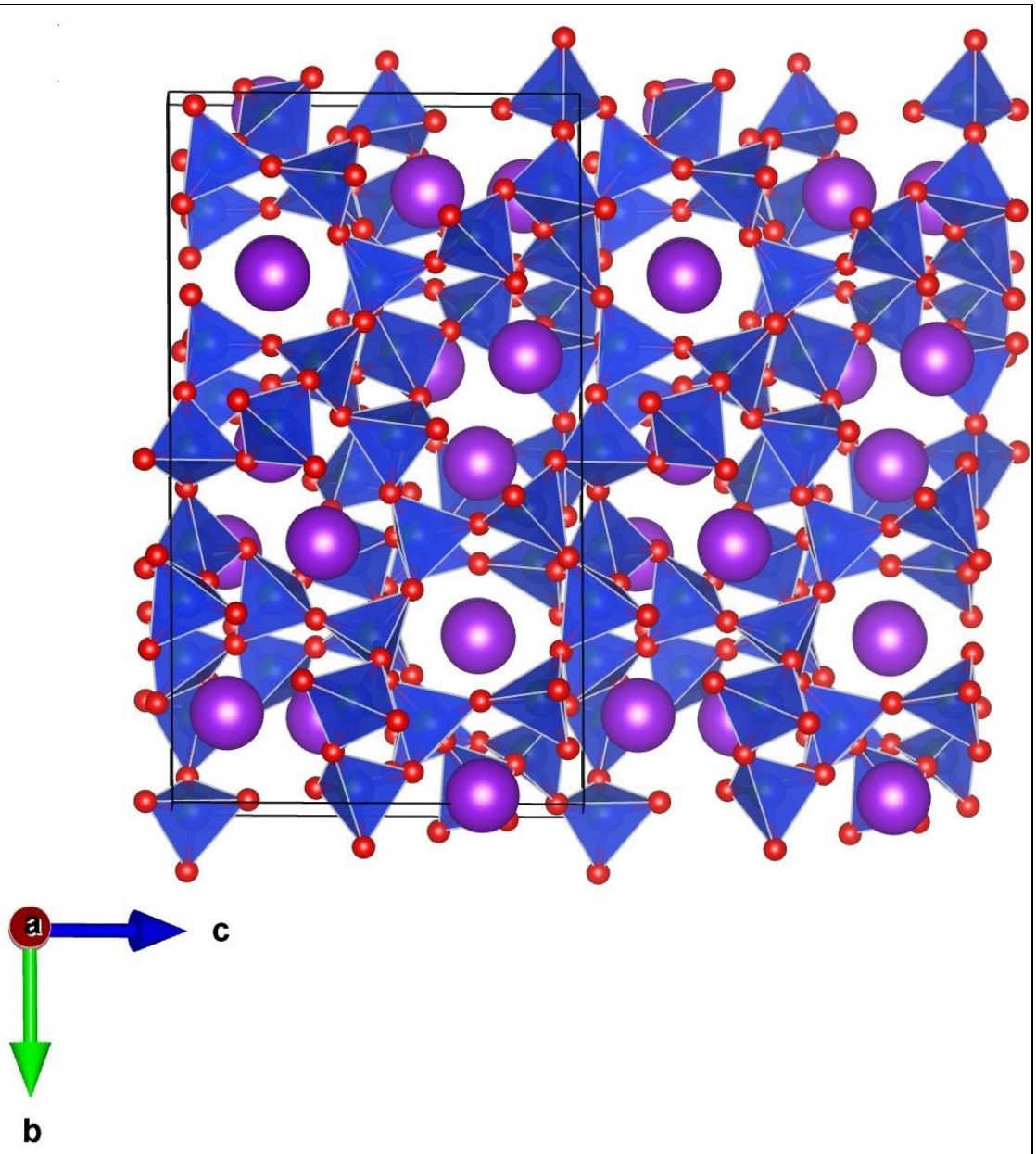

Figure 10. $P2_1/a$ structure for $KBSi_2O_6$ [***(68, 69)***] Purple spheres represent K^+ cations, red spheres represent O^{2-} anions. Blue tetrahedra represent disordered $(Si,B)O_4$.

3. Leucite phase transitions.

5.1 Initial leucite phase transitions

Even before the development of X-ray crystallography ***(70, 71)***a synthetic form of leucite $KAlSi_2O_6$ ***(72)***already showed a tetragonal form at room temperature and a cubic form of leucite at high temperature, this work was published in 1890. The first crystal structure determination of leucite ***(16)*** showed that the ambient temperature $I4_1/a$ tetragonal leucite structure had a phase transition to cubic at 898 K.

The crystal structure was determined for the Fe analogue of leucite, $KFeSi_2O_6$ has an $I4_1/a$ tetragonal structure which is isostructural with $KAlSi_2O_6$ leucite ***(73)***. This paper also reports a differential thermal analysis study on synthetic $KFeSi_2O_6$ and $KAlSi_2O_6$ samples and 6 natural leucite samples. These suggest phase transitions between 823 and 958 K.

The crystal structure of the Fe analogue of pollucite, $CsFeSi_2O_6$ has an *Ia*-3*d* cubic structure which is isostructural with $CsAlSi_2O_6$ pollucite ***(74)***. This *Ia*-3*d* cubic structure is retained for synthetic mixed $Cs(Al_xFe_{1-x})Si_2O_6$ pollucite samples ***(75)***

A high temperature diffraction study on two samples of natural leucite ***(76)*** showed a $I4_1/a$ tetragonal to *Ia*-3*d* cubic phase transition between 933-938 K.

Another high temperature diffraction study ***(36)***was done on samples of natural leucite, $KAlSi_2O_6$, $RbAlSi_2O_6$ and $CsAlSi_2O_6$. All but the $CsAlSi_2O_6$ samples show phase transitions from $I4_1/a$ tetragonal to *Ia*-3*d* cubic. The transition temperatures are 963 K (natural leucite), 878 K ($KAlSi_2O_6$) and 583 K ($RbAlSi_2O_6$), the transition temperature for $RbAlSi_2O_6$ is lower than $KAlSi_2O_6$ and natural leucite. The larger Cs^+ cation size means that the silicate framework structure is fully expanded at room

temperature and has the *Ia*-3*d* cubic structure. However, the smaller K^+ and Rb^+ cations mean that the framework partially collapses to the lower symmetry tetragonal structure. As Rb^+ has a larger crystal ionic radius than K^+ the $RbAlSi_2O_6$ structure is less collapsed than the $KAlSi_2O_6$ and consequently a lower temperature is needed for the structure to expand from tetragonal to cubic. The 12 coordinate crystal ionic radii for these alkali metal cations are:- K^+ 1.78Å; Rb^+ 1.86Å; Cs^+ 2.02Å ***(35)***.

A high temperature single-crystal structure determination ***(77)*** on a sample of natural leucite shows an *Ia*-3*d* cubic structure (isostructural with pollucite) at 908±5 K.

A high temperature diffraction study on $RbAlSi_2O_6$ and $RbFeSi_2O_6$ ***(78)*** showed similar $I4_1/a$ tetragonal to *Ia*-3*d* cubic phase transitions. These transition temperatures were 843 K ($RbAlSi_2O_6$) and 593 K ($RbFeSi_2O_6$).

Details of these phase transitions are given in Table 2.

Stoichiometry	Ambient SG	HTSG	TT (K)	Ref
$KAlSi_2O_6$	tetragonal	cubic	898	***(16)***
Natural leucite	$I4_1/a$	*Ia*-3*d*	963	***(36)***
$KAlSi_2O_6$	$I4_1/a$	*Ia*-3*d*	878	***(36)***
$RbAlSi_2O_6$	$I4_1/a$	*Ia*-3*d*	583	***(36)***
Natural leucite			905	***(73)***
Natural leucite			904	***(73)***
Natural leucite			897	***(73)***
Natural leucite			891	***(73)***
$KFeSi_2O_6$			823	***(73)***
$KFeSi_2O_6$			823	***(73)***
Natural leucite	$I4_1/a$	*Ia*-3*d*	933-938	***(76)***

(K,Na)$AlSi_2O_6$	*I*4$_1$/*a*	*Ia*-3*d*	903-913	***(77)***
$KAlSi_2O_6$	*I*4$_1$/*a*	*Ia*-3*d*	893	***(78)***
$RbAlSi_2O_6$	*I*4$_1$/*a*	*Ia*-3*d*	633	***(78)***
$KFeSi_2O_6$	*I*4$_1$/*a*	*Ia*-3*d*	843	***(78)***
$RbFeSi_2O_6$	*I*4$_1$/*a*	*Ia*-3*d*	593	***(78)***

Table 2. Initial leucite Phase transitions. SG = space group. HTSG = high temperature space group. TT = transition temperature. No space group assignments were given by Wyart ***(16)***. Differential thermal analysis used to study phase transitions by Faust ***(73)***.

5.2 Non-cation disordered leucite phase transitions since 1990.

More phase transitions have been studied on non-cation ordered leucites since 1990. These studies have used synchrotron radiation ***(79)*** and laboratory X-ray sources [***(49)***,***(69)(75, 80-84)(85)***] as well as neutron sources ***(20)*** for diffraction experiments. These mostly show phase transitions from *I*4$_1$/*a* tetragonal to *Ia*-3*d* cubic. However, for boroleucites, a *I*-43*d* cubic to *Ia*-3*d* cubic phase transition is observed for $KBSi_2O_6$ ***(79)***. Another phase transition study for $KBSi_2O_6$ ***(69)*** shows an intermediate *P*2$_1$/*a* monoclinic phase between *I*-43*d* and *Ia*-3*d*. A phase transition from an unknown Primitive orthorhombic to *Ia*-3*d* cubic is observed for $CsBSi_2O_6$. Table 3 shows details of these leucite phase transitions.

Stoichiometry	Ambient SG	HTSG	TT (K)	Ref
Natural leucite	*I*4$_1$/*a*	*Ia*-3*d*	943	***(20)***
Rb-leucite	*I*4$_1$/*a*	*Ia*-3*d*	753	***(20)***
$KFeSi_2O_6$	*I*4$_1$/*a*	*Ia*-3*d*	853	***(20)***

Cs-leucite	$I4_1/a$	*Ia*-3*d*	373	***(20)***
$KGaSi_2O_6$	$I4_1/a$	*Ia*-3*d*	673-973	***(49)***
$KBSi_2O_6$ ++	*I*-43*d*	$P2_1/a$	573	***(69)***
$KBSi_2O_6$ ++	$P2_1/a$	*Ia*-3*d*	823	***(69)***
$KBSi_2O_6$	*I*-43*d*	*Ia*-3*d*	848	***(79)***
$CsBSi_2O_6$	+	*Ia*-3*d*	1273	***(80)***
$RbFeSi_2O_6$	$I4_1/a$	*Ia*-3*d*	673	***(82)***
$RbGaSi_2O_6$	$I4_1/a$	*Ia*-3*d*	733	***(81)***
$RbAlSi_2O_6$	$I4_1/a$	*Ia*-3*d*	673	***(75)***
$Rb_{0.9}Al_{0.9}Si_{2.1}O_6$	$I4_1/a$	*Ia*-3*d*	630	***(75)***
$Rb_{0.8}Al_{0.8}Si_{2.2}O_6$	$I4_1/a$	*Ia*-3*d*	600	***(75)***
$KAlSi_2O_6$	tetragonal	cubic	823	***(83)***
$RbBSi_2O_6$	*I*-43*d*	*Ia*-3*d*	648	***(84, 86)***
$Rb_{0.8}Cs_{0.2}BSi_2O_6$	*I*-43*d*	*Ia*-3*d*	473	***(84)***
$Rb_{0.6}Cs_{0.4}BSi_2O_6$	*I*-43*d*	*Ia*-3*d*	423	***(84)***

Table 3. More recent non cation ordered leucite Phase transitions. $CsBSi_2O_6$ + ***(80)***has an amorphous glass phase at ambient temperature, an unknown Primitive orthorhombic phase crystallises out at 1073K and then an *Ia*-3*d* cubic phase forms at 1273K. $KBSi_2O_6$ ++ ***(69)***shows two phase transitions; *I*-43*d* to $P2_1/a$ at 573K and $P2_1/a$ to *Ia*-3*d* at 823K, the $P2_1/a$ structure at 573K is similar to another ambient temperature structure ***(68)***.

Figure 11 shows variation of lattice parameters for tetragonal to cubic phase transitions. Figure 12 shows the crystal structure of $RbAlSi_2O_6$. It has the $I4_1/a$ leucite structure but with a smaller c/a ratio than $KAlSi_2O_6$ ***(78)***.

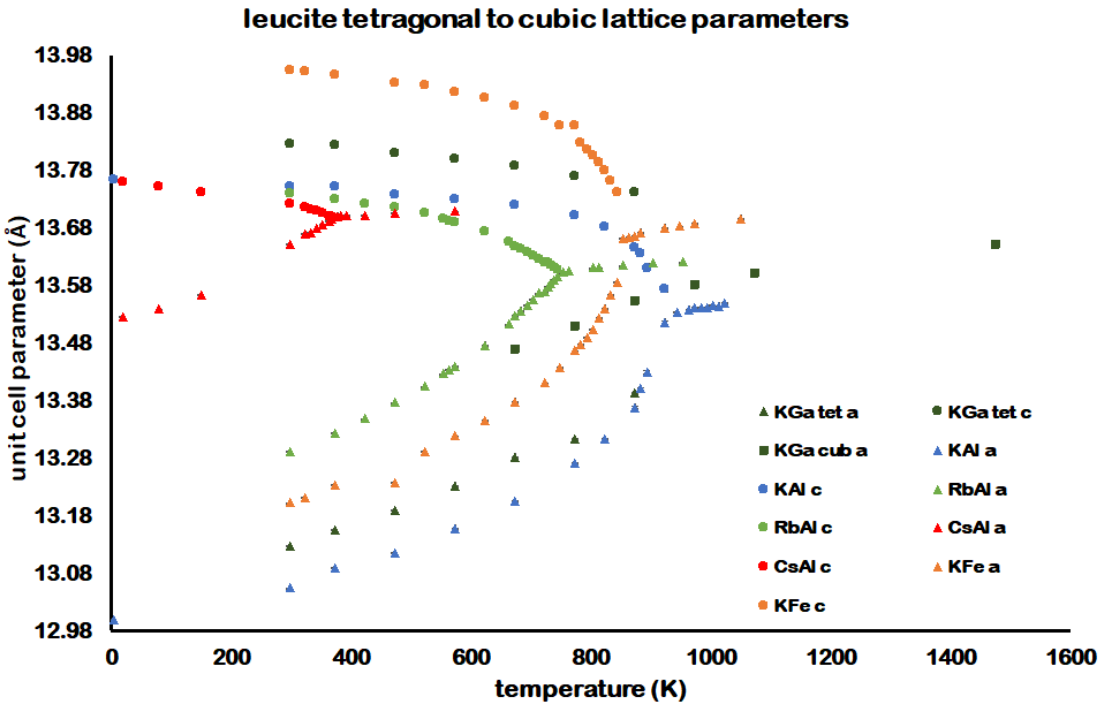

Figure 11, variation of lattice parameters for tetragonal to cubic phase transitions. KGa = $KGaSi_2O_6$, KAl = $KAlSi_2O_6$, RbAl = $RbAlSi_2O_6$, CsAl = $CsAlSi_2O_6$, KFe = $KFeSi_2O_6$.

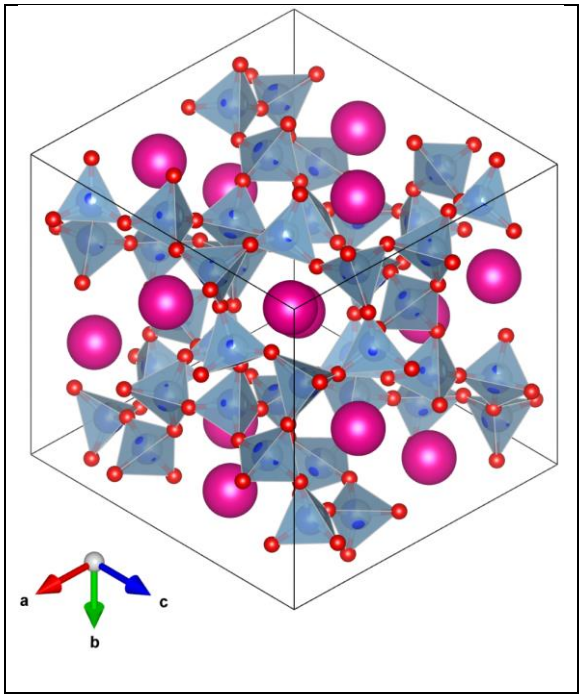

Figure 12. $I4_1/a$ tetragonal crystal structure of $RbAlSi_2O_6$ leucite. Mauve spheres show Rb^+ cations, red spheres show O^{2-}anions. Grey tetrahedra show $(Si/Al)O_4$ units. $RbAlSi_2O_6$ is isostructural with $KAlSi_2O_6$ but has a smaller c/a ratio.

5.3 Cation ordered leucite phase transitions

One year after the publication of the details of the new $P2_1/c$ ***(52, 53)*** and *Pbca* ***(59)*** leucite structures, a paper was published ***(87)*** showing how these two structures are related. A high temperature X-ray powder diffraction study on $K_2MgSi_5O_{12}$ showed the ambient temperature structure ***(52, 53)*** undergoes a phase transition to a *Pbca* structure at 622K. This *Pbca* structure is isostructural with the $Cs_2CdSi_5O_{12}$ structure ***(59)***. A similar $P2_1/c$ to *Pbca* phase transition is observed for $K_2ZnSi_5O_{12}$ over the range 848-863K ***(55)***. Figure 13 shows how the lattice parameters vary for these two monoclinic to orthorhombic phase transitions.

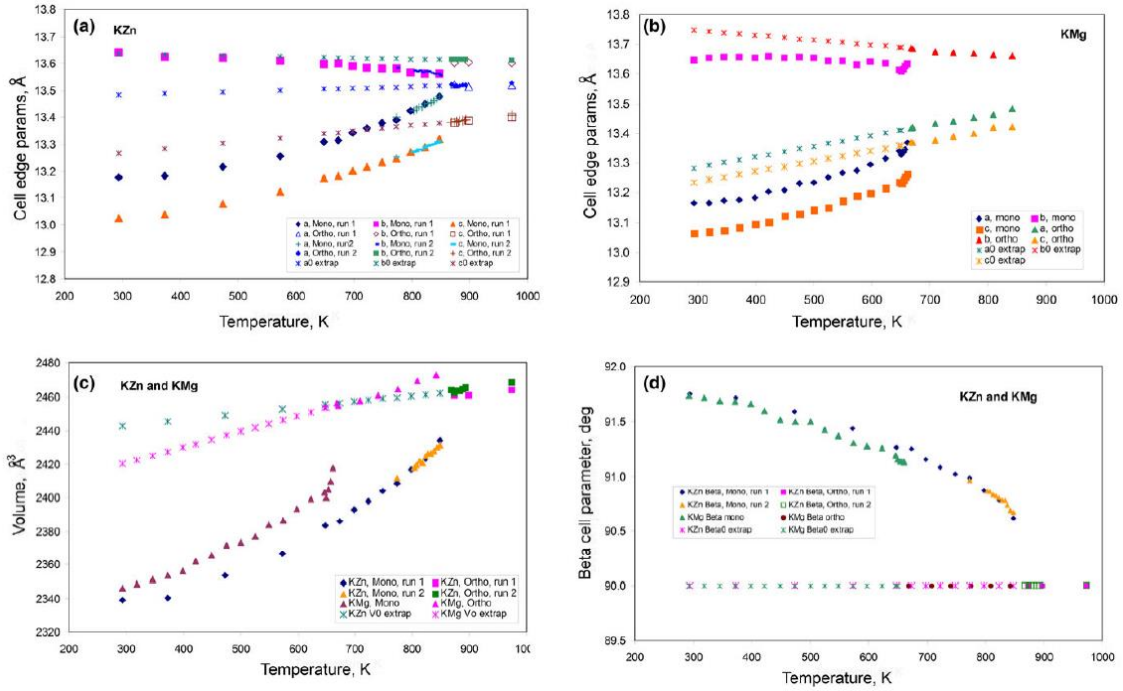

Figure 13, variation of lattice parameters on heating for $K_2MgSi_5O_{12}$ (KMg ***(87)***) and $K_2ZnSi_5O_{12}$ (KZn ***(55)***). Figure from ***(55)***.

A high temperature synchrotron X-ray powder diffraction study on $Cs_2CuSi_5O_{12}$ ***(62, 88)*** shows that the ambient temperature *Pbca* structure is retained but there is a first-order phase transition to a less collapsed *Pbca* structure with a larger unit-cell volume at ~333 K. Figure 14 shows the variation in lattice parameters for $Cs_2CuSi_5O_{12}$ leucite on heating***(62)***.

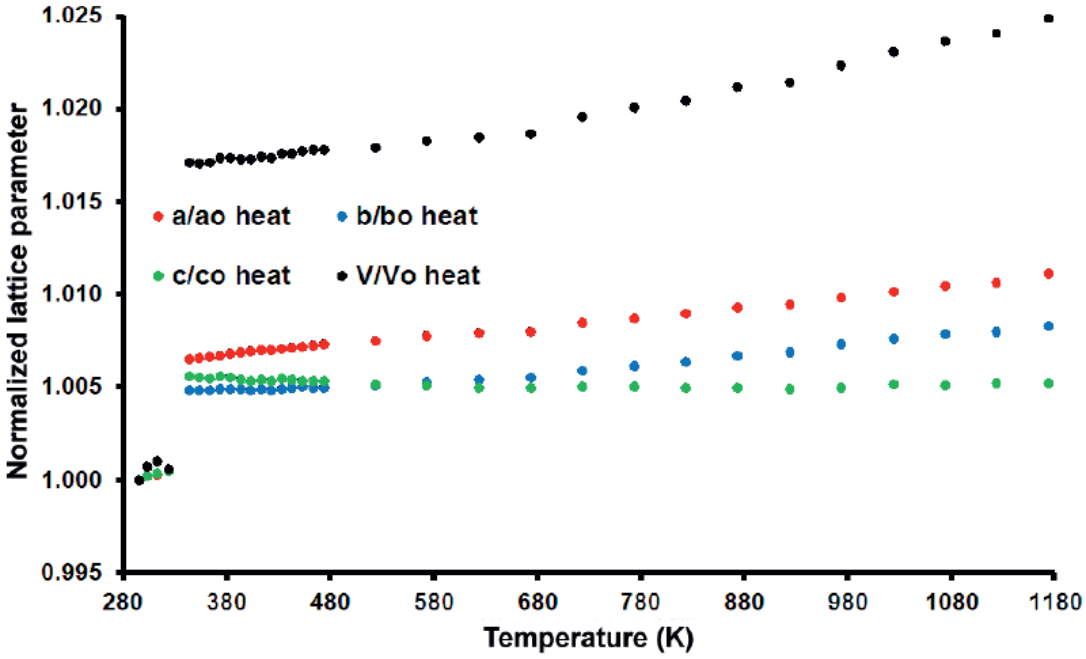

Figure 14 Variation in lattice parameters for $Cs_2CuSi_5O_{12}$ leucite on heating, lattice parameters are normalised to those at 295K, note the change in normalised parameters at ~333K.

A similar high temperature synchrotron X-ray powder diffraction study on $Cs_2ZnSi_5O_{12}$ ***(62)*** shows a phase transition from cation-ordered *Pbca* orthorhombic to a previously unknown *Pa*-3 cubic structure at 566K on heating. This transition is reversible on cooling with a transition at 633K. This *Pa*-3 structure has some partial T-site cation disorder. Figure 15 ***(62)***shows the variation of $Cs_2ZnSi_5O_{12}$ lattice parameters on heating and cooling.

There is another *Pbca* to *Pa*-3 transition at 457K on heating the $Rb_2CoSi_5O_{12}$ leucite analogue ***(89)***. These are the first known phase transitions in leucite structures from complete cation ordering to partial cation disorder. Figures 16ab shows the changes in crystal structure either side of the phase transition. Figure 17 ***(89)*** shows the variation of lattice parameters for $Rb_2CoSi_5O_{12}$ leucites with temperature.

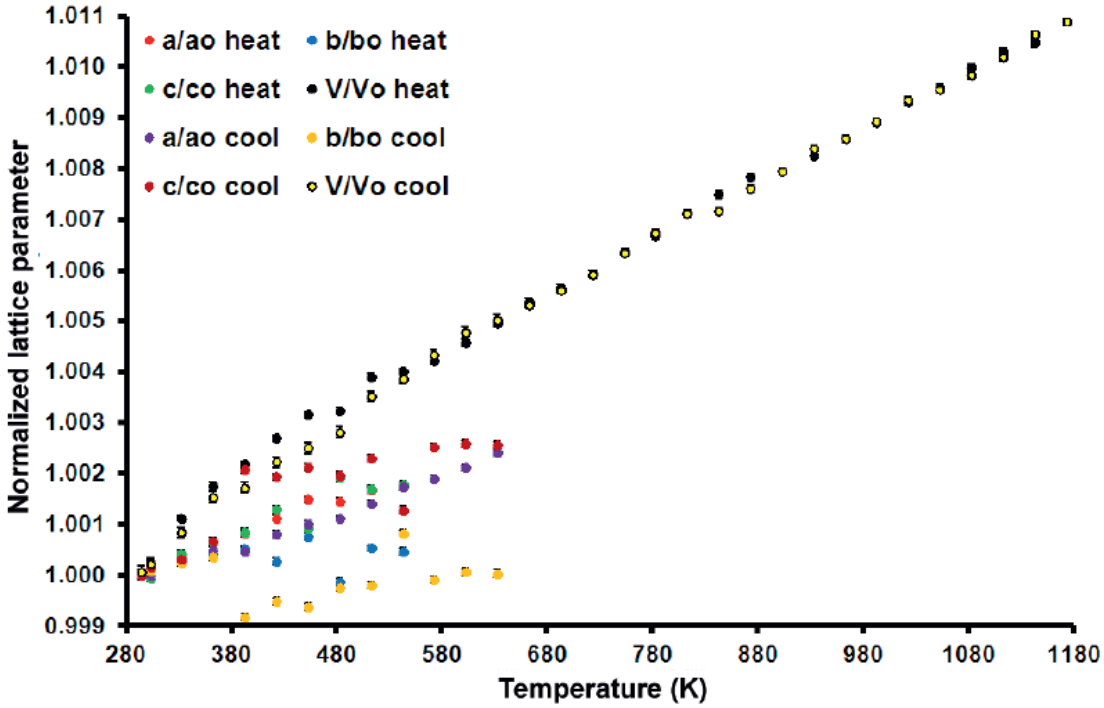

Figure 15 ***(62)***Variation in unit cell volumes and orthorhombic lattice parameters for $Cs_2ZnSi_5O_{12}$ leucite on heating and cooling, lattice parameters are normalised to those at 295K.

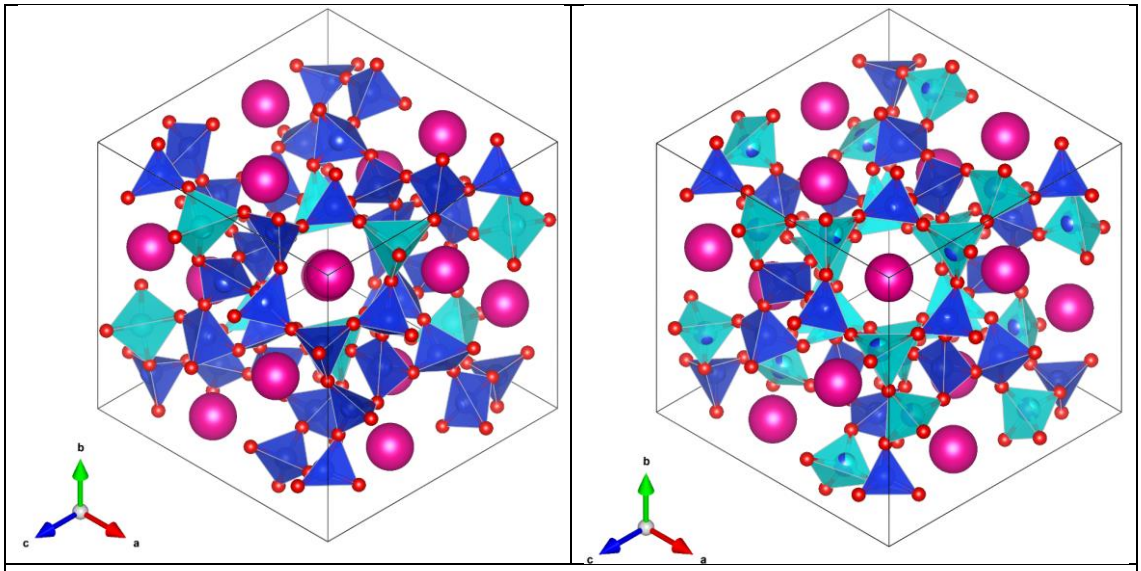

Figures 16a (left) and 16b (right). Plots of crystal structures for $Rb_2CoSi_5O_{12}$. Left structure is for *Pbca* orthorhombic cation ordered $Rb_2CoSi_5O_{12}$ at 447K. Right is for *Pa*-3 cubic partially cation disordered $Rb_2CoSi_5O_{12}$ at 457K. SiO_4 units are shown in

blue, CoO_4 and (Si/CoO_4) units are shown in pale blue. Mauve spheres show Rb^+ cations, red spheres show O^{2-}anions. Note how cubic structure is less distorted than orthorhombic structure.

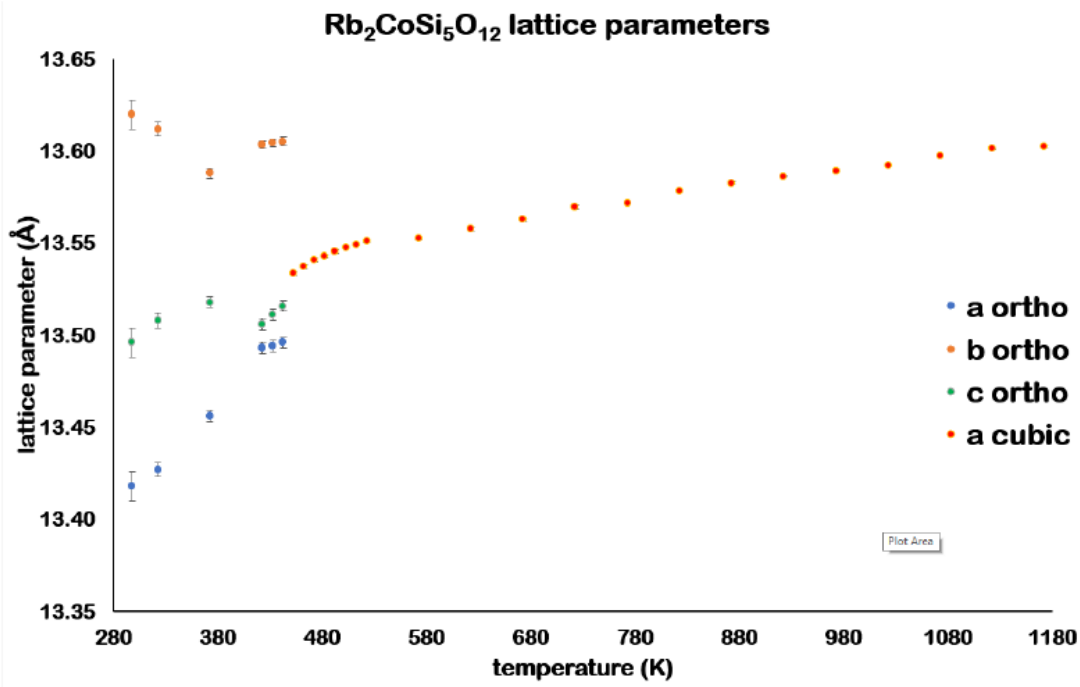

Figure 17 Variation of lattice parameters on heating for $Rb_2CoSi_5O_{12}$.

An X-ray powder diffraction study on Eu-doped $Cs_2ZnSi_5O_{12}$ shows an ambient temperature *Pa*-3 cubic structure ***(90)*** with a cubic lattice parameter a= 13.6582(1)Å.

Low temperature phase transitions from $I4_1/acd$ to *Ia*-3*d* cation have been observed for $CsAlSi_2O_6$ and $Cs_{0.9}Al_{0.9}Si_{2.1}O_6$ ***(31, 75)***. These are the first leucite phase transitions changing from completely cation ordered to completely cation disordered structures.

Table 4 shows details of the phase transitions in cation-ordered leucites.

Stoichiometry	LTSG	HTSG	TT (K)	Ref
$CsAlSi_2O_6$	$I4_1/acd$	*Ia*-3*d*	248	***(31, 75)***

$Cs_{0.9}Al_{0.9}Si_{2.1}O_6$	$I4_1/acd$	Ia-3d	173	***(75)***
$Cs_2ZnSi_5O_{12}$	*Pbca*	*Pa*-3	573 (heat) 633 (cool)	***(62)***
$K_2MgSi_5O_{12}$	$P2_1/c$	*Pbca*	622	***(87)***
$K_2ZnSi_5O_{12}$	$P2_1/c$	*Pbca*	848−863	***(55)***
$Cs_2CuSi_5O_{12}$	*Pbca*	*Pbca*	333	***(62, 88)***
$Rb_2CoSi_5O_{12}$	*Pbca*	*Pa*-3	457	***(89)***

Table 4. Phase transitions, cation-ordered leucites. LTSG = low temperature space group, HTSG = high temperature space group, TT = transition temperature.

5.4 Pressure induced leucite phase transitions

The symmetry of the crystal structures of leucite analogues is dependent on the size of the extraframework cation. The smaller the cation size then the more the framework structure can collapse ***(36)***, which can cause the symmetry of the crystal structure to be reduced. $CsAlSi_2O_6$ pollucite has an ambient temperature Ia-3d crystal structure. However, replacing Cs by K gives $KAlSi_2O_6$, which has a lower symmetry ambient temperature $I4_1/a$ tetragonal crystal structure.

Another way of collapsing a framework structure is the application of pressure. High pressure X-ray diffraction studies on natural mineral samples of leucite, pollucite and analcime, all show first-order phase transitions from Ia-3d cubic or $I4_1/a$ tetragonal to P-1 triclinic structures, see Table 5. Figure 18 shows how the unit cell volumes vary with increasing pressure. All Gatta et al ***(91-93)*** phase transitions were noticed at ambient temperature. Choi et al ***(94)*** noticed a phase transition in pollucite to P-1

triclinic at 1.3(1)GPa and 373K. After further compression to 4.1(1)GPa and at 523K, a new hexagonal phase with a hexacelsian framework is formed.

Phase	APSG	HPSG	TP (GPa)	Ref
Leucite	$I4_1/a$	*P*-1	2.4(2)	***(91)***
Pollucite	*Ia*-3*d*	*P*-1	0.79(3)	***(92)***
Pollucite	*Ia*-3*d*	*P*-1	1.3(1)	***(94)***
Analcime	*Ia*-3*d*	*P*-1	1.08(5)	***(93)***

Table 5. Details of high-pressure phase transitions in natural leucite $((K_{15.17}Na_{0.42})\Sigma=15.59(Fe^{3+}_{0.162}Ti_{0.03}Al_{15.86}Si_{32.04})\Sigma=48.11O_{96})$, pollucite $((Cs_{10.976}Rb_{0.352}K_{0.064}Na_{1.824})\Sigma=13.216(Al_{12.304}Si_{35.472})\Sigma=47.776O_{96}\cdot 3.79H_2O$ ***(92)***, $Cs_{2.1(1)}Na_{0.3(1)}Rb_{0.1(1)}Al_{2.4(1)}Si_{6.1(1)}O_{16}$ ***(94)***) and analcime $((Na_{0.887}K_{0.001}Ca_{0.001})(Al_{0.905}Si_{2.102})O_6\cdot 0.994H_2O)$ samples. APSG = ambient pressure space group, HPSG = high pressure space group, TP = transition pressure.

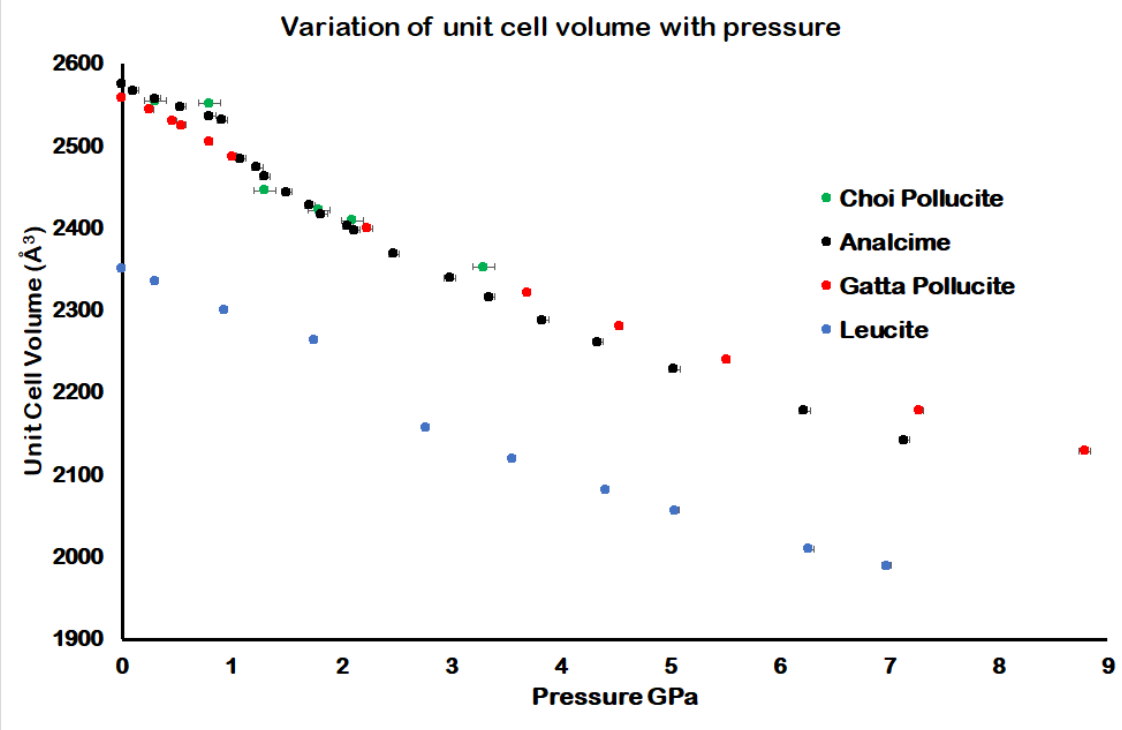

Figure 18. Variation of unit cell volumes with pressure for phase transitions in natural leucite, pollucite and analcime samples.

4. Ge leucites.

This paper has referred to many analogues of $KAlSi_2O_6$ leucite in which the extraframework K cation in these silicate framework structures can be replaced by other monovalent cations. The framework Al cation can also be replaced by other divalent and trivalent cations. However, it is also possible to synthesise ACX_2O_6 and $A_2BX_5O_{12}$ leucite analogues where X = Ge. In these analogues Si has been replaced by Ge, another quadrivalent element directly below Si in Group 14 of the Periodic Table. These Ge-leucites have the general formulae $ACGe_2O_6$ and $A_2BGe_5O_{12}$, many of these Ge-leucites were synthesised by the research group of Professor West. Tables S7a and S7b show lattice parameters for $ACGe_2O_6$ and $A_2BGe_5O_{12}$.

Ge^{4+} (4 coordinate crystal 0.53Å) has a larger ionic radius [32] compared to Si^{4+} (4 coordinate crystal ionic radius 0.40Å), *I*-43*d* is most common space group for the crystal structures for Ge-leucites instead of the highest symmetry cubic space group *Ia*-3*d*, which is one of the most common space groups for silicon containing leucites. As Ge is larger than Si therefore a germanate framework structure will contain larger pores than a corresponding silicate framework. Therefore, it will take larger cation sizes to prevent even a partial collapse of the germanate framework from *Ia*-3*d* cubic. The only Ge-leucite with the *Ia*-3*d* structure is $CsCdGe_2O_6$ ***(95)***, the larger Cs extraframework and Cd framework cations prevent framework collapse from *Ia*-3*d* to *I*-43*d*. All known Ge-leucite crystal structures have disordered T-sites.

Figures 19ab show the crystal structures for $KAlGe_2O_6$ and $CsAlGe_2O_6$ ***(96)***, these are the structures for the Ge analogues of leucite and pollucite, as was observed in the silicate analogues the $KAlGe_2O_6$ structure is more distorted than that for $CsAlGe_2O_6$

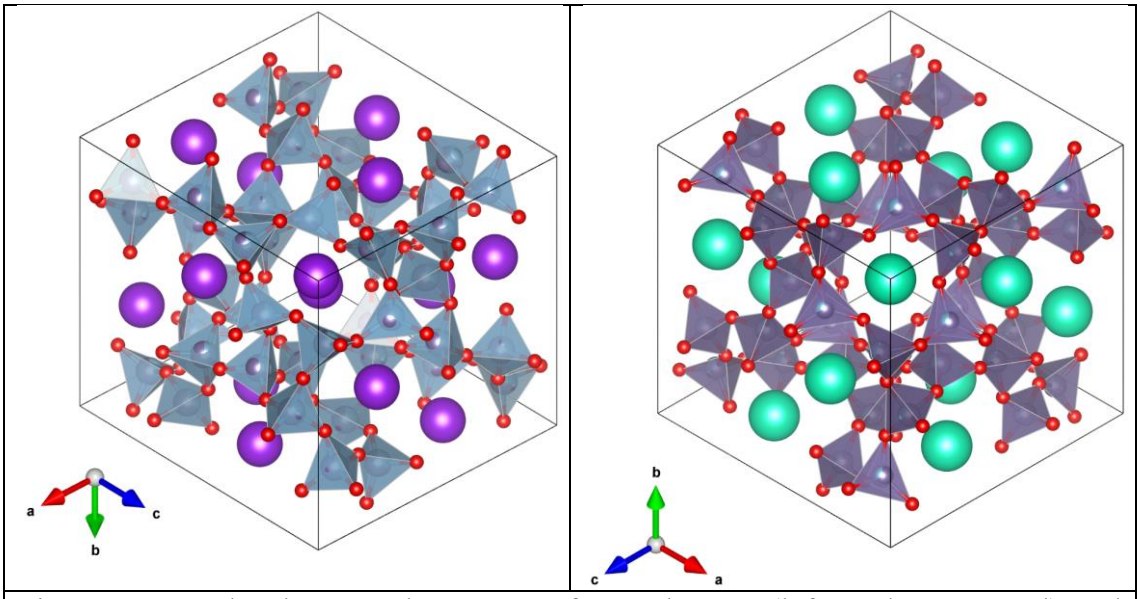

Figures 19a and 19b. Crystal structures for $KAlGe_2O_6$ (left, $I4_1/a$ tetragonal) and $CsAlGe_2O_6$ (right, I-43d cubic). Grey tetrahedra are (Ge/AlO_4) units, purple spheres are K^+ cations, turquoise spheres are Cs^+ cations and red spheres show O^{2-}anions.

5. Comparison of leucite structure types.

Ambient temperature and pressure crystal structures have been determined for leucite analogues in 8 different space groups. These crystal structures have differing degrees of cation ordering. Table 6 shows details of these different structure types. Figures 20a-h show plots of these different structure types, note how the silicate frameworks are becoming more collapsed with the lowering of the symmetry of the crystal structures, this is particularly apparent in the shape of the central 6-ring channel.

SG	Symmetry	T-sites	Example	Reference
Ia-3*d*	Cubic	D	$CsAlSi_2O_6$	***(30)***
I-43*d*	Cubic	D	$KBSi_2O_6$	***(97)***
Pa-3	Cubic	P	$Rb_2CoSi_5O_{12}$ +	***(89)***
$I4_1/acd$	Tetragonal	O	$K_{0.01}Cs_{1.02}B_{0.96}Si_{2.02}O_6$	***(67)***
$I4_1/a$	Tetragonal	D	$KAlSi_2O_6$	***(19)***
Pbca	Orthorhombic	O	$Cs_2CdSi_5O_{12}$	***(59)***
$P2_1/c$	Monoclinic	O	$K_2MgSi_5O_{12}$	***(52, 53)***
$P2_1/a$	Monoclinic	D	$KBSi_2O_6$ +	***(68, 69)***

Table 6. Different space groups with leucite structures. SG = space group, D = complete T-side disorder, O = complete T-side order, P = partial T-site order. + indicates a crystal structure determined at non-ambient temperature.

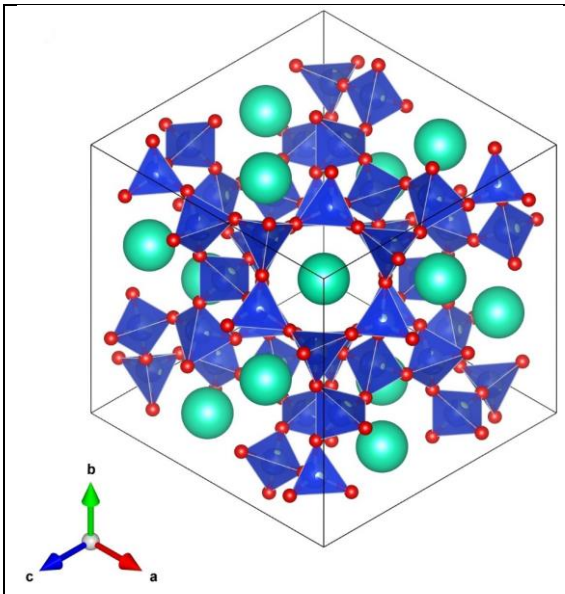	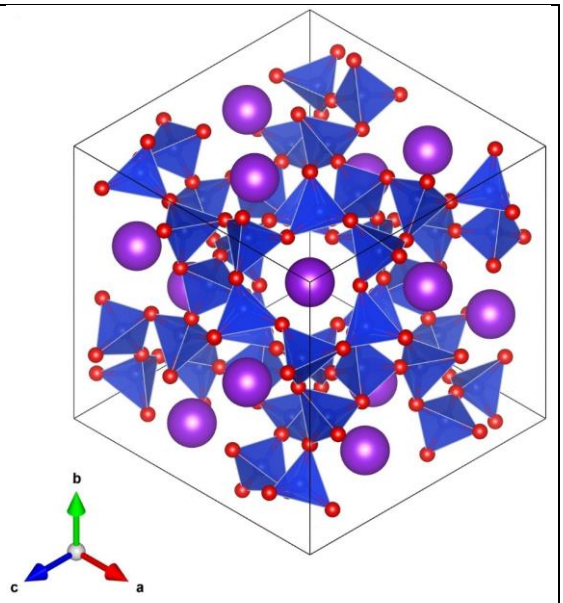
(a) *Ia*-3*d* $CsAlSi_2O_6$	(b) *I*-43*d* $KBSi_2O_6$
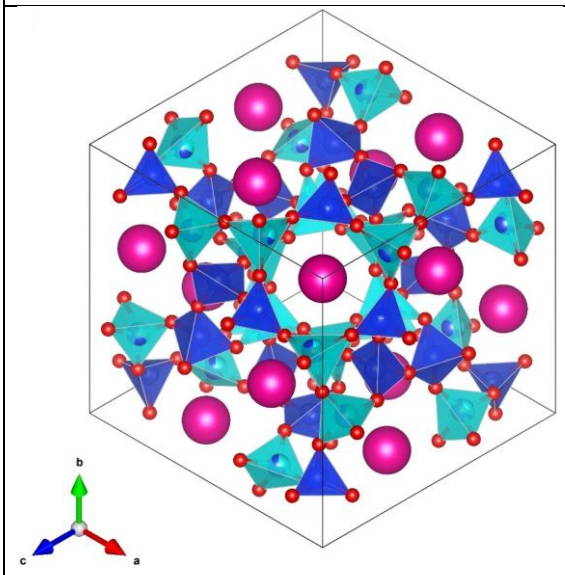	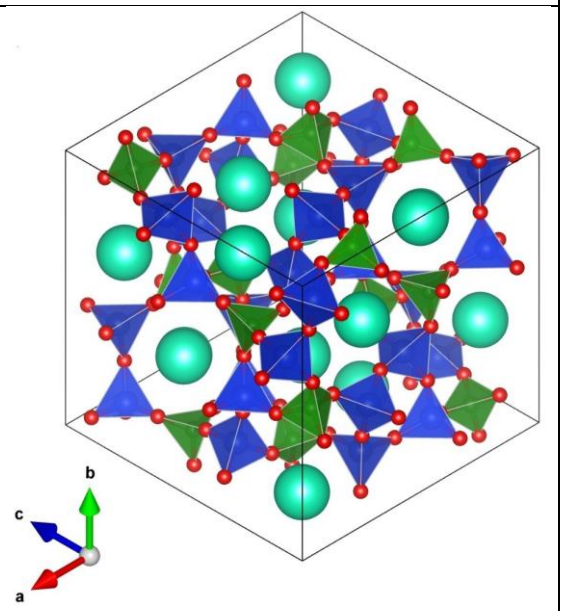
(c) *Pa*-3 $Rb_2CoSi_5O_{12}$	(d) $I4_1/acd$ $K_{0.01}Cs_{1.02}B_{0.96}Si_{2.02}O_6$

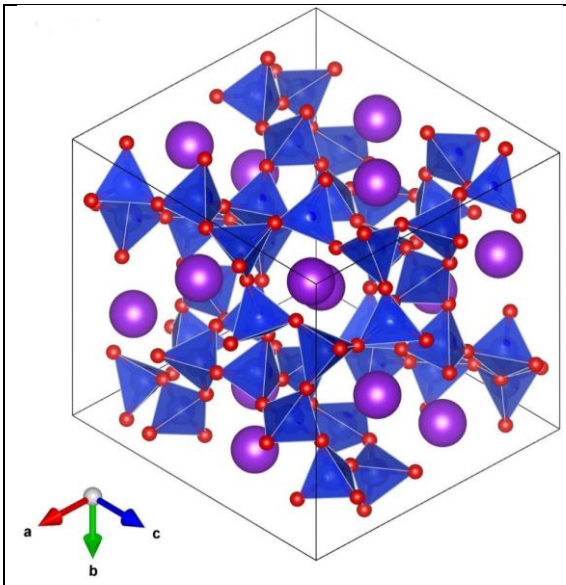

(e) $I4_1/a$ $KAlSi_2O_6$

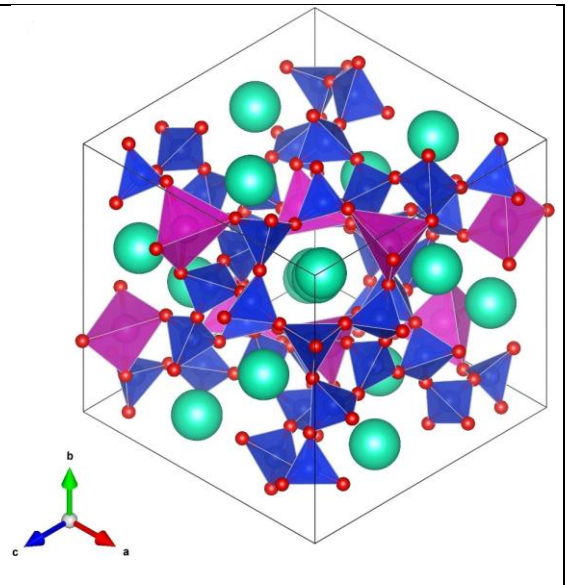

(f) *Pbca* $Cs_2CdSi_5O_{12}$

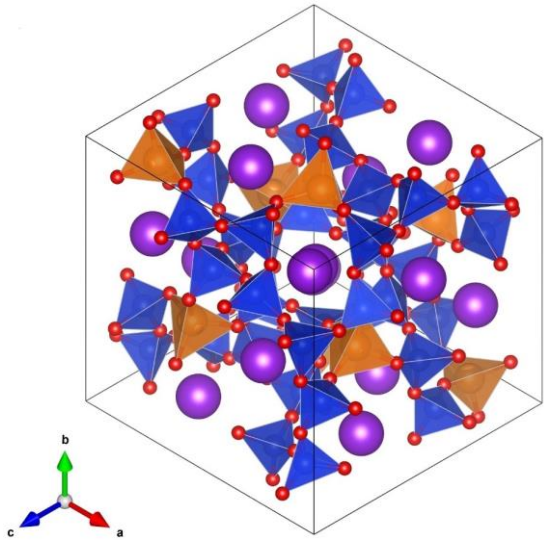

(g) $P2_1/c$ $K_2MgSi_5O_{12}$

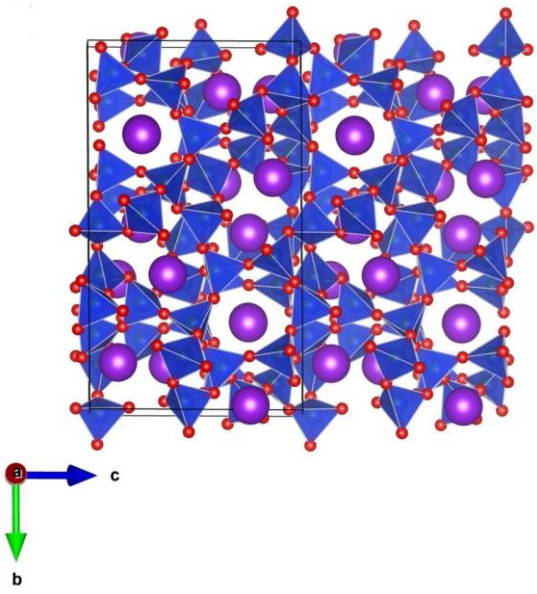

(h) $P2_1/a$ $KBSi_2O_6$

Figure 20. Plots showing the different leucite structure types:- Purple spheres represent K^+ cations, maroon spheres represent Rb^+ cations, turquoise spheres represent Cs^+ cations, red spheres represent O^{2-} anions. Blue tetrahedra represent ordered SiO_4 (c, d, f, g) or disordered (Si,*C*)O_4 units (a, b, e, h), where *C* is a trivalent cation. Light blue tetrahedra represent disordered (Si,Co)O_4 units (c). Green

tetrahedra represent ordered AlO_4 units (d). Pink tetrahedra represent ordered CdO_4 units (f). Orange tetrahedra represent ordered MgO_4 units (g).

All leucite structures have the same framework topology, for most structures the cube root of the unit cell volume is approximately 13.5Å. However, the $P2_1/a$ monoclinic structure of $KBSi_2O_6$ ***(68, 69)*** has a cube root of the unit cell volume which is very different from 13.5Å.

Figures 21a ($A_2BSi_5O_{12}$) and 21b ($ACSi_2O_6$), which show the cube root of the unit cell volume plotted against B^{2+} and C^{3+} crystal ionic radii ***(35)*** for A = K, Rb, Cs. Only the leucite structures with B = Be and C = B show average unit cell lengths significantly lower than about 13.5 Å. The small crystal ionic radii for Be and B mean that there will be a larger framework collapse ***(36)*** and consequently smaller unit cell volumes Errors in unit cell parameters are given on the y-axes, although these are sometimes too small to be seen on the plots.

Figures 21a and 21b show that the cube root of the unit cell volume tends to decrease with B^{2+} and C^{3+} crystal ionic radii. This is less apparent for the $K_2BSi_5O_{12}$ plot as these show cube root of the unit cell volumes for both Ia-3d cubic cation disordered and $P2_1/c$ monoclinic cation ordered structures, see Table 8.

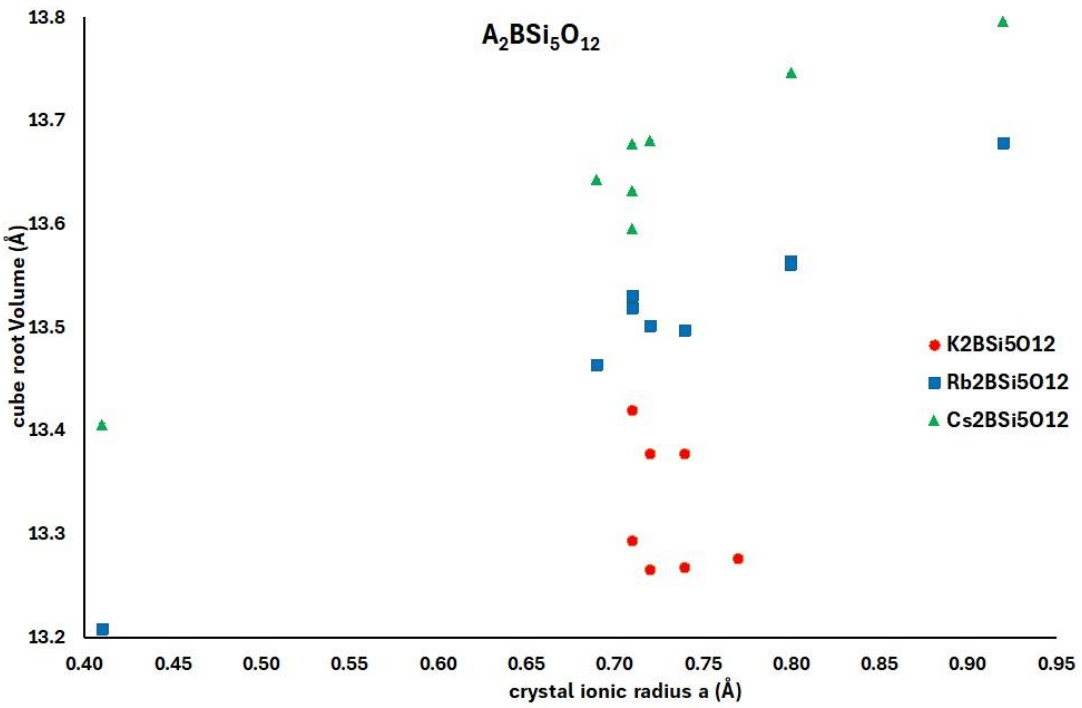

Figure 21a. Variation of the cube root of the unit cell volume with the B^{2+} crystal ionic radii for $A_2BSi_5O_{12}$ leucites (with only one monovalent A^+ cation). Ionic radii from Shannon ***(35)***.

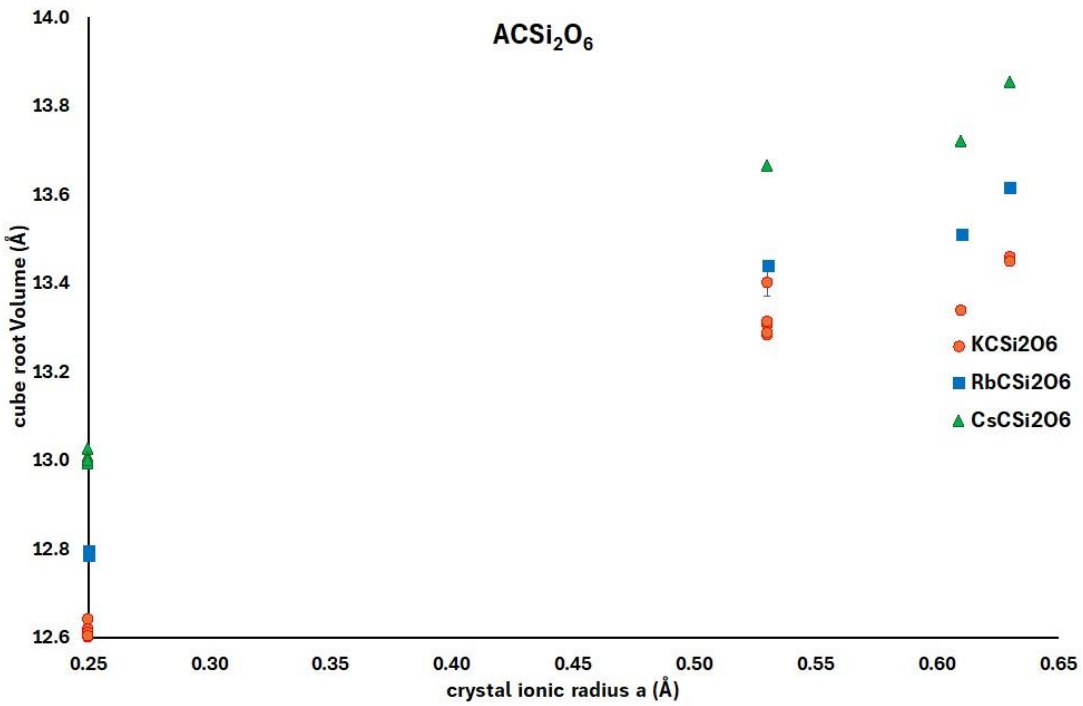

Figure 21b. Variation of the cube root of the unit cell volume with the C^{3+} crystal ionic radii for $ACSi_2O_6$ leucites (with only one monovalent A^+ cation). Ionic radii from Shannon ***(35)***.

Substitution of extraframework *A*, and framework *B* and *C* cations into the silicate framework structure will cause changes in the unit cell size due to different cation sizes ***(35)***. Incorporation of different *A*, *B* and *C* cations of different sizes will cause the unit cell to expand or contract. Only changes in extraframework *A* cations will cause changes in the degree of framework collapse ***(36)***. Ambient temperature cation ordered leucite structures with *A* = Rb and/or Cs collapse down to *Pbca* orthorhombic. However ambient temperature cation ordered leucite structures with *A* = K collapse down to $P2_1/c$ monoclinic, due to the *A* smaller cation size. As was discussed by Palmer

et al***(20)***, changing the size of the *B* and *C* framework cations will cause a change in the size of the unit cell but will have virtually no change on the degree of framework collapse.

However, it should be noticed for $ACSi_2O_6$, where *C* is the smallest trivalent boron cation (crystal ionic radius 0.25 Å these boroleucites have the body centred space group symmetry *I*-43*d*, instead of the usual body centred space group symmetry *Ia*-3*d*, see Table 6. The incorporation of this small boron cation into the silicate framework apparently changes the space group symmetry from the centrosymmetric *Ia*-3*d* to the noncentrosymmetric *I*-43*d*. Table 6 also shows that $CsGaSi_2O_6$ is also *I*-43*d* cubic, which doesn't follow the trend. It may be expected that this structure with such a large *C* cation as gallium would also be *Ia*-3*d*, similar to that for $CsAlSi_2O_6$ pollucite, possibly the space group for the $CsGaSi_2O_6$ structure refinement ***(50)*** was misassigned?

Figures 22a-l show how the incorporation of different *A* and *B* cations (in $A_2BSi_5O_{12}$) and *A* and *C* cations (in $ACSi_2O_6$) affects the unit cell size for ambient temperature structures with different space groups. These figures show how the *A*-O and *T*-O distance vary with unit cell size for leucite structures with the *Ia*-3*d* cubic, *I*-43*d* cubic, $I4_1/a$ tetragonal, *Pbca* orthorhombic and $P2_1/c$ monoclinic space groups. These figures have the a lattice parameter on the x-axes for cubic structures and the cube root of the unit cell volume on the x-axes for the lower symmetry structures.

Generally, the larger the *A*, *B* and *C* cations, the larger the unit cell size. There are more *A*-O and *T*-O distances for low symmetry crystal structures, and consequently a wider spread of distances, than for high symmetry crystal structures. If there are multiple crystal structures with the same *AB* or *AC* combinations, then these are plotted

with the same colour. Errors in unit cell parameters are given on the x-axes, although these are sometimes too small to be seen on the plots.

Table 7 shows how different combinations of extraframework, and framework cations affect the cube root of the unit cell volume for ambient temperature $A_2BSi_5O_{12}$ and $ACSi_2O_6$ leucite crystal structures. The sizes of both the extraframework *A*, and framework *B* or *C* cations will affect the unit cell size. Even though the ionic radius ***(35)***for Rb^+ is greater than that for K^+, the greater ionic radius for Fe^{3+} compared to Al^{3+} means that $KFeSi_2O_6$ has a larger unit cell size than $RbAlSi_2O_6$.

$A_2BSi_5O_{12}$ ambient temperature crystal structures.	
SG	*AB* combinations showing which combinations have the largest to smallest cube root of the unit cell volume.
Ia-3*d*	CsCu > RbMn > RbMg > RbZn > KMg > KZn ≈ KCo
Pbca	CsCd > RbCsCd > CsMn > CsMg > CsCo ≈ RbCd > CsNi > RbCsMg > CsCu > RbMn > RbCsNi > RbMg > RbCo > RbNi
$P2_1/c$	KMg > KFe > KZn > KCo
$ACSi_2O_6$ ambient temperature crystal structures.	
SG	*AC* combinations showing which combinations have the largest to smallest cube root of the unit cell volume.
Ia-3*d*	CsFe > CsAl > KAl > CsB
I-43*d*	CsGa > KCsB > RbB > KRbB > KB
$I4_1/a$	RbFe > RbGa > KFe > RbAl > KGa > KAl

Table 7. Relative unit cell sizes for $A_2BSi_5O_{12}$ and $ACSi_2O_6$ ambient temperature crystal structures for different combinations of *AB* and *AC* cations.

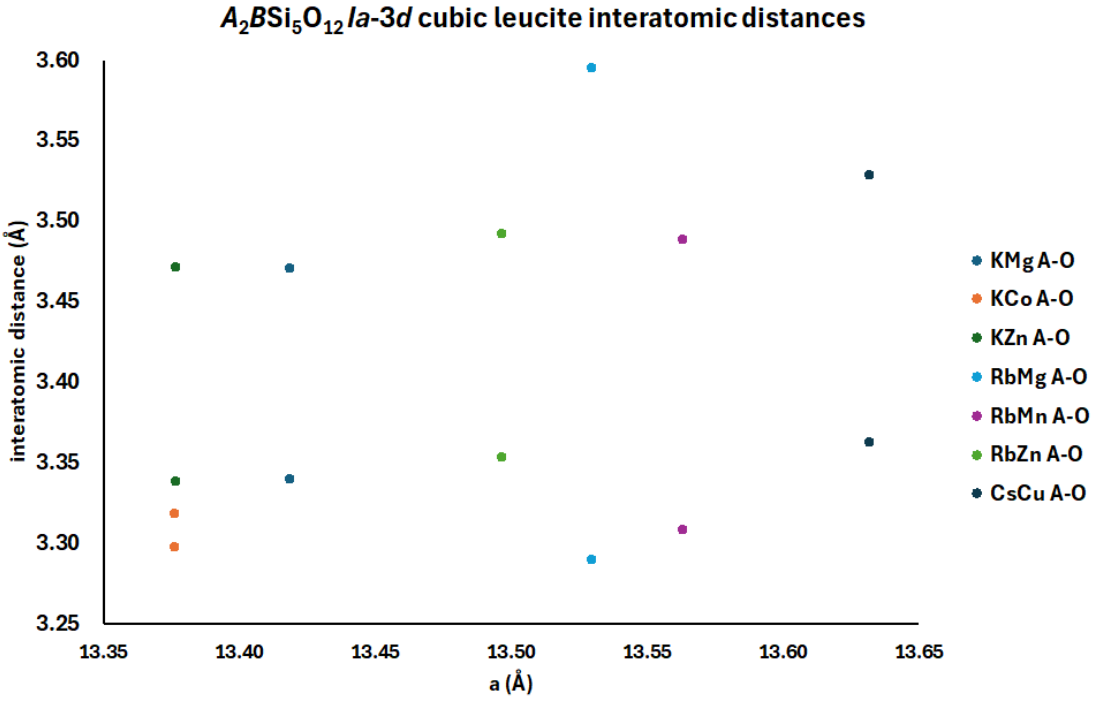

Figure 22a. Variation of *A*-O interatomic distances with unit cell size in different $A_2BSi_5O_{12}$ *Ia*-3*d* cubic leucites.

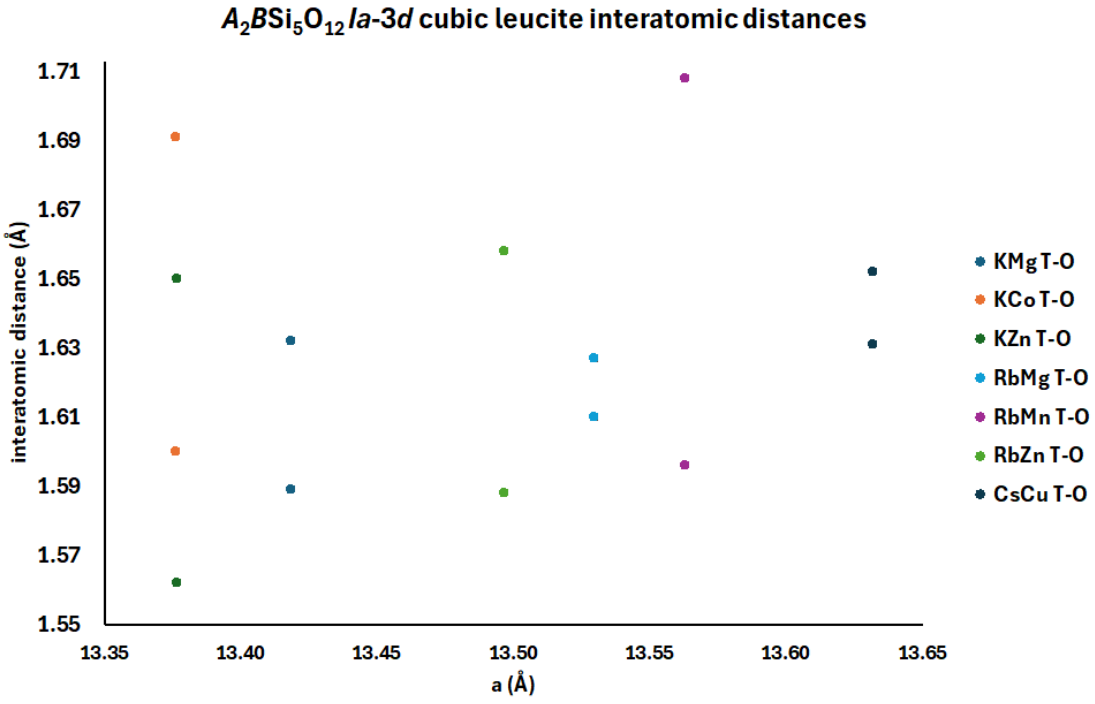

Figure 22b. Variation of *T*-O interatomic distances with unit cell size in different $A_2BSi_5O_{12}$ *Ia*-3*d* cubic leucites.

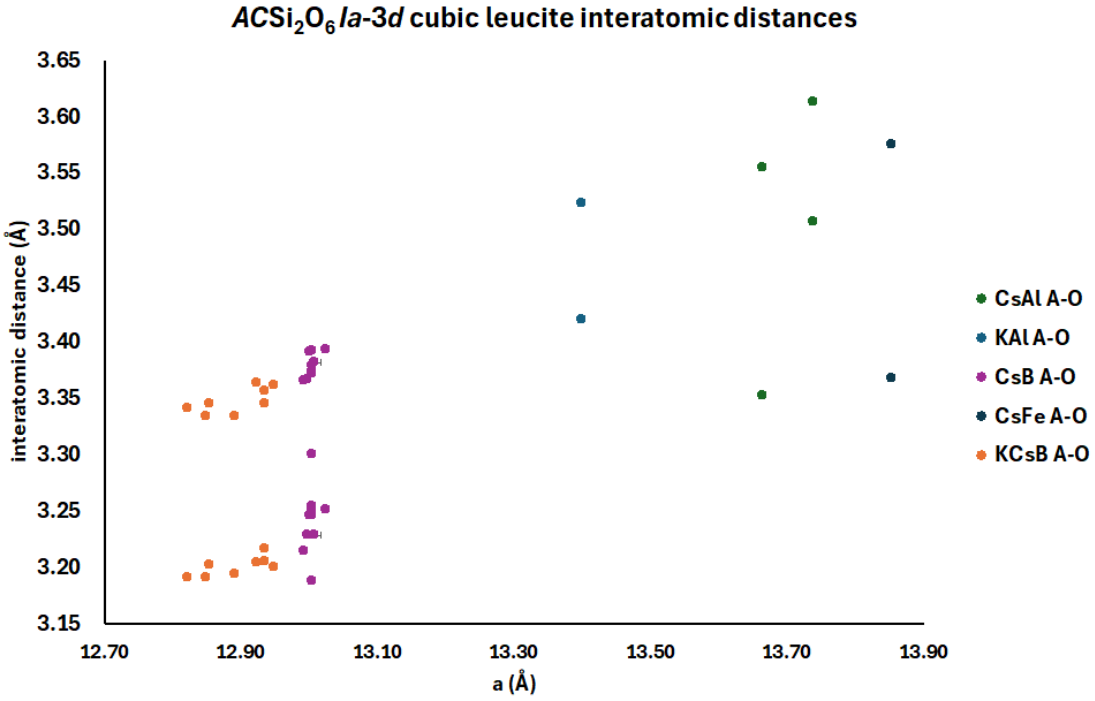

Figure 22c. Variation of *A*-O interatomic distances with unit cell size in different ACSi$_2$O$_6$ *Ia*-3*d* cubic leucites.

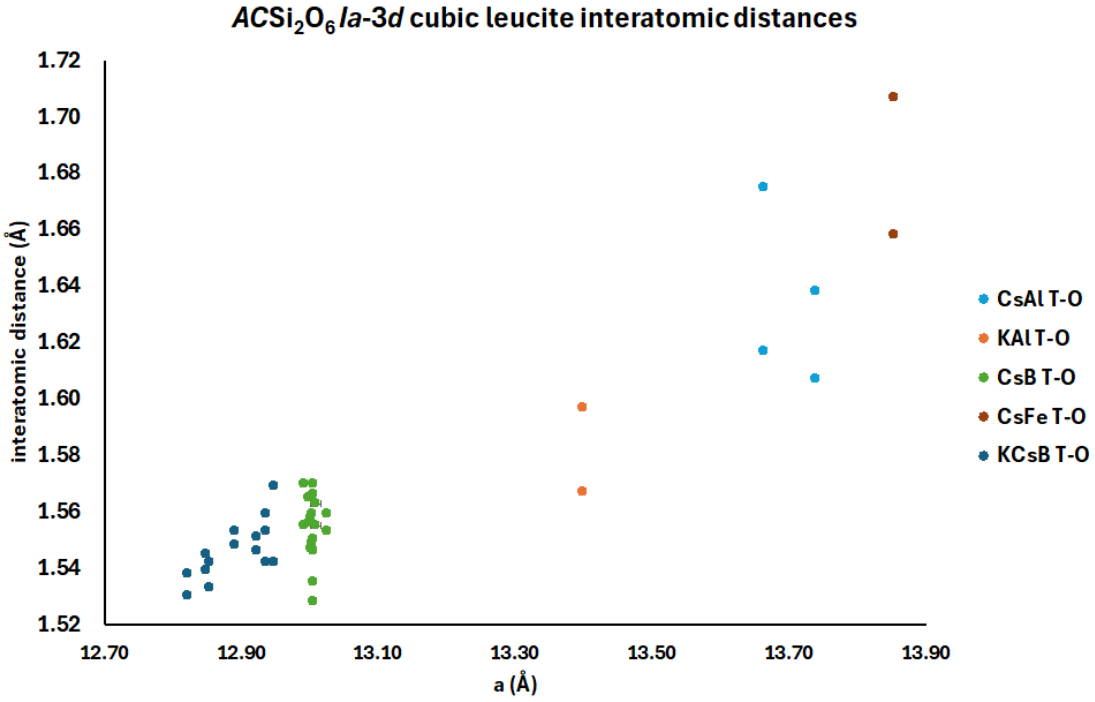

Figure 22d. Variation of *T*-O interatomic distances with unit cell size in different ACSi$_2$O$_6$ *Ia*-3*d* cubic leucites.

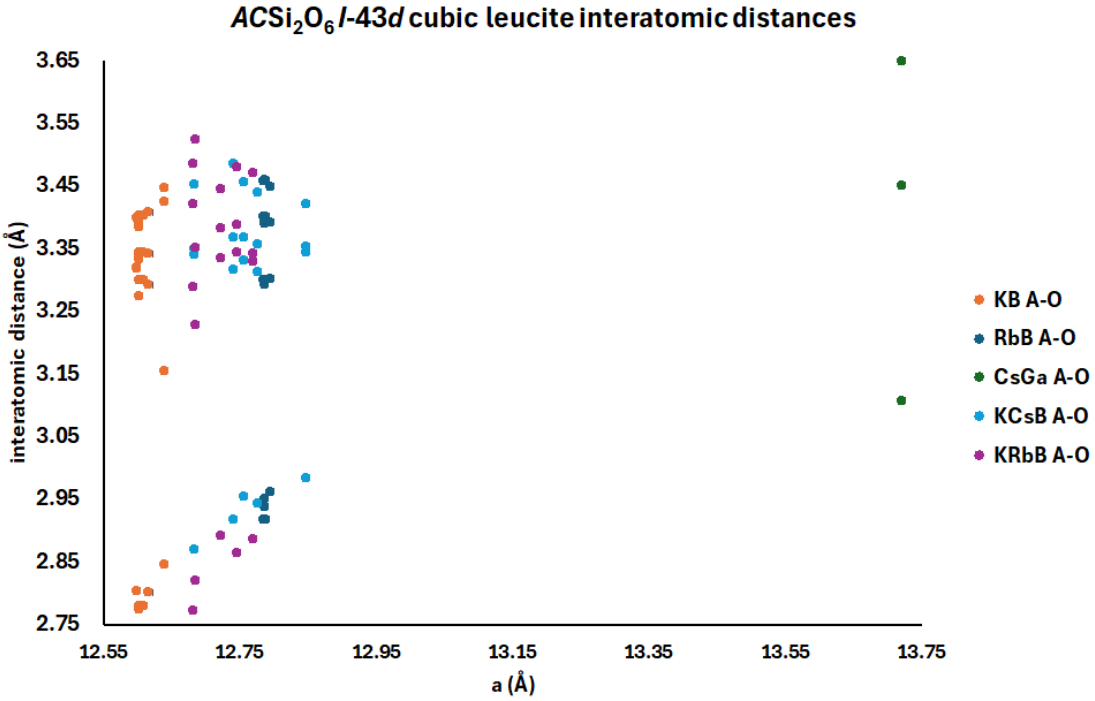

Figure 22e. Variation of *A*-O interatomic distances with unit cell size in different $ACSi_2O_6$ *I*-43*d* cubic leucites.

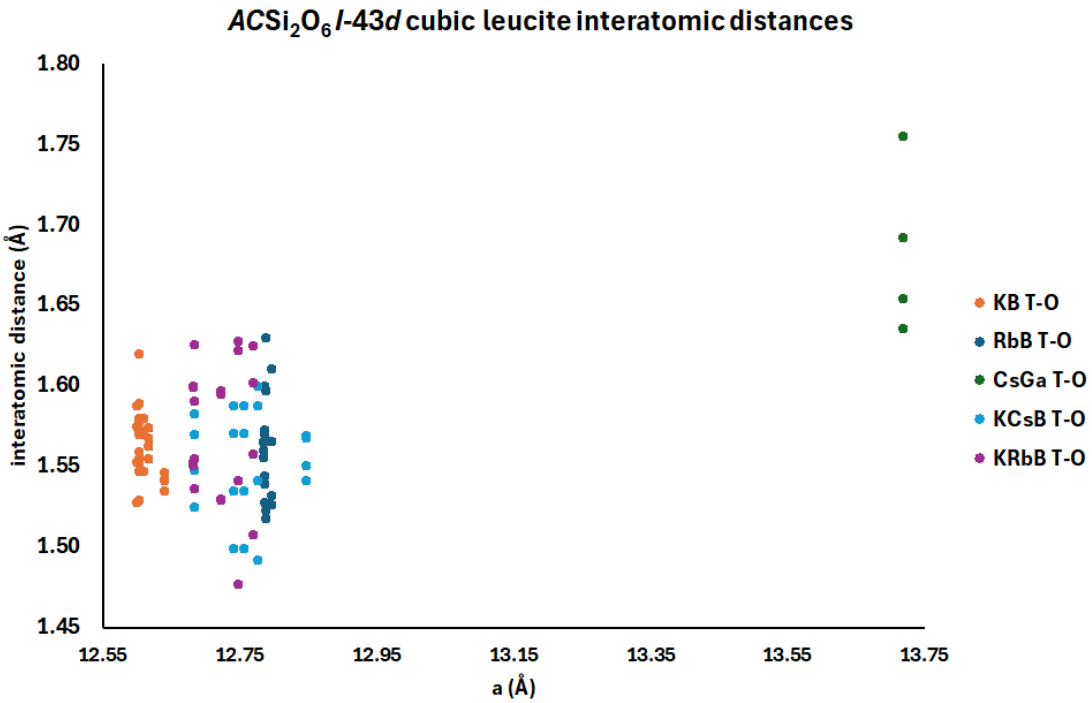

Figure 22f. Variation of *T*-O interatomic distances with unit cell size in different $ACSi_2O_6$ *I*-43*d* cubic leucites.

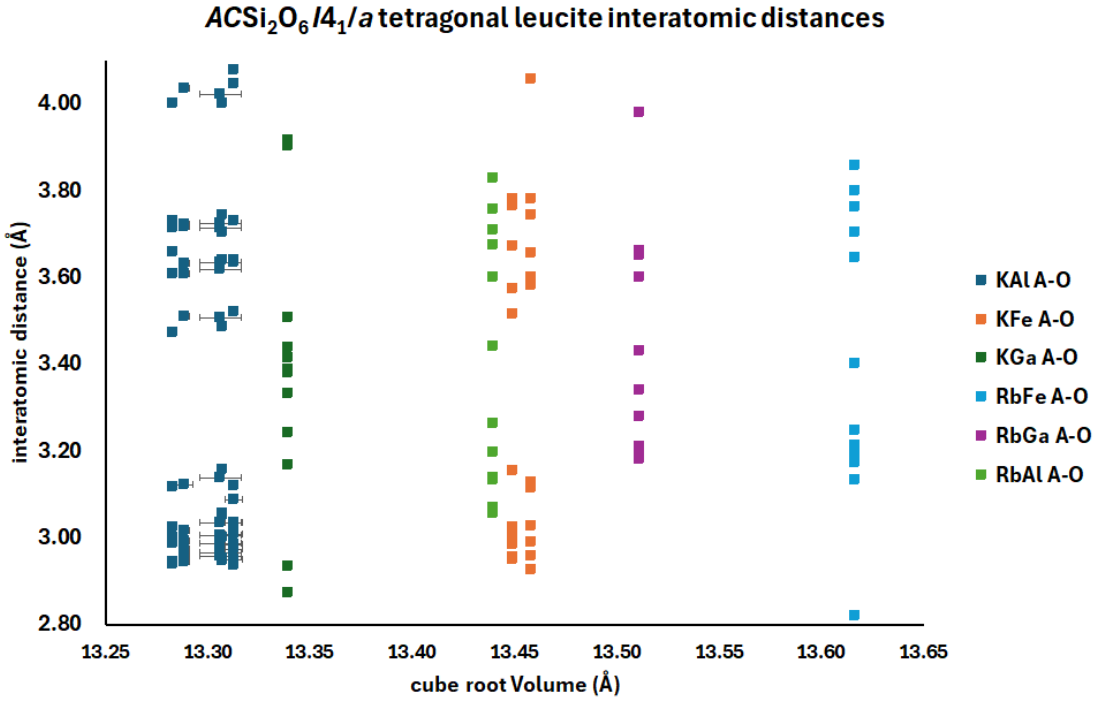

Figure 22g. Variation of *A*-O interatomic distances with unit cell size in different $ACSi_2O_6$ $I4_1/a$ tetragonal leucites.

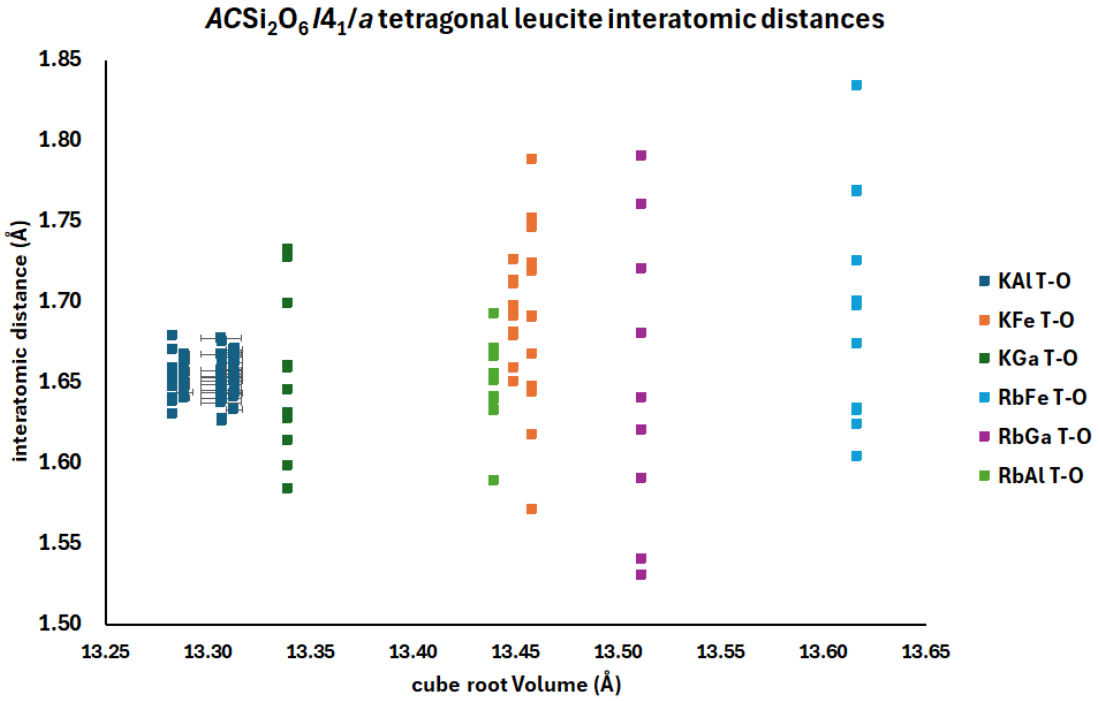

Figure 22h. Variation of *T*-O interatomic distances with unit cell size in different $ACSi_2O_6$ $I4_1/a$ tetragonal leucites.

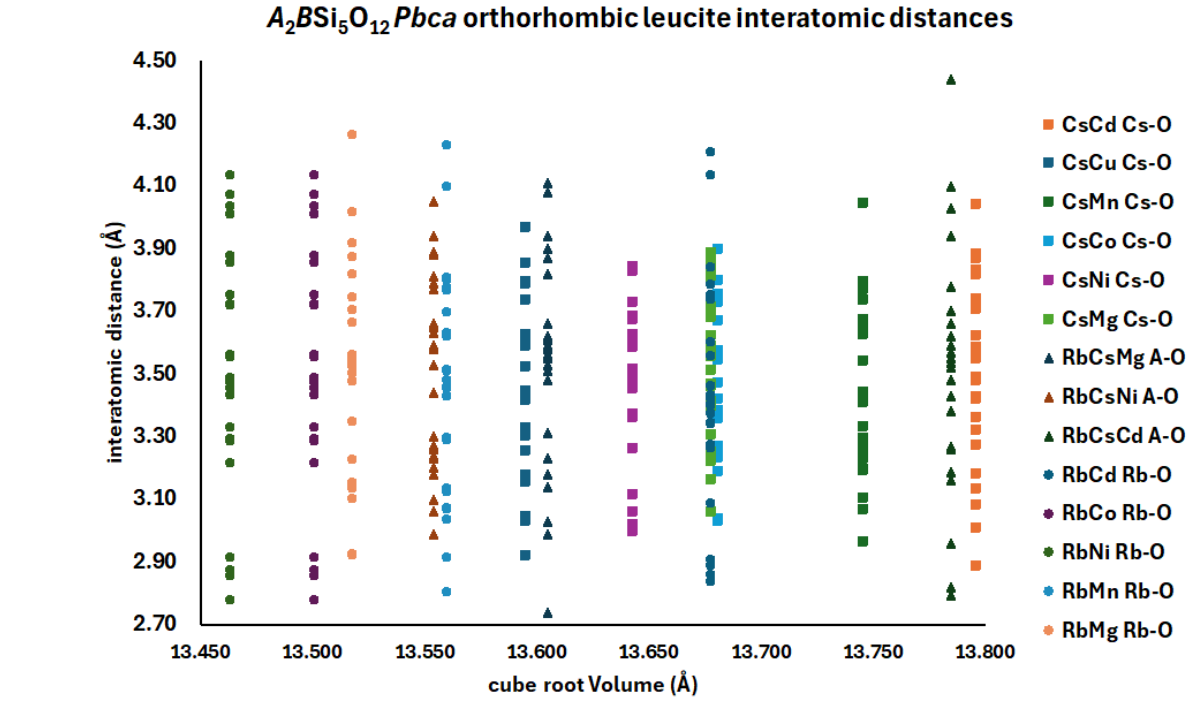

Figure 22i. Variation of *A*-O interatomic distances with unit cell size in different $A_2BSi_5O_{12}$ *Pbca* orthorhombic leucites.

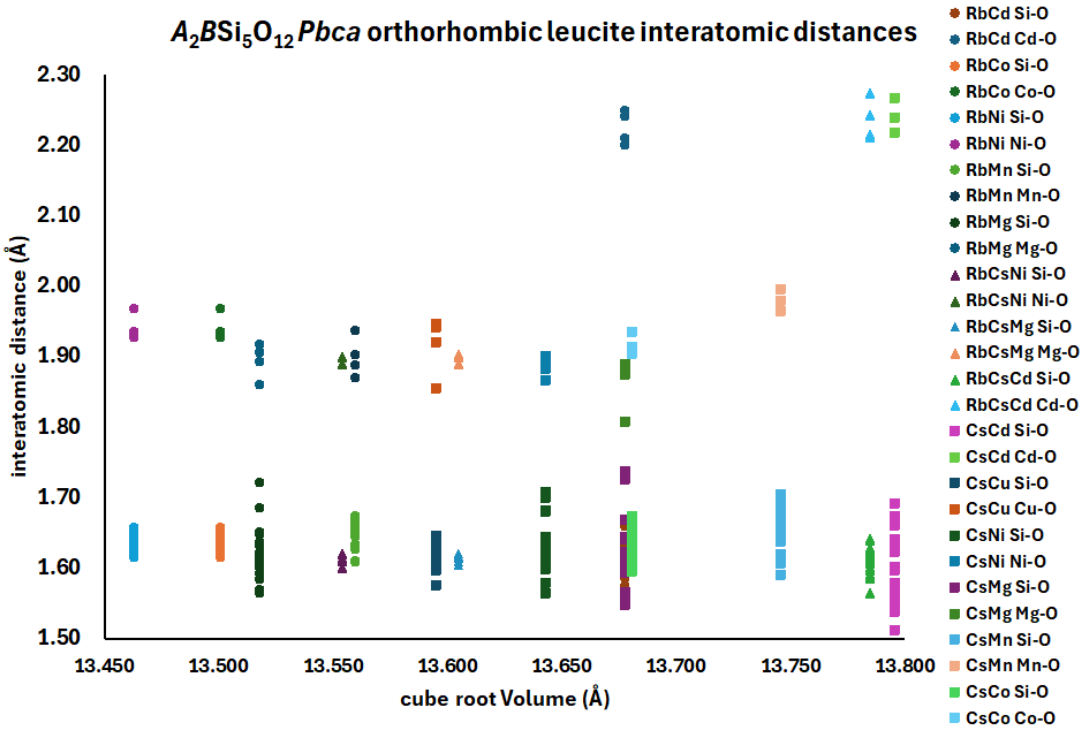

Figure 22j. Variation of *T*-O interatomic distances with unit cell size in different $A_2BSi_5O_{12}$ *Pbca* orthorhombic leucites.

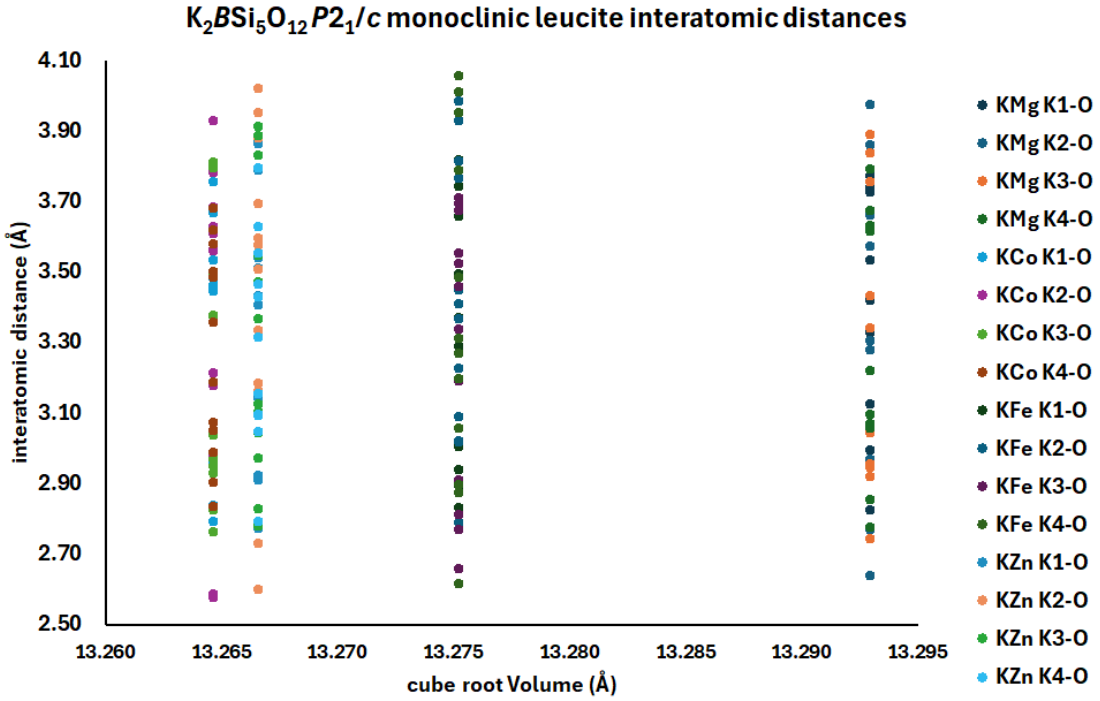

Figure 22k. Variation of *A*-O interatomic distances with unit cell size in different $A_2BSi_5O_{12}$ $P2_1/c$ monoclinic leucites

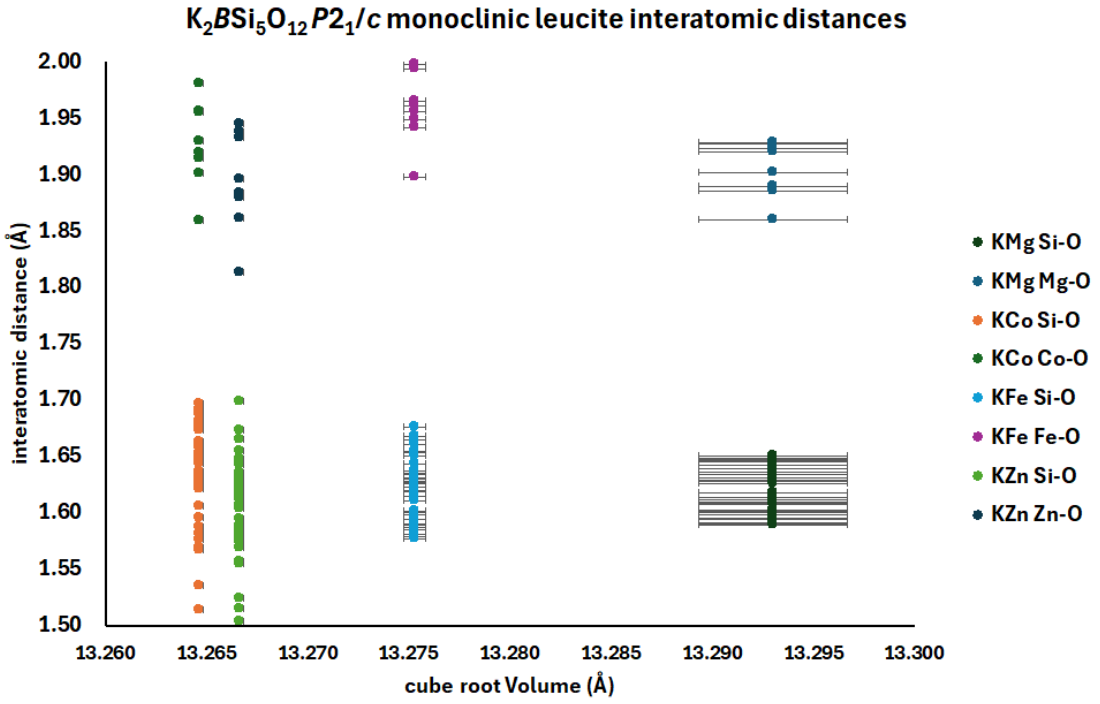

Figure 22k. Variation of *T*-O interatomic distances with unit cell size in different $A_2BSi_5O_{12}$ $P2_1/c$ monoclinic leucites.

Some $A_2BSi_5O_{12}$ leucite structures have both cation-disordered and cation-ordered structures with the same stoichiometry. Table 8 shows a comparison of the unit cell volumes for these cation-disordered and cation-ordered structures. Note that in each case the cation-ordered structures all have smaller unit cell volumes than the corresponding cation-disordered structures. The cation-ordered structures have more collapsed tetrahedral frameworks and hence smaller unit-cell volumes.

	Cation-disordered		Cation-ordered		
Stoichiometry	SG	V (Å^3)	SG	V (Å^3)	Ref.
$K_2MgSi_5O_{12}$	*Ia*-3*d*	2416.33(5)	*P*2$_1$/*c*	2348(2)	***(52, 53)***
$K_2CoSi_5O_{12}$	*Ia*-3*d*	2393.57(10)	*P*2$_1$/*c*	2333.96(4)	***(55)***
$K_2ZnSi_5O_{12}$	*Ia*-3*d*	2393.87(6)	*P*2$_1$/*c*	2334.98(6)	***(55)***
$Cs_2CuSi_5O_{12}$	*Ia*-3*d*	2533.4(2)	*Pbca*	2512.85(1)	***(65)***
$Rb_2MnSi_5O_{12}$	*Ia*-3*d*	2495.24(10)	*Pbca*	2493.5(3)	***(55)(98)***
$Rb_2MgSi_5O_{12}$	*Ia*-3*d*	2476.8(5)	*Pbca*	2470.6(4)	***(61, 99)***

Table 8. Comparison of unit cell volumes for cation-disordered and cation ordered leucite analogues with the same stoichiometries.

6. Future work.

Most leucite analogues studied have had stoichiometries $ACSi_2O_6$ and $A_2BSi_5O_{12}$ where A = K, Rb or Cs, only a few analogues with A = Tl or NH_4^+ have been studied so far. Analcime ion-exchange experiments ***(39)*** showed that monovalent Ag^+ could also be ion-exchanged into the leucite silicate framework, but there have been no A = Ag structural studies. A lot more work could be done with these non-alkali metal extraframework cations. Similarly, there are potentially a lot more $ACGe_2O_6$ and $A_2BGe_5O_{12}$ Ge-leucite analogues that could be synthesised, would it be possible to synthesise any cation-ordered Ge leucites? No non-ambient temperature work has been done on Ge-leucites, there may well be more phase transitions that could be discovered including some possible previously unknown cation ordered Ge-leucites?

Comparatively few leucites have been synthesised with more than one monovalent alkali metal cation. It would be interesting to see how having two or more extraframework alkali metal cations in the structure would affect the framework collapse and consequently the crystal structure symmetry. $K_2BSi_5O_{12}$ leucite analogues with cation ordering are all $P2_1/c$ monoclinic at ambient temperature. However, $Rb_2BSi_5O_{12}$ and $Cs_2BSi_5O_{12}$ cation ordered leucite analogues are all *Pbca* orthorhombic at ambient temperature. Would an $A_2BSi_5O_{12}$ analogue with both K and Rb extraframework cations have sufficient framework collapse to form a $P2_1/c$ monoclinic structure?

The only high-pressure studies done so far have all been on naturally occurring aluminosilicates, these all show first order phase transitions from high symmetry structures to P-1 triclinic, no intermediate structures are observed between these two

extremes. What phase transitions would be observed from lower-symmetry cation-ordered leucite structures under high pressure?

Phase transitions have been observed on heating leucite analogues with the following space-group changes; $I4_1/a$ to *Ia*-3*d*, *I*-43*d* to *Ia*-3*d, I*-43*d* to $P2_1/a$ to *Ia*-3*d*, $I4_1/acd$ to *Ia*-3*d*, unknown Primitive orthorhombic to *Ia*-3*d*, *Pbca* to *Pa*-3 and $P2_1/c$ to *Pbca*. Would there be further transitions from *Pa*-3 to body centred cubic structures on heating to higher temperatures resulting in the complete loss of cation ordering?

Most of the non-ambient temperature studies of leucite analogues have been done above ambient temperature. Would any low (below ambient) temperature studies show lowering of symmetry on cooling? Would *Pbca* go to $P2_1/c$? Would any cation disordered structures change to cation ordered?

Leucite analogues are of technological interest as possible hosts for radioactive Cs from nuclear waste. An *in-situ* synchrotron X-ray powder diffraction experiment showing the changes in crystal structure during the ion-exchange of one alkali metal cation with Cs^+ would be potentially very interesting.

Mössbauer spectroscopy, combined with non-ambient temperature synchrotron X-ray and neutron powder diffraction, has been used to study structural changes with temperature in iron oxides ***(100-102)***. An ambient temperature Mössbauer study has been done on Fe containing leucites ***(103)***. A combined Mössbauer and non-ambient temperature XRD study on Fe containing leucite analogues could give more information on phase transitions in these materials.

Most leucite structures have alkali metal (*A* = K, Rb, Cs) extraframework cations. The size differences of these cations affect the crystal structures. The larger sized cations result in higher symmetry structures ($KAlSi_2O_6$ and $RbAlSi_2O_6$ are both tetragonal, but $CsAlSi_2O_6$ is cubic). The radioactive alkali metal element **Francium** (Fr)

is one place below Cs in Group 1 of the Periodic Table, the element is analogous to Cs, it was discovered ***(104)*** by co-precipitating with Cs salts. However, Fr has a very low natural occurrence and has a very short half-life (22 minutes for the longest-lived Fr isotope). Synthesis of macroscopic Fr compounds is not currently practical and probably may never be practical. However, the structures of any hypothetical Fr-leucites would be of interest due to the larger Fr^{+} cation size ***(35)*** compared to other alkali metal extraframework cations, would they be isostructural with any known leucite analogues?

7. Conclusions.

The structural chemistry of natural and synthetic analogues of the silicate framework mineral leucite has been investigated from 1890 to the present day.

The crystal structures of leucite ($KAlSi_2O_6$) and pollucite ($CsAlSi_2O_6$) consist of tetrahedrally coordinated aluminosilicate frameworks with alkali metal extraframework cations. The relationship between these structures and that for the zeolite analcime ($NaAlSi_2O_6.H_2O$) is discussed.

The work of Professor Barrer in the 1950s showed how these extraframework cations can be ion-exchanged. Consequently, more leucite analogues were synthesised with different monovalent extraframework cations and with different divalent and trivalent cations partially substituting for silicon in the framework structures. The work of Professor West in the 1980s helped to synthesise many more new leucite analogues. These new analogues included Ge-leucites, with divalent and trivalent cations partially substituting into germanate framework structures. These Ge-leucites have the same topology as their silicon analogues.

Up to the end of the 1980s almost all leucites had silicon and other divalent and trivalent cations disordered over the tetrahedrally coordinated sites (T-sites). These all had body centred tetragonal or cubic crystal structures. In the 1990s Bell, Henderson et al discovered new cation-ordered leucite structures in which silicon and other framework cations were ordered onto their own T-sites. These new cation-ordered structures had lower symmetry primitive monoclinic and cubic structures.

High temperature diffraction experiments have shown that there are phase transitions from lower to higher symmetry crystal structures on heating. These include tetragonal-cubic, monoclinic-orthorhombic, and orthorhombic-cubic phase transitions.

High pressure diffraction experiments on naturally occurring samples of pollucite, leucite and analcime show phase transitions from tetragonal or cubic ambient temperature structures down to triclinic with increasing pressure.

8. References.

Supplementary Materials.

Cation	symmetry	a (Å)	c (Å)	V (Å^3)
K^+	tetragonal	12.92	13.7	2287
NH_4^+	tetragonal	13.17	13.69	2375
Rb^+	tetragonal	13.64	13.33	2480
Tl^+	tetragonal			
Cs^+	cubic	13.66		2549

Table S1. lattice parameters for anhydrous AAlSi$_2$O$_6$ samples***(43)***, no lattice parameters quoted for TlAlSi$_2$O$_6$. If the original reference doesn't quote a unit cell volume, then these have been calculated.

Stoichiometry	a (Å)	c (Å)	V (Å^3)	SG	Ref
$CsAl_{0.875}Fe_{0.125}Si_2O_6$	13.67		2554	*Ia*-3*d*	***(32)***
$CsAl_{0.75}Fe_{0.25}Si_2O_6$	13.696		2569.1	*Ia*-3*d*	***(32)***
$CsAl_{0.625}Fe_{0.375}Si_2O_6$	13.718		2581.5	*Ia*-3*d*	***(32)***

$CsAl_{0.5}Fe_{0.5}Si_2O_6$	13.737		2592.2	*Ia*-3*d*	***(32)***
$CsAl_{0.375}Fe_{0.625}Si_2O_6$	13.758		2604.2	*Ia*-3*d*	***(32)***
$CsAl_{0.25}Fe_{0.75}Si_2O_6$	13.768		2609.8	*Ia*-3*d*	***(32)***
$CsAl_{0.125}Fe_{0.875}Si_2O_6$	13.803		2629.8	*Ia*-3*d*	***(32)***
$CsFeSi_2O_6$	13.816		2637.2	*Ia*-3*d*	***(32)***
$CsBSi_2O_6$	12.985		2189.4	*Ia*-3*d*	***(33)***
$CsBSi_2O_6$	13.02		2207	*Ia*-3*d*	***(33)***
$CsFeSi_2O_6$	13.847		2655	*Ia*-3*d*	***(33)***
$NH_4AlSi_2O_6$	13.214(1)	13.713(2)	2394.4(5)	$I4_1/a$	***(47)***
$K_{0.2}Rb_{0.8}GaSi_2O_6$	**13.15(7)**	**13.89(7)**	**2402(25)**	***I*4$_1$/*a***	***(48)***

$CsFeSi_2O_6$	**13.66(3)**		**2549**	***Ia*-3*d***	***(74)***
$RbAlSi_2O_6$	13.297	13.747	2430.6	$I4_1/a$	***(78)***
$RbFeSi_2O_6$	13.42	13.91	2505	$I4_1/a$	***(78)***
$KFeSi_2O_6$	13.206	13.97	2436.3	$I4_1/a$	***(78)***
$CsBSi_2O_6$	12.991(1)		2192.4(2)	*Ia*-3*d*	***(95)***
$CsGaSi_2O_6$	13.732(1)		2589.4(2)	*I*-43*d*	***(95)***
$RbGaSi_2O_6$	13.363(1)	13.835(1)	2470.5(4)	$I4_1/a$	***(95)***
$KGaSi_2O_6$	13.125(2)	13.878(3)	2390.7(9)	$I4_1/a$	***(95)***
$RbBSi_2O_6$	12.78		2087	*I*-43*d*	***(105)***
$KBSi_2O_6$	12.615(3)		2007.5(5)	*I*-43*d*	***(106)***

Table S2a. *AC*Si_2O_6 lattice parameters, up to 1989 (excepting leucite and pollucite). If the original reference doesn't quote a unit cell volume, then these have been calculated. SG = space group. **Bold type shows that crystal structure is given in this reference.**

Stoichiometry	a (Å)	c (Å)	V ($Å^3$)	SG	Ref

$K_2MgSi_5O_{12}$	13.39		2401	*Ia*-3*d*	***(45, 46)***
$Cs_2CuSi_5O_{12}$	13.598(1)		2514.3(2)	P(?)	***(95)***
$Rb_2NiSi_5O_{12}$	13.498(4)		2459.3(7)	P(?)	***(95)***
$Rb_2CuSi_5O_{12}$	13.4(1)		2406(18)	*Ia*-3*d*	***(95)***
$Rb_2ZnSi_5O_{12}$	13.5(1)		2460(18)	*Ia*-3*d*	***(95)***
$Rb_2CdSi_5O_{12}$	13.614(5)		2523.2323	*Ia*-3*d*	***(95)***
$K_2BeSi_5O_{12}$	12.900(4)	13.431(5)	2235(2)	$I4_1/a$	***(95)***
$K_2ZnSi_5O_{12}$	13.3(l)		2353(18)	*Ia*-3*d*	***(95)***
$Cs_2MgSi_5O_{12}$	13.695(1)		2568.5(2)	*Ia*-3*d*	***(99)***
$Cs_2FeSi_5O_{12}$	13.834(2)		2647.5(4)	*Ia*-3*d*	***(99)***

$Cs_2CoSi_5O_{12}$	13.672(1)		2555.6(2)	*Ia-3d*	***(99)***
$Cs_2NiSi_5O_{12}$	13.654(1)		2545.5(2)	*Ia-3d*	***(99)***
$Cs_2ZnSi_5O_{12}$	13.662(1)		2550.0(2)	*Ia-3d*	***(99)***
$Cs_2CdSi_5O_{12}$	13.791(2)		2622.9(4)	*Ia-3d*	***(99)***
$Rb_2MgSi_5O_{12}$	**13.530(1)**		**2476.8(2)**	***Ia-3d***	***(99)***
$Rb_2FeSi_5O_{12}$	13.650(4)		2543.3(7)	*Ia-3d*	***(99)***
$Rb_2CoSi_5O_{12}$	13.4(l)		2406(18)	*Ia-3d*	***(99)***
$Cs_2MgSi_5O_{12}$	13.695(1)		2568.5(2)	*Ia-3d*	***(99)***
$Cs_2FeSi_5O_{12}$	13.834(2)		2647.5(4)	*Ia-3d*	***(99)***
$Cs_2CoSi_5O_{12}$	13.672(1)		2555.6(2)	*Ia-3d*	***(99)***

$Cs_2NiSi_5O_{12}$	13.654(1)		2545.5(2)	*Ia*-3*d*	***(99)***
$Cs_2ZnSi_5O_{12}$	13.662(2)		2550.0(4)	*Ia*-3*d*	***(99)***
$Cs_2CdSi_5O_{12}$	13.791(2)		2622.9(4)	*Ia*-3*d*	***(99)***
$Rb_2MgSi_5O_{12}$	13.530(1)		2476.8(2)	*Ia*-3*d*	***(99)***
$Rb_2FeSi_5O_{12}$	13.650(4)		2543.3(7)	*Ia*-3*d*	***(99)***
$Cs_2BeSi_5O_{12}$	**13.4059(11)**		**2409.3(2)**	***Ia*-3*d***	***(107)***
$Rb_2BeSi_5O_{12}$	13.109(3)	13.407(5)	2304(2)	$I4_1/a$	***(108)***

Table S2b. $A_2BSi_5O_{12}$ lattice parameters, up to 1989. If the original reference doesn't quote a unit cell volume, then these have been calculated. SG = space group. **Bold type shows that crystal structure is given in this reference.**

Stoichiometry	a(Å)	b(Å)	c(Å)	β(°)	V(Å^3)	Ref
$K_2MgSi_5O_{12}$	13.168(5)	13.652(1)	13.072(5)	91.69(5)	2348(2)	***(52, 53)***
$K_2FeSi_5O_{12}$	13.2574(5)	13.6739(6)	12.9240(5)	93.048(3)	2339.54(16)	***(55)***
$K_2CoSi_5O_{12}$	13.1773(2)	13.6106(2)	13.0248(2)	91.9994(8)	2333.96(4)	***(55)***

$K_2ZnSi_5O_{12}$	13.1773(2)	13.6106(2)	13.0248(2)	91.6981(9)	2334.98(6)	***(55)***

Table S3. Ambient temperature $P2_1/c$ leucite structures. Note that even though $K_2MgSi_5O_{12}$ data (1992) were collected with synchrotron radiation and the others were collected with an X-ray tube (2018), advances in detector technology in the intervening years result in much smaller errors in lattice parameters in the newer structures.

Stoichiometry	a(Å)	b(Å)	c(Å)	V(Å^3)	Ref
$Cs_2CdSi_5O_{12}$	13.6714(1)	13.8240(1)	13.8939(1)	2625.83(6)	***(59)***
$RbCsMgSi_5O_{12}$	13.5676(9)	13.7115(1)	13.5366(9)	2518.2(3)	***(109)***
$RbCsNiSi_5O_{12}$	13.5399(5)	13.563(1)	13.560(1)	2490.1(3)	***(109)***
$RbCsCdSi_5O_{12}$	13.6935(3)	13.8030(3)	13.8592(4)	2619.6(1)	***(109)***
$Rb_2MgSi_5O_{12}$	13.422(1)	13.406(1)	13.730(1)	2470.6(4)	***(61)***
$Cs_2MgSi_5O_{12}$	13.6371(5)	13.6689(5)	13.7280(5)	2559.0(2)	***(61)***
$Cs_2ZnSi_5O_{12}$	13.6415(9)	13.6233(8)	13.6653(9)	2539.6(3)	***(61)***
$Cs_2CuSi_5O_{12}$	13.58943(6)	13.57355(5)	13.62296(4)	2512.847(13)	***(65)***
$Rb_2CoSi_5O_{12}$	13.370(4)	13.639(4)	13.497(4)	2461.4(20)	***(89)***
$Rb_2NiSi_5O_{12}$	13.469(3)	13.480(3)	13.442(2)	2440.7(8)	***(98)***
$Rb_2MnSi_5O_{12}$	13.4085(10)	13.6979(11)	13.5761(10)	2493.5(3)	***(98)***
$Rb_2CdSi_5O_{12}$	13.4121(1)	13.6816(1)	13.8558(1)	2542.51(5)	***(110)***
$Cs_2MnSi_5O_{12}$	13.6878(3)	13.7931(3)	13.7575(3)	2597.4(2)	***(110)***
$Cs_2CoSi_5O_{12}$	13.6487(4)	13.7120(4)	13.6828(4)	2560.7(2)	***(110)***
$Cs_2NiSi_5O_{12}$	13.6147 (3)	13.6568(5)	13.6583(5)	2539.5(1)/	***(110)***

Table S4. Ambient temperature *Pbca* leucite structures.

Stoichiometry	a(Å)	b(Å)	c(Å)	V(Å^3)	T (K)
$Cs_2CdSi_5O_{12}$	13.6760(3)	13.8008(4)	13.8666(4)	2617.17(12)	10
$Cs_2CuSi_5O_{12}$	13.56321(14)	13.52837(14)	13.60617(14)	2496.57(5)	8
$Cs_2ZnSi_5O_{12}$	13.6356(7)	13.6440(11)	13.6358(10)	2536.9(3)	8

Table S5. Low temperature *Pbca* leucite structures, data collected with synchrotron radiation ***(63)***.

Stoichiometry	a(Å)	c(Å)	V(Å^3)	SG	Ref
$K_{0.97}Al_{1.01}Fe_{0.01}Si_{1.99}O_6$	13.0548(2)	13.7518(2)	2343.69(1)	*I*4$_1$/*a*	*(20)*
$Rb_{0.99}Cs_{0.01}Al_{0.99}Si_{1.99}O_6$	13.2918(2)	13.7412(2)	2427.69(1)	*I*4$_1$/*a*	*(20)*
$Cs_{0.96}K_{0.01}Ca_{0.01}Al_{1.00}Si_{1.99}O_6$	13.6524(4)	13.7216(4)	2557.54(1)	*I*4$_1$/*a*	*(20)*
$K_{0.90}Fe_{0.95}Si_{2.01}O_6$	13.2036(2)	13.9543(3)	2432.76(1)	*I*4$_1$/*a*	*(20)*
$KGaSi_2O_6$	13.1099(4)	13.8100(4)	2373.51	*I*4$_1$/*a*	*(49)*
$RbGaSi_2O_6$	13.3703(2)	13.7983(2)	2466.66(7)	*I*4$_1$/*a*	*(50)*
$CsGaSi_2O_6$	13.72124(8)		2583.33(2)	*I*-43*d*	*(50)*
$Cs_2NiSi_5O_{12}$	13.64694(9)		2541.59(3)	*Ia*-3*d*	*(50)*
$K_2MgSi_5O_{12}$	13.4190(1)		2416.35	*Ia*-3*d*	*(52, 53)*
$K_2ZnSi_5O_{12}$	13.3772(2)		2393.87(6)	*Ia*-3*d*	*(55)*
$Rb_2MnSi_5O_{12}$	13.5635(3)		2495.24(10)	*Ia*-3*d*	*(55)*
$K_2CoSi_5O_{12}$	13.3767(3)		2393.57(10)	*Ia*-3*d*	*(55)*
$Cs_2CuSi_5O_{12}$	13.6322(4)		2533.37	*Ia*-3*d*	*(65)*
$Cs_{0.7\text{-}0.8}Na_{0.1}Al_{0.8}Si_{2.2}O_6.(0.3\text{-}0.2)H_2O$	13.677(2)	13.691(2)	2561.2	*I*4$_1$/*acd*	*(66)*
$K_{0.01}Cs_{1.02}B_{0.96}Si_{2.02}O_6$	13.019(2)	12.900(2)	2186.5(1)	*I*4$_1$/*acd*	*(67)*
$KBSi_2O_6$	12.641(1)		2019.9(1)	*I*-43*d*	*(79)* PDF 04-018-9625
$Cs_{0.2}Rb_{0.8}BSi_2O_6$	12.8296(5)		2111.73	*I*-43*d*	*(84)* PDF 04-013-6855
$Cs_{0.4}Rb_{0.6}BSi_2O_6$	12.8787(5)		2136.07	*I*-43*d*	*(85)* PDF 04-013-6856

$Cs_{4.8}Rb_{3.2}B_8Si_{16}O_{48}$	**12.9322(5)**		**2162.80**	***Ia-3d***	***(85)*** **PDF 04-013-6857**
$Cs_{6.4}Rb_{1.6}B_8Si_{16}O_{48}$	**12.9553(5)**		**2174.42**	***Ia-3d***	***(85)*** **PDF 04-013-6858**
$Cs_{0.54}Rb_{0.4}B_{0.94}Si_{2.06}O_6$	**12.9004(5)**		**2146.89**	***Ia-3d***	***(85)*** **PDF 04-015-2977**
$KBSi_2O_6$	**12.604(8)**		**2002.28**	***I*-43*d***	***(97)*** **PDF 04-012-8488**
$CsFeSi_2O_6$	**13.8542(1)**		**2659.16**	***Ia*-3*d***	***(111)***
$KFeSi_2O_6$	**13.2207(3)**	**13.9464(3)**	**2437.65**	***I*4$_1$/*a***	***(111)***
$RbFeSi_2O_6$	**13.4586(1)**	**13.9380(1)**	**2524.64**	***I*4$_1$/*a***	***(111)***
$Rb_2ZnSi_5O_{12}$	**13.4972(1)**		**2458.84**	***Ia*-3*d***	***(112, 113)***
$RbFeSi_2O_6$	13.486(6)	13.922(10)		*I*4$_1$/*a*	***(114)***
$RbBSi_2O_6$	12.831(3)			*I*-43*d*	***(114)***
$NH_4AlSi_2O_6$	**13.2106(6)**	**13.7210(7)**		***I*4$_1$/*a***	***(115)***
$TlAlSi_2O_6$	13.269(2)	13.718(2)	2415.1(9)	*	***(116)***

$NH_4AlSi_2O_6$	13.23	13.735	2403.9	$I4_1/a$	*(117)* PDF 00-056-1348
$ND_4AlSi_2O_6$	13.224	13.751	2404.86	$I4_1/a$	*(117)* PDF 00-057-0527
$NH_4AlSi_2O_6$	13.17954	13.75266	2388.801	$I4_1/a$	*(118)* PDF 04-023-8932
$KBSi_2O_6$	12.6109(2)		2005.57	*I*-43*d*	*(119)* PDF 01-080-7595
$RbBSi_2O_6$	12.7898(1)		2092.14	*I*-43*d*	*(119)* PDF 04-018-4390
$K_{0.84}Rb_{0.16}B_{0.99}Si_2O_6$	12.6859(5)		2041.57	*I*-43*d*	*(119)* PDF 01-080-7596
$K_{0.84}Rb_{0.16}B_{0.99}Si_2O_6$	12.6832(2)		2040.26	*I*-43*d*	*(119)* PDF 01-080-7597
$K_{0.65}Rb_{0.35}BSi_2O_6$	12.7238(2)		2059.92	*I*-43*d*	*(119)* PDF 01-080-7598
$K_{0.42}Rb_{0.58}BSi_2O_6$	12.7483(2)		2071.84	*I*-43*d*	*(119)* PDF 01-080-7599
$K_{0.21}Rb_{0.79}BSi_2O_6$	12.7716(2)		2083.22	*I*-43*d*	*(119)* PDF 01-080-7600
$K_{0.8}Rb_{0.2}BSi_2O_6$	12.6832(2)		2040.26	*I*-43*d*	*(119)* PDF 04-018-4385
$K_{6.4}Rb_{1.6}Si_{16}B_8O_{48}$	12.7502(9)		2072.77	*I*-43*d*	*(119)* PDF 04-018-4386

$K_{0.6}Rb_{0.4}Si_2BO_6$	12.7238(2)		2059.92	*I*-43*d*	*(119)* PDF 04-018-4387
$K_{0.4}Rb_{0.6}Si_2BO_6$	12.7483(2)		2071.84	*I*-43*d*	*(119)* PDF 04-018-4388
$K_{0.2}Rb_{0.8}Si_2BO_6$	12.7716(2)		2083.22	*I*-43*d*	*(119)* PDF 04-018-4389
$K_{0.981}B_{1.041}Si_{1.959}O_6$	12.618(4)		2008.96	*I*-43*d*	*(120)* PDF 01-081-0530 PDF 04-011-4049
$KBSi_2O_6$	12.6418(7)			*Ia*-3*d*	*(121)*
$Rb_{0.89}B_{0.89}Si_{2.11}O_6$	12.7973(1)		2095.83	*I*-43*d*	*(122)* PDF 01-082-8756
$Rb_{0.89}B_{0.89}Si_{2.11}O_6$	12.7879(1)		2091.21	*I*-43*d*	*(122)* PDF 01-082-8757
$Rb_{0.93}B_{0.93}Si_{2.07}O_6$	12.7881(1)		2091.31	*I*-43*d*	*(122)* PDF 01-082-8758
$KBSi_2O_6$	12.626	12.745	2031.76	*I41/a*	*(123)* PDF 00-052-0129
$Rb_{0.96}Si_{2.18}B_{0.77}O_6$	12.858(1)		2125.79	*I*-43*d*	*(124)* PDF 04-026-5688
$Rb_{0.92}Si_{2.42}B_{0.46}O_6$	12.914(1)		2153.69	*I*-43*d*	*(124)* PDF 04-026-5689
$RbBSi_2O_6$	12.785(1)		2090.0	*I*-43*d*	*(124, 125)*

$Rb_{0.96}B_{0.77}Si_{2.18}O_6$	12.858(1)		2125.7	*I*-43*d*	*(125)*
$Rb_{0.92}B_{0.46}Si_{2.42}O_6$	12.914(1)		2153.9	*I*-43*d*	*(125)*
$CsBSi_2O_6$	13.009(1)			*Ia*-3*d*	*(126)*
$Cs_{0.82}B_{1.09}Si_{1.98}O_6$	13.009(8)		2202.4(23)	*Ia*-3*d*	*(126)*
$KBSi_2O_6$	12.6037(5)		2002.14	*I*-43*d*	*(127)* PDF 01-081-9563
$K_{0.63}Cs_{0.37}BSi_2O_6$	12.8554(6)		2124.50	*Ia-3d*	*(127)* PDF 01-081-9566
$K_{0.8}Cs_{0.2}Si_2BO_6$	12.7300(1)		2062.93	*I*-43*d*	*(127)* PDF 04-017-8348
$K_{0.65}Cs_{0.35}Si_2BO_6$	12.7963(3)		2095.33	*I*-43*d*	*(127)* PDF 04-017-8349
$K_5Cs_3B_8Si_{16}O_{48}$	12.8554(6)		2124.50	*Ia-3d*	*(127)* PDF 04-017-8350
$K_{4.8}Cs_{3.2}B_8Si_{16}O_{48}$	12.8230(5)		2108.48	*Ia-3d*	*(127)* PDF 04-017-8351
$K_4Cs_4B_8Si_{16}O_{48}$	12.8499(2)		2121.77	*Ia-3d*	*(127)* PDF 04-017-8352
$K_{2.4}Cs_{5.6}B_8Si_{16}O_{48}$	12.9244(2)		2158.89	*Ia-3d*	*(127)* PDF 04-017-8353
$K_{1.6}Cs_{6.4}B_8Si_{16}O_{48}$	12.9496(2)		2171.55	*Ia-3d*	*(127)* PDF 04-017-8354

$KBSi_2O_6$	12.6007(2)		2000.71	*I*-43*d*	*(128)* PDF 01-088-6658
$K_{0.88}Cs_{0.12}B_{1.09}Si_{1.91}O_6$	12.6858(4)		2041.52	*I*-43*d*	*(129)* PDF 01-072-6041
$K_{0.5}Cs_{0.5}B_{1.08}Si_{1.92}O_6$	12.8480(2)		2120.83	*I*-43*d*	*(129)* PDF 01-072-6040
$K_{0.88}Cs_{0.12}Si_2BO_6$	12.6858(4)		2041.52	*I*-43*d*	*(129)* PDF 04-012-1447
$K_{0.5}Cs_{0.5}Si_2BO_6$	12.8480(2)		2120.83	*I*-43*d*	*(129)* PDF 04-012-1448
$Cs_{0.87}(B_{0.290}Si_{0.710})_3O_6$	12.9992(7)		2196.6(2)	*Ia-3d*	*(86)*
$Rb(B_{0.333}Si_{0.667})_3O_6$	12.7867(7)		2090.7(2)	*I*-43*d*	*(86)*
$K_{0.68}Cs_{0.29}BSi_2O_{5.98}$	12.7785(1)		2086.60	*I*-43*d*	*(130)* PDF 01-083-8305
$K_{0.66}Cs_{0.28}BSi_2O_{5.98}$	12.7572(1)		2076.19	*I*-43*d*	*(130)* PDF 01-083-8306
$K_{0.61}Cs_{0.26}BSi_2O_{5.98}$	12.74224(1)		2068.89	*I*-43*d*	*(130)* PDF 01-083-8307
$K_{0.28}Cs_{0.65}BSi_2O_{5.96}$	12.93664(7)		2165.03	*Ia-3d*	*(130)* PDF 01-083-8308
$K_{0.26}Cs_{0.61}BSi_2O_{5.94}$	12.93664(7)		2165.03	*Ia-3d*	*(130)* PDF 01-083-8309
$K_{0.25}Cs_{0.59}BSi_2O_{5.92}$	12.8924(2)		2142.90	*Ia-3d*	*(130)* PDF 01-083-8310

$CsBSi_2O_6$	13.011(2)	12.900(2)	2183.79	*I41/acd*	PDF 64-274
$Cs_{0.86}B_{1.38}Si_{1.62}O_{5.77}$	13.0020(18)		2198.01	*I*-43*d*	PDF 01-070-8061
$Cs_{0.86}B_{1.38}Si_{1.62}O_{5.77}$	13.0049(14)		2199.49	*I*-43*d*	PDF 01-070-8062
$Cs_{0.86}B_{1.35}Si_{1.65}O_{5.77}$	13.0052(13)		2199.64	*I*-43*d*	PDF 01-070-8063
$Cs_{0.86}B_{1.29}Si_{1.71}O_{5.77}$	13.0057(7)		2199.89	*I*-43*d*	PDF 01-070-8064
$Cs_{0.86}B_{1.29}Si_{1.71}O_{5.77}$	13.0062(4)		2200.14	*I*-43*d*	PDF 01-070-8065
$Cs_{0.85}B_{1.32}Si_{1.68}O_{5.77}$	13.0263(3)		2210.36	*I*-43*d*	PDF 01-071-3371
$Cs_{0.814}B_{1.092}Si_{1.977}O_6$	13.009(8)		2201.57	*I*-43*d*	PDF 01-073-5206
$CsBSi_2O_6$	12.9935(4)		2193.71	*I*-43*d*	PDF 04-017-8355
$CsBSi_2O_6$	13.019(2)	12.899(3)	2186.31	*I41/acd*	PDF 04-019-1461
$Cs_{6.56}B_{8.72}Si_{15.84}O_{48}$	13.009(1)		2201.57	*I*-43*d*	PDF 04-015-1926
$Cs_{6.8}B_{10.56}Si_{13.44}O_{46.08}$	13.0263(3)		2210.36	*I*-43*d*	PDF 04-015-6724
$Cs_{6.88}B_{11.04}Si_{12.96}O_{46.08}$	13.0020(18)		2198.01	*I*-43*d*	PDF 04-015-6725

$Cs_{6.88}B_{11.04}Si_{12.96}O_{46.08}$	**13.0049(14)**		**2199.49**	***I*-43*d***	**PDF 04-015-6726**
$Cs_{6.88}B_{10.8}Si_{13.2}O_{46.08}$	**13.0052(13)**		**2199.64**	***I*-43*d***	**PDF 04-015-6727**
$Cs_{6.88}B_{10.32}Si_{13.68}O_{46.08}$	**13.0057(7)**		**2199.89**	***I*-43*d***	**PDF 04-015-6728**
$Cs_{6.8}B_{10.32}Si_{13.68}O_{46.08}$	**13.0062(4)**		**2200.14**	***I*-43*d***	**PDF 04-015-6729**
$Cs_{6.96}B_{6.96}Si_{17.04}O_{48}$	**12.9992(7)**		**2196.59**	***I*-43*d***	**PDF 04-026-5125**

Table S6. Non cation-ordered leucite structures since 1990. PDF refers to a pattern in the Powder Diffraction File database ***(131)***. If the original reference doesn't quote a unit cell volume, then these have been calculated.

SG = space group. **Bold type shows that crystal structure is given in this reference.**

*$TlAlSi_2O_6$ ***(116)*** no space group given.

There is also a $KBSi_2O_6$ $P2_1/a$ monoclinic leucite with complete Si/B cation disorder, with lattice parameters a =10.9320(3) Å, ***(68, 128)*** b = 17.9111(4) Å, c = 11.0672(3) Å, β =110.284(5)° and volume = 2032.62 Å^3 ***(68, 69)***. The cation ordered $K_2MgSi_5O_{12}$ structure is $P2_1/c$ monoclinic ***(52, 53)*** but this is a different structure to $KBSi_2O_6$.

Stoichiometry	a (Å)	c (Å)	V (Å^3)	**SG**	**Ref**
$CsAlGe_2O_6$	13.919		2696.6		***(33)***
$CsAlGe_2O_6$	13.932		2704.2		***(33)***
$CsFeGe_2O_6$	14.115		2812.2		***(33)***
$CsFeGe_2O_6$	14.103		2805		***(33)***
$CsCrGe_2O_6$	13.82		2639		***(33)***
$K_{0.8}Rb_{0.2}AlGe_2O_6$	13.41	14.36	2582	$I4_1/a$	***(48)***
$CsBGe_2O_6$	13.698(1)		2570.2(2)	*I*-43*d*	***(95)***
$CsAlGe_2O_6$	13.906(1)		2689.1(2)	*I*-43*d*	***(95)***
$CsGaGe_2O_6$	13.960(1)		2720.5(2)	*I*-43*d*	***(95)***
$CsFeGe_2O_6$	13.822(1)		2640.7(2)	*I*-43*d*	***(95)***
$CsCrGe_2O_6$	13.811(1)		2634.4(2)	P(?)	***(95)***

$RbBGe_2O_6$	13.194(1)		2296.8(2)	*I*-43*d*	***(95)***
$RbGaGe_2O_6$	13.725(1)		2585.5(2)	*I*-43*d*	***(95)***
$RbFeGe_2O_6$	13.822(1)		2640.7(2)	*I*-43*d*	***(95)***
$RbCrGe_2O_6$	13.633(3)		2533.8(6)	P(?)	***(95)***
$KAlGe_2O_6$	13.302(8)	14.316(4)	2533.1189	$I4_1/a$	***(95)*** PDF 37-1349
$KGaGe_2O_6$	13.538(2)		2481.2(4)	*I*-43*d*	***(95)***
$RbAlGe_2O_6$	13.698		2570	*I*-43*d*	***(95)*** PDF 37-348
$CsAlGe_2O_6$	13.906		2689.0983	*I*-43*d*	***(95)*** PDF 37-347
$CsAlGe_2O_6$	**13.8939(5)**		**2682.06(31)**	***I*-43*d***	***(96)***

$KAlGe_2O_6$	**13.3314(5)**	**14.3205(3)**	**2545.13(19)**	***I*4$_1$/*a***	***(96)***
$RbAlGe_2O_6$	**13.7153(5)**		**2579.97(26)**	***I*-43*d***	***(96)***
$CsAlGe_2O_6$	**13.9827(1)**		**2733.84(3)**	***I*-43*d***	***(132)*** **PDF 04-012-2039**
$(NH_4)AlGe_2O_6$	**13.6958(1)**		**2568.99(3)**	***I*-43*d***	***(132)*** **PDF 04-012-2037**
$CsAlGe_2O_6$	**13.945(2)**		**2711.8(5)**	***I*-43*d***	***(133)*** **PDF 04-011-7944**
$CsFeGe_2O_6$	**14.0839(8)**		**2793.6(5)**	***I*-43*d***	***(134)*** **PDF 04-026-5014**

Table S7a. Lattice parameters $ACGe_2O_6$ – PDF refers to a pattern in the Powder Diffraction File database ***(131)***. If the original reference doesn't quote a unit cell volume, then these have been calculated. SG = space group. **Bold type shows that crystal structure is given in this reference.** Attempts to synthesise Cr containing Ge-leucites ***(33)*** produced products that were not stable and decomposed on contact with water, these products also contain GeO_2 as an impurity phase. No space group information was given for Cr containing Ge-leucites.

Stoichiometry	a (Å)	V (Å^3)	SG	Ref

$Cs_2FeGe_5O_{12}$	13.959(1)	2720.0(2)	*I*-43*d*	***(96)***
$Cs_2NiGe_5O_{12}$	13.865(1)	2665.4(2)	*I*-43*d*	***(96)***
$Cs_2CuGe_5O_{12}$	13.860(1)	2662.5(2)	*I*-43*d*	***(96)***
$Cs_2CdGe_5O_{12}$	13.900(2)	2685.6(4)	*I*-43*d*	***(96)***
$Rb_2FeGe_5O_{12}$	13.744(1)	2596.2(2)	*I*-43*d*	***(96)***
$Rb_2NiGe_5O_{12}$	13.672(2)	2555.6(4)	*I*-43*d*	***(96)***
$Rb_2CdGe_5O_{12}$	13.656(2)	2546.7(4)	*I*-43*d*	***(96)***
$Cs_2BeGe_5O_{12}$	13.7245(8)	2585.2(2)	*I*-43*d*	***(135)***

$Cs_2MgGe_5O_{12}$	13.9748(6)	2729.2(1)	*I*-43*d*	***(135)***
$Cs_2ZnGe_5O_{12}$	13.9985(5)	2743.1(1)	*I*-43*d*	***(135)***
$Cs_2CoGe_5O_{12}$	14.0021(8)	2745.2(2)	*I*-43*d*	***(135)***
$Cs_2ZnGe_5O_{12}$	13.999(1)	2743.4(2)	*I*-43*d*	***(135)***
$Rb_2BeGe_5O_{12}$	13.4728(7)	2445.5(1)	*I*-43*d*	***(135)***
$Rb_2MgGe_5O_{12}$	13.7826(7)	2618.1(1)	*I*-43*d*	***(135)***
$Rb_2ZnGe_5O_{12}$	**13.7374(8)**	**2592.5(2)**	***I*-43*d***	***(135)***
$Rb_2CoGe_5O_{12}$	13.7307(8)	2588.7(2)	*I*-43*d*	***(135)***

Table S7b. lattice parameters $A_2BGe_5O_{12}$ – If the original reference doesn't quote a unit cell volume, then these have been calculated. SG = space group. **Bold type shows known crystal structures.**

References only referred to in Supplementary Materials.

[106] Voldan J. Crystallization of Rb_2O-B_2O_3-$4SiO_2$. Silikaty. 1981;**25:**165-167.

[107] Voldan J. Krystalizace Trislozkove Slouceniny v Soustave K_2O-B_2O_3-SiO_2 [Crystallization of the Tricomponent Compound in the System K_2O-B_2O_3-SiO_2] Silikaty. 1979;23:133-141. Czech.

[108] Torres-Martinez LM, Gard JA, Howie RA, et al. Synthesis of $Cs_2BeSi_5O_{12}$ with a Pollucite Structure. J. Solid State Chem. 1984;51:100-103.

[109] Torres-Martinez LM, West AR. Synthesis of $Rb_2BeSi_5O_{12}$ with a leucite structure, J. Mat. Sci. Lett. 1984;3:1093-1094

[110] Bell AMT, Henderson CMB. Rietveld Refinement of the Orthorhombic Pbca Structures of $Rb_2CdSi_5O_{12}$, $Cs_2MnSi_5O_{12}$, $Cs_2CoSi_5O_{12}$ and $Cs_2NiSi_5O_{12}$ Leucites by Synchrotron X-ray Powder Diffraction. Acta Cryst. 1996;C52:2132-2139. https://doi.org/10.1107/S0108270196003162

[111] Bell AMT, Henderson CMB. Rietveld Refinement of the Structures of Dry-Synthesized $MFeIIISi_2O_6$ Leucites (M = K, Rb, Cs) by Synchrotron X-ray Powder Diffraction. Acta Cryst. 1994;C50:1531-1536. https://doi.org/10.1107/S0108270194004014

[112] Bell AMT, Henderson CMB. Rietveld Refinement of Dry-Synthesized $Rb_2ZnSi_5O_{12}$ Leucite by Synchrotron X-ray Powder Diffraction. Acta Cryst. 1994;C50:984-986. https://doi.org/10.1107/S0108270194002039

[113] Bell AMT, Henderson CMB. Rietveld Refinement of Dry-Synthesized $Rb_2ZnSi_5O_{12}$ Leucite by Synchrotron X-ray Powder Diffraction. Erratum. Acta Cryst. 1996;C52:490. https://doi.org/10.1107/S0108270196099775

[114] Mazza D, Lucco Bolera M. New X-ray powder diffraction data for Fe, B substituted Rb-leucites ($RbFeSi_2O_6$ and $RbBSi_2O_6$) Powder Diffraction 1997;12(2):87-89.

[115] Yamada M, Riyawaki R, Nakai I, et al. A Rietveld analysis of the crystal structure of ammonioleucite. Mineral. Journ. 1998;20(3):105-112

[116] Kyono A, Kimita M, Shimizu M, et al. Synthesis of thallium-leucite ($TlAlSi_2O_6$) pseudomorph after analcime. Min. Mag. 1999;63(1):75-83. DOI: 10.1180/002646199548321

[117] Andrut M, Harlov DE, Najorka J. Characterization of ammonioleucite $(NH_4)[AlSi_2O_6]$ and ND_4-ammonioleucite $(ND_4)[AlSi_2O_6]$ using IR spectroscopy and Rietveld refinement of XRD spectra. Min. Mag. 2004;68(1):177–189

[118] Yuan J, Yang J, Ma H, et al. Crystal structural transformation and kinetics of NH_4^+/Na^+ ion-exchange in analcime. Micro. Meso. Mat. 2016;222:202-208. https://doi.org/10.1016/j.micromeso.2015.10.020.

[119] Filatov SK, Paufler P, Georgievskaya MI, et al. Crystal formation from glass, crystal structure refinement and thermal behavior of $K_{1-x}Rb_xBSi_2O_6$ boroleucite solid solutions from X-ray powder diffraction data. Z. Krist. 2011;226:602–612. DOI 10.1524/zkri.2011.1390

[120] Miklos D, Smrcok L, Durovic S, et al. Refinement of the Structure of Boroleucite, $K(BSi_2O_6)$ Acta Cryst. 1992;C48:1831-1832 https://doi.org/10.1107/S0108270192002270

[121] Millini R, Montanari L, Bellussi G. Synthesis and characterization of a potassium borosilicate with ANA framework type structure. Microporous Mat. 1993;1:9-15

[122] Levin AA, Filatov SK, Paufler P, et al. Temperature-dependent evolution of $RbBSi_2O_6$ glass into crystalline Rb-boroleucite according to X-ray diffraction data. Z. Kristallogr. 2013;228:259–270 / DOI 10.1524/zkri.2013.1609

[123] Mazza D, Borlera ML, Brisi C, et al. Boron for Aluminium Substitution in the $KAlSi_2O_6$ leucite structure. Journal of the European Ceramic Society, 1997:17;951-955

[124] Krzhizhanovskaya MG, Bubnova RS, Filatov SK, et al. Transformations of the Crystal Structure in a Series of Rubidium Boroleucite Solid Solutions from the X-ray Powder Diffraction Data. Glass Physics and Chemistry, 2003;29(6):599–607.

[125] Bubnova RS, Polyakova IG, Krzhizhanovskaya MG, et al. Structure–density relationship for crystals and glasses in the Rb_2O–B_2O_3–SiO_2 system Phys. Chem. Glasses, 2000;41(6):389–91

[126] Bubnova RS, Stepanov NK, Levin AA, et al. Crystal structure and thermal behaviour of boropollucite $CsBSi_2O_6$. Solid State Sci. 2004;6:629–637.

[127] Derkacheva ES, Krzhizhanovskaya MG, Bubnova RS, et al. Transformation of the Crystal Structure in the Series of $K_{1-x}Cs_xBSi_2O_6$ Borosilicate Solid Solutions. Glass Physics and Chemistry, 2011;37(5):572–578. DOI: 10.1134/S108765961105004X

[128] Krzhizhanovskaya MG, Bubnova RS, Derkacheva ES, et al. Thermally induced reversible phase transformations of boroleucite, $KBSi_2O_6$. Eur. J. Mineral.2016;28:15–21 DOI: 10.1127/ejm/2015/0027-2505

[129] Bubnova RS, Levin AA, Stepanov NK, Crystal structure of $K_{1-x}Cs_xBSi_2O_6$ (x = 0.12, 0.50) boroleucite solid solutions and thermal behaviour of $KBSi_2O_6$ and $K_{0.5}Cs_{0.5}BSi_2O_6$. Z. Krist. 2002;217:55–62

[130] Derkacheva ES, Krzhizhanovskaya MG, Bubnova RS, et al. Thermal Decomposition of $K_{1-x}Cs_xBSi_2O_6$ Borosilicates. Glass Physics and Chemistry, 2013;39(6):659–663. DOI: 10.1134/S1087659613060035

[131] Kabekkodu, S, Dosen, A, Blanton T. 2024. PDF-5+: a comprehensive Powder Diffraction File™ for materials characterization. Powder Diffraction 2024;39(2):47-59. doi: 10.1017/S0885715624000150

[132] Tripathi A, Parise JB. Hydrothermal synthesis and structural characterization of the aluminogermanate analogues of JBW, montesommaite, analcime and paracelsian. Micro. Meso. Mat. 2002;52:65–78.

[133] Usman M, Kocevski V, Smith MD, et al. Polymorphism and Molten Nitrate Salt-Assisted Single Crystal to Single Crystal Ion Exchange in the Cesium Ferrogermanate

Zeotype: $CsFeGeO_4$. Inorg. Chem. 2020;59:9699−9709. https://dx.doi.org/10.1021/acs.inorgchem.0c00936

[134] Bu X, Feng P, Gier TE, et al. Hydrothermal Synthesis and Structural Characterization of Zeolite-like Structures Based on Gallium and Aluminum Germanates. J. Am. Chem. Soc. 1998;120:13389-13397.

[135] Torres-Martinez LM, Gard JA, West AR. Synthesis and Structure of a New Family of Phases, $A_2MGe_5O_{12}$: A = Rb, Cs; M = Be, Mg, Co, Zn. J. Solid State Chem. 1984;53:354-359

1. References.

[1] Deer WA, Howie RA, Zussman J. An Introduction to the Rock-Forming Minerals. Mineralogical Society of Great Britain and Ireland; 2013. https://doi.org/10.1180/DHZ

[2] d'Amour H, Denner W, Schulz H. Structure determination of alpha-quartz up to 68*10exp8 Pa. Acta Cryst. 1979;B35:550-555. https://doi.org/10.1107/S056774087900412X

[3] Downs RT, Palmer DC. The pressure behavior of alpha-cristobalite. Am. Mineral. 1994;79:9-14.

[4] Kihara, K. Thermal change in unit-cell dimensions, and a hexagonal structure of tridymite. Z. Krist.1978;148:237-254.

[5] Araki T, Zoltai T. Refinement of a coesite structure. Z. Krist.1969;129;381-387.

[6] Henderson CMB. Composition, Thermal Expansion and Phase Transitions in Framework Silicates: Revisitation and Review of Natural and Synthetic Analogues of Nepheline-, Feldspar- and Leucite-Mineral Groups. Solids. 2021;2:1–49. https://doi.org/10.3390/ solids2010001

[7] Henderson CMB, Bell AMT, Knight KS. Variable stoichiometry in tectosilicates having the leucite/pollucite-type structure with particular emphasis on modelling the interframework cavity cation environment J. Solid State Chem. 2016;251: 90–104 http://dx.doi.org/10.1016/j.jssc.2017.04.013

[8] Sels BF, Kustov LM (editors). Zeolites and Zeolite-Like Materials. Elsevier; 2016. https://doi.org/10.1016/C2014-0-00257-2)

[9] International Zeolite Association. Database of Zeolite structures. [Internet] Available from http://www.iza-structure.org/databases/.

[10] Taylor WH, The structure of analcite ($NaAlSi_2O_6.H_2O$). Z. Krist. 1930;74:1-5. https://doi.org/10.1524/zkri.1930.74.1.1

[11] Ferraris G, Jones DW, Yerkess J. A neutron-diffraction study of the crystal structure of analcime, $NaAlSi_2O_6.H_2O$. Z. Krist. 1972;135:240-252 DOI: 10.1524/zkri.1972.135.3-4.240

[12] Taylor WH. Note on the Structures of Analcite and Pollucite. Z. Krist. 1938;99:283-290.

[13] Takéuchi Y, Mazzi F, Haga N, et al. The crystal structure of wairakite. Am. Mineral. 1979;64:993-1001.

[14] Henderson CMB, Bell AMT, Kohn SC, et al. Leucite-pollucite structure-type variability and the structure of a synthetic end-member calcium wairakite ($CaAl_2Si_4O_{12}.2H_2O$) Min. Mag. 1998;62(2):165-178.

[15] Momma K, Izumi F. VESTA 3 for three-dimensional visualization of crystal, volumetric and morphology data. J. Appl. Cryst. 2011;44:1272-1276. https://doi.org/10.1107/S0021889811038970

[16] Wyart J. Étude sur la leucite [Study of leucite]. Bull. Soc. Franc. Mineral. 1938;61(4-6):228-238. French. doi : https://doi.org/10.3406/bulmi.1938.4444

[17] Wyart J. Etude cristallographique d'une leucite artificielle. Structure atomique et symétrie du minéral. [Crystallographic study of an artificial leucite. Atomic structure and mineral symmetry]. Bull. Soc. Franc. Mineral. 1940;63(1-12):5-17. French. doi : https://doi.org/10.3406/bulmi.1940.4477

[18] Náray-Szabó SV, Die Struktur des Leucits $KAlSi_2O_6$ [The structure of leucite $KAlSi_2O_6$] Z. Krist. 1942;104:39-44. German.

[19] Mazzi F, Galli E, Gottardi G. The crystal structure of tetragonal leucite. Am. Mineral. 1976;61:108-115.

[20] Palmer DC, Dove MT, Ibberson RM, et al. Structural behavior, crystal chemistry, and phase transitions in substituted leucite: High-resolution neutron powder diffraction studies. Am. Mineral. 1997;82:16-29.

[21] Mineral Data Company [Internet]; 2001. Details of leucite mineral. https://rruff.info/doclib/hom/leucite.pdf

[22] Ritzberger C, Apel A, Höland W, et al, Properties and Clinical Application of Three Types of Dental Glass-Ceramics and Ceramics for CAD-CAM Technologies. Materials (Basel). 2010;19;3(6):3700–3713. doi: 10.3390/ma3063700

[23] Mineral Data Company [Internet]; 2001. Details of pollucite mineral. https://rruff.info/doclib/hom/pollucite.pdf

[24]. Yi Liu, Shuai Deng, Yaxin Feng et al (2025) Synthesis of Pollucite Ceramics for Immobilizing Molten Salt Waste via Sub/Supercritical Hydrothermal. Ceramics International. https://doi.org/10.1016/j.ceramint.2025.07.082

[25]. Ga-Yeong Kim, Seong-Sik Shin, Byeonggwan Lee et al (2024) Characteristics of Cs pollucite synthesized at various Cs loadings for immobilization of radioactive Cs. Journal of Nuclear Materials. 2023; :154781. https://doi.org/10.1016/j.jnucmat.2023.154781

[26] Diego Gatta G, Rinaldi R, McIntyre GJ, et al. On the crystal structure and crystal chemistry of pollucite, $(Cs,Na)_{16}Al_{16}Si_{32}O_{96}.nH_2O$: A natural microporous material of

interest in nuclear technology**.** Am. Mineral. 2009;94:1560–1568. DOI: 10.2138/am.2009.3237

[27] Strunz H, Die chemische Zusammensetzung von Pollucit [The chemical composition of pollucite]. Z. Krist. 1936;95:1-8. German.

[28] Náray-Szabó SV, Die Struktur des Pollucits $CsAlSi_2O_6.xH_2O$ [The structure of pollucite $CsAlSi_2O_6.xH_2O$] Z. Krist. 1938;99:277-282. German.

[29] Newnham RE. Crystal structure and optical properties of pollucite. Am. Mineral. 1967;52:1515-1518.

[30] Beger RM. The crystal structure and chemical composition of pollucite. Z. Krist. 1969;129:280-302. https://doi.org/10.1524/zkri.1969.129.16.280.

[31] Yanase I, Kobayashi H, Shibasaki Y, et al. Tetragonal-to-cubic structural phase transition in pollucite by low-temperature X-ray powder diffraction. J. Amer. Ceram. Soc. 1997;80:2693-2695. https://doi.org/10.1111/j.1151-2916.1997.tb03175.

[32] Kume S, Koizumi M. Synthetic pollucites in the system $Cs_2O.Al_2O_3.4SiO_2$-$Cs_2O.Fe_2O_3.4SiO_2.H_2O$. Their phase relationship and physical properties. Am. Mineral. 1965;50:587-592.

[33] Richerson DW, Hummel FA. Synthesis and Thermal Expansion of Polycrystalline Cesium Minerals. J. Amer. Ceram. Soc. 1972;55(5):269-273.

[34] Yanase I, Kobayashi H, Mitamura T. Thermal property and phase transition of the synthesized new cubic leucite-type compounds. J. Therm. Anal. Calorim. 1999;57:695-705.

[35] Shannon RD, Revised Effective Ionic Radii and Systematic Studies of Interatomic Distances in Halides and Chalcogenides. Acta Cryst. 1976;A32:751-767. https://doi.org/10.1107/S0567739476001551

[36] Henderson CMB, Taylor D. The thermal expansion of the leucite group of minerals. Am. Mineral. 1968;53:1476-1489.

[37] Clark JR, Appleman DE, Papike JJ. Crystal-chemical characterization of clinopyroxenes based on eight new structure refinements. Min. Soc. America, Special Paper. 1969;2:31-50

[38] Cameron M, Sueno S, Prewitt CT, et al. High-temperature crystal chemistry of acmite, diopside, Hedenbergite, jadeite, spodumene, and ureyite. Am. Mineral. 1973;58:594-618.

[39] Barrer RM. Ion–exchange and ion-sieve processes in crystalline zeolites. J. Chem. Soc**.** 1950;2342-2350 https://doi.org/10.1039/JR9500002342

[40] Taylor HFW, Hydrothermal reactions involving thallium. J. Chem. Soc. 1949;1253-1256 https://doi.org/10.1039/JR9490001253

[41] Barrer RM. Hinds L. Ion-exchange in crystals of analcite and leucite. J. Chem. Soc. 1953;1879-1888 DOI https://doi.org/10.1039/JR9530001879

[42] Barrer RM, McCallum N. Hydrothermal chemistry of silicates. Part IV. Rubidium and caesium aluminosilicates. J. Chem. Soc. 1953;4029-4035. https://doi.org/10.1039/JR9530004029

[43] Barrer RM, Baynham JW, McCallum N. Hydrothermal chemistry of silicates. Part V. Compounds structurally related to analcite. J. Chem. Soc. 1953;4035-4041. https://doi.org/10.1039/JR9530004035

[44] Goldsmith JR. Gallium and Germanium Substitutions in Synthetic Feldspars. J. Geology. 1950;58(5):518-536. https://www.jstor.org/stable/30068568

[45] Roedder EW. The system K_2O-MgO-SiO_2 Part 1. Amer. J. Sci. 1951;249:81-130. https://doi.org/10.2475/ajs.249.2.81

[46] Roedder EW. The system K_2O-MgO-SiO_2 Part 2. Amer. J. Sci. 1951;249:224-248. https://doi.org/10.2475/ajs.249.3.224

[47] Hori H, Nagashima K, Yamada M, et al. Ammonioleucite, a new mineral from Tataruzrwu, Fujioka, Japan. Am. Mineral. 1986;71:1022-1027.

[48] Klaska R. Ein synthetischer Leucit-typ mit Ordnungstenenz [A synthetic leucite-type with ordering]. Naturwissenschaften. 1978;65:592-593. German.

[49] Bell AMT, Henderson CMB. Tetragonal-cubic phase transition in $KGaSi_2O_6$ synthetic leucite analogue and its probable mechanism. J. Solid State Chem. 2020;284:121142 https://doi.org/10.1016/j.jssc.2019.121142

[50] Bell AMT, Stone AH. Crystal structures and X-ray powder diffraction data for $Cs_2NiSi_5O_{12}$, $RbGaSi_2O_6$, and $CsGaSi_2O_6$ synthetic leucite analogues. Powder Diffraction. 2021;November:1-9. http://dx.doi.org/10.1017/s0885715621000580

[51] Kohn SC, Dupree R, Mortuza MG, et al. An NMR Study of Structure and Ordering in Synthetic $K_2MgSi_5O_{12}$, a Leucite Analogue. Phys Chem Min. 1991;18:144-152.

[52] Bell AMT. Ab-initio structure determination of monoclinic K-Mg-leucite from Synchrotron X-ray Powder Diffraction [master's thesis]. Keele (UK): University of Keele; 1992.

[53] Bell AMT, Henderson CMB, Redfern SAT, et al. Structures of Synthetic $K_2MgSi_5O_{12}$ Leucites by Integrated X-ray Powder Diffraction, Electron Diffraction and 29Si MAS NMR Methods. Acta Cryst. 1994;B50:31-41. https://doi.org/10.1107/S0108768193008754

[54] Rietveld HM. A profile refinement method for nuclear and magnetic structures. J. Appl. Cryst. 1969;2:65-71. https://doi.org/10.1107/S0021889869006558

[55] Bell AMT, Henderson CMB. Crystal structures of $K_2ZnSi_5O_{12}$ (X = Fe^{2+}, Co, Zn) and $Rb_2XSi_5O_{12}$ (X = Mn) leucites: comparison of monoclinic *P*2_1/*c* and *Ia*-3*d* polymorph structures and inverse relationship between tetrahedral cation (T = Si and X)—O bond distances and intertetrahedral T—O—T angles. Acta Cryst. 2018;B74:274-286. https://doi.org/10.1107/S2052520618004092

[56] Kohn SC, Henderson CMB, Dupree R. NMR Studies of the Leucite Analogues $X_2YSi_5O_{12}$, where X = K, Rb, Cs; Y = Mg, Zn, Cd Phys Chem Min. 1994;21:176-190

[57] Kohn SC, Henderson CMB, Dupree R. Si-Al order in leucite revisited: New information from an analcite-derived analogue. Am. Mineral. 1995;80:705–714.

[58] Kohn SC, Henderson CMB, Dupree R. Si-Al ordering in leucite group minerals and ion-exchanged analogues: An MAS NMR study. Am. Mineral. 1997;82:1133–1140.

[59] Bell AMT, Redfern SAT, Henderson CMB, et al. Acta Cryst. 1994;B50:560-566. Structural Relations and Tetrahedral Ordering Pattern of Synthetic Orthorhombic $Cs_2CdSi_5O_{12}$ Leucite: A Combined Synchrotron X-ray Powder Diffraction and Multinuclear MAS NMR Study. https://doi.org/10.1107/S0108768194003393

[60] Bell AMT, Henderson CMB. A study of possible extra-framework cation ordering in *Pbca* leucite structures with stoichiometry $RbCsX^{2+}Si_5O_{12}$ (X = Mg, Ni, Cd). Powder Diffraction. 2018;34(S1):S2-S7. doi:10.1017/S0885715619000071

[61] Bell AMT, Henderson CMB. Crystal structures and cation ordering in $Cs_2MgSi_5O_{12}$, $Rb_2MgSi_5O_{12}$ and $Cs_2ZnSi_5O_{12}$ leucites. Acta Cryst. 2009;B65:435-444. https://doi.org/10.1107/S0108768109024860

[62] Bell AMT, Henderson CMB. High-temperature synchrotron X-ray powder diffraction study of $Cs_2X^{2+}Si_5O_{12}$ (X = Cd, Cu, Zn) leucites. Min. Mag. 2012;76(5):1257–1280. DOI: 10.1180/minmag.2012.076.5.12

[63] Bell AMT. Rietveld refinement of the low temperature crystal structures of $Cs_2XSi_5O_{12}$ (X = Cu, Cd, Zn). Eur. J. Chem. 2021;12(1):60-63. https://dx.doi.org/10.5155/eurjchem.12.1.60-63.2089

[64] Heinrich AR, Baerlocher, C. X-ray Rietveld structure determination of $Cs_2CuSi_5O_{12}$, a pollucite analogue. Acta Cryst. 1991;C47:237-241. https://doi.org/10.1107/S0108270190004711

[65] Bell AMT, Knight KS, Henderson CMB, et al. Revision of the structure of $Cs_2CuSi_5O_{12}$ leucite as orthorhombic Pbca. Acta Cryst. 2010;B66:51–59. https://doi.org/10.1107/S0108768109054895

[66] Frank-Kamenetskaya OV, Rozhdestvenskaya IV, Bannova II, et al. Dissymmetrization of crystal structures of sodium pollucites. Crystallogr. Rep. 1995;**40**, 645-654.

[67] Agakhanov AA, Pautov LA, Karpenko VY, et al. Kirchhoffite, $CsBSi_2O6$, a new mineral species from the Darai-Pioz alkaline massif, Tajikistan: description and crystal structure. Can. Mineral. 2012;50: 523-529. DOI : 10.3749/canmin.50.2.523

[68] Belokoneva EL, Dimitrova OV, Stefanovich SY. New Isoformula Potassium Borosilicates with Different Zeolite Frameworks: Monoclinic Centrosymmetric Boroleucite $K(BSi_2)O_6$ and Chiral $KBSi_2O_6$. Crystallography Reports, 2010;55(4):575–582. DOI: 10.1134/S1063774510040073

[69] Krzhizhanovskaya MG, Bubnova RS, Derkacheva ES, et al. Thermally induced reversible phase transformations of boroleucite, $KBSi_2O_6$. European Journal of Mineralogy 2016;28:15–21. DOI: 10.1127/ejm/2015/0027-2505

[70] Friedrich W, Knipping P, von Laue M. "Interferenz-Erscheinungen bei Röntgenstrahlen" [Interference phenomena in X-rays]. Sitzungsber. K. Bayer. Akad. Wiss. Math. Phys. Kl, 1912;303–322. German.

[71] Bragg WH, Bragg WL, The Reflection of X-rays by Crystals. Proc. Roy. Soc. London Ser. A. 1913;**88**:428-438.

[72] Friedel C, Friedel G. Action des alcalis et des silicates alcalins sur le mica: production de néphéline, de I'amphigène, de l'orthose [Action of alkalis and alkali

silicates on mica: production of nepheline, amphigene and orthose.] Bull. Soc. Franc. Mineral. 1890;**13**:129-139. French.

[73] Faust GT. Phase transition in synthetic and natural leucite. Schweiz. Mineral. und petrograph. Mitteil. 43 1963;43:165-195. https://doi.org/10.5169/seals-33447

[74] Kopp OC, Harris LA, Clark GW, et al. A hydrothermally synthesized iron analog of pollucite-its structure and significance. Am. Mineral. 1963;48:100-109.

[75] Sadanaga R, Ozawa T. Thermal transition of leucite. Mineral. J. 1968;**5**:321-333.

[76] Peacor DR. A high temperature single crystal diffractometer study of leucite, $(K,Na)AlSi_2O_6$. Z. Krist. 1968;127:213-224.

[77] Hirao K, Soga N, Masanaga M. Thermal Expansion and Structure of Leucite-Type Compounds. J. Phys. Chem. 1976;80(14):1612-1616.

[78] Martucci A, Pecorari P, Cruciani G. Dehydration process and transient channel deformations of slightly hydrated boron leucite: An ‘‘in situ’’ time-resolved synchrotron powder diffraction study. Micro. Meso. Mat. 2011;142:570-576. doi:10.1016/j.micromeso.2010.12.046

[79] Hübner R, Belger A, Meyer DC, et al. Crystallisation of caesium borosilicate glasses with approximate boroleucite composition. Z. Krist. 2002;217:223–232.

[80] Bell AMT. High temperature XRD study of $RbFeSi_2O_6$ leucite analogues. Unpublished work.

[81] Bell AMT. Tetragonal - cubic phase transition in $RbGaSi_2O_6$ synthetic leucite analogue. 2025, submitted to Powder Diffraction.

[82] Yanase I, Kobayashi H, Mitamura T. Thermal expansion property of synthetic cubic leucite-type compounds. J. Ceram. Soc. Japan. 2000;108[1]:26-31.

[83] Novotna M, Maixner J. X– ray powder diffraction study of leucite crystallisation Z. Krist. Suppl. 2006;23:455-459 DOI https://doi.org/10.1524/9783486992526-076

[84] Krzhizhanovskaya MG, Bubnova RS, S. Filatov SK et al.
Crystal structure and thermal behaviour of $(Rb,Cs)BSi_2O_6$ solid solutions. Cryst. Res. Technol. 2006;41(3):285 – 292 DOI 10.1002/crat.200510575

[85] Eremina TA, Belokoneva EL, Dimitrova OV, et al. Single-Crystal Synthesis and Structures of Rb-Boroleucite $Rb(BSi_2)O_6$ and Boropollucite $Cs(BSi_2)O_6$ at 293 and 120 K Crystallography Reports, 2019;64(1):57–62. **DOI:** 10.1134/S1063774519010073

[86] Krzhizhanovskaya MG, Bubnova RS, Ugolkov VL, et al. Thermal Expansion and Polymorphism in a Series of Rubidium Cesium Boroleucites. Glass Physics and Chemistry, 2007;33(3):242–249. DOI: 10.1134/S1087659607030091

[87] Redfern SAT, Henderson CMB. Monoclinic-orthorhombic phase transition in the $K_2MgSi_5O_{12}$ leucite analog. Am. Mineral. 1996;81:369-374

[88] Bell AMT, Clegg F, Henderson CMB. Monoclinic–orthorhombic first-order phase transition in $K_2ZnSi_5O_{12}$ leucite analogue; transition mechanism and spontaneous strain analysis. Min. Mag. 2021;85:752–771. doi:10.1180/mgm.2021.67

[89] Bell AMT, Henderson CMB. $Cs_2CuSi_5O_{12}$ phase transition? Z. Krist. Proc. 2011;1:337-342 DOI 10.1524/zkpr.2011.0051

[90] Bell AMT. Orthorhombic-Cubic Phase Transition in $Rb_2CoSi_5O_{12}$ Leucite Analogue. Minerals. 2023;13:210. https://doi.org/10.3390/min13020210

[91] Hariyani S, Armijo E, Brgoch J. Broad Green Emission in the Leucite-Like $Cs_2ZnSi_5O_{12}:Eu^{2+}$ Phosphor ECS J. of Solid State Sci. Tech. 2020;9: 016015 DOI: 10.1149/2.0222001JSS

[92] Diego Gatta G, Rotiroti N, Boffa Ballaran T, et al. Leucite at high pressure: Elastic behavior, phase stability, and petrological implications. Am. Mineral. 2008;93:1588–1596. DOI: 10.2138/am.2008.2932

[93] Diego Gatta G, Rotiroti N, Boffa Ballaran T, et al. Elastic behavior and phase stability of pollucite, a potential host for nuclear waste. Am. Mineral. 2009;94:1137-1143. DOI: 10.2138/am.2009.3195 1137.

[94] Choi W, Choi J, Hwang H, et al. Transformation of natural pollucite into hexacelsian under high pressure and temperature. Phys Chem Minerals 2022;**49**:15 https://doi.org/10.1007/s00269-022-01190-w

[95] Diego Gatta G, Nestola F, Boffa Ballaran T. Elastic behavior, phase transition, and pressure induced structural evolution of analcime. Am. Mineral. 2006;91(4):568-578. 10.2138/am.2006.1994

[96] Torres-Martinez LM, West AR. Pollucite- and Leucite-related Phases: $A_2BX_5O_{12}$ and ACX_2O_6 (A = K, Rb, Cs; B = Be, Mg, Fe, Co, Ni, Cu, Zn, Cd; C = B, Al, Ga, Fe, Cr; X = Si, Ge). Zeit. Anorg. Allg. Chem. 1989;578:223-230.

[97] Bell AMT. Crystal structures and powder diffraction data for $AAlGe_2O_6$ (A = K, Rb, Cs) leucite analogues. Powder Diffraction. 2024;39(3):162-169. https://doi.org/10.1017/S088571562400023X

[98] Ihara M, Kamei F. Crystal Structure of Potassium Borosilicate, $K_2O \cdot B_2O_3 \cdot 4SiO_2$ Yogyo-Kyokai-Shi 1980;88[1]:32-25.

[99] Bell AMT, Henderson CMB. Rietveld refinement of the crystal structures of $Rb_2X^{2+}Si_5O_{12}$ (X = Ni, Mn). Acta Cryst. 2016;E72:249–252. https://doi.org/10.1107/S2056989016001390

[100] Torres-Martinez LM, West AR. New family of silicate phases with the pollucite structure. Z. Krist. 1986;175:1-7.

[101] Attfield JP, Bell AMT, Rodriguez-Martinez LM, et al. Synthesis, structure and properties of a semivalent iron oxoborate, Fe_2OBO_3. J. Mat. Chem., 1999;9(1):205-209.

[102] Attfield JP, Bell AMT, Rodriguez-Martinez LM, et al. Electrostatically driven charge-ordering in Fe_2OBO_3. Nature. 1998;396:655-658.

[103] Bell AMT. Structural studies using synchrotron X-ray powder diffraction and other techniques [dissertation]. Cambridge (UK): University of Cambridge; 1999. 10.17863/CAM.41650

[104] Brown IWM, Cardile CM, MacKenzie KJD, et al. Natural and synthetic leucites studied by solid state 29-Si and 27-Al NMR and 57-Fe Mossbauer spectroscopy. *Phys Chem Minerals.* 1987;**15**:78–83. https://doi.org/10.1007/BF00307612

[105] Adloff J-P, Kauffman GB. Francium (Atomic Number 87), the Last Discovered Natural Element. Chem. Educator. 2005;**10**:387–394

Subject Index

alkali metal, 20, 31, 60, 61, 62
ammonioleucite, 20, 102, 103
analcime, 2, 7, 8, 9, 11, 13, 14, 19, 20, 41, 42, 63, 87, 100, 103, 106
boroleucite, 20, 96, 97, 103, 104, 105
boron, 21, 50, 97
caesium, 10, 91, 97
cation ordering, 2, 21, 25, 37, 45, 60, 61, 94
cation-disordered, 28, 59
crystallography, 30
electron diffraction, 22
extraframework, 2, 6, 9, 13, 19, 20, 24, 40, 43, 50, 51, 60, 62, 63
framework collapse, 13, 26, 43, 48, 50, 60
framework structure, 7, 9, 31, 40, 43, 50
Francium, 62, 101
gallium, 51
Ge leucites, 3, 43, 60
germanate, 43, 63
High pressure, 40, 63
high temperature diffraction, 30, 31
Hydrothermal synthesis, 19, 106
ion exchange, 3, 19
leucite analogues, 3, 19, 20, 21, 23, 24, 26, 28, 40, 43, 45, 59, 60, 61, 62, 63, 92, 97, 100
mineral, 2, 6, 9, 10, 26, 40, 62, 88, 89, 92, 95
Mössbauer spectroscopy, 61
neutron powder diffraction, 26, 61, 88
NMR spectroscopy, 22, 24
nuclear waste, 61
partial cation disorder, 37
phase transitions, 3, 6, 30, 31, 32, 34, 35, 36, 37, 39, 40, 41, 42, 60, 61, 62, 63, 88
pollucite, 3, 9, 10, 11, 12, 13, 14, 17, 19, 20, 22, 30, 31, 40, 41, 42, 44, 51, 62, 63, 67, 86, 87, 89, 90, 95, 96, 99, 100
potassium, 9, 104
Powder Diffraction File, 80, 83, 106
Rietveld refinement, 22, 24, 95, 100, 103
Rubidium, 91, 98, 104
silicate framework, 2, 3, 6, 7, 9, 31, 43, 50, 60, 62
structure type, 20
synchrotron, 1, 2, 21, 22, 24, 25, 26, 32, 36, 37, 61, 71, 72, 94, 97, 101
topology, 2, 7, 9, 13, 23, 26, 28, 48, 63
transition temperature, 30, 32, 40
wairakite, 7, 8, 9, 14, 87
X-ray powder diffraction, 1, 2, 19, 21, 24, 35, 36, 37, 39, 61, 90, 92, 94, 101, 102, 103
zeolite, 6, 7